NASA CR-
ERIM 109600-66-F
7.7-10162
NASA CR-
150997

NASA

Final Report

WHEAT SIGNATURE MODELING AND ANALYSIS FOR IMPROVED TRAINING STATISTICS

W.A. MALILA, R.C. CICONE, AND J.M. GLEASON
Infrared and Optics Division

MAY 1976

(E77-10162) WHEAT SIGNATURE MODELING AND ANALYSIS FOR IMPROVED TRAINING STATISTICS Final Report, 15 May 1975 - 14 May 1976 (Environmental Research Inst. of Michigan) 170 p HC A08/MF A01 CSCL 02C G3/43
N77-24557
Unclas
00162

Prepared for
NATIONAL AERONAUTICS AND SPACE ADMINISTRATION

Johnson Space Center
Earth Observations Division
Houston, Texas 77058
Contract No. NAS9-14123, Task 17
Technical Monitor: Dr. A. Potter/TF3

ENVIRONMENTAL
RESEARCH INSTITUTE OF MICHIGAN
FORMERLY WILLOW RUN LABORATORIES THE UNIVERSITY OF MICHIGAN
BOX 618 • ANN ARBOR • MICHIGAN 48107

NOTICE

Sponsorship. The work reported herein was conducted by the Environmental Research Institute of Michigan under Contract NAS9-14123 for the National Aeronautics & Space Administration, Johnson Space Center, Houston, Texas 77058. Dr. Andrew E. Potter was Technical Monitor for NASA. Contracts and grants to the Institute for the support of sponsored research are administered through the Office of Contracts Administration.

Other Final Reports. This is one of 6 final reports on this contract.

Disclaimers. This report was prepared as an account of Government sponsored work. Neither the United States, nor the National Aeronautics & Space Administration (NASA), nor any person acting on behalf of NASA:

(A) Makes any warranty expressed or implied, with respect to the accuracy, completeness, or usefulness of the information, apparatus, method, or process disclosed in this report may not infringe privately owned rights; or

(B) Assumes any li·bilities with respect to the use of, or for damages resulting from the use of any information, apparatus, method, or process disclosed in this report.

As used above, "person acting on behalf of NASA" includes any employee or contractor of NASA, or employee of such contractor, to the extent that such employee or contractor of NASA or employee of such contractor prepares, disseminates, or provides access to any information pursuant to his employment or contract with NASA, or his employment with such contractor.

Availability Notice. Request for copies of this report should be referred to:

National Aeronautics & Space Administration
Scientific & Technical Information Facility
P. O. Box 33
College Park, Maryland 20740

Final Disposition. After this document has served its purpose, it may be destroyed. Please do not return it to the Environmental Research Institute of Michigan.

1. Report No. NASA CR- ERIM 109600-66-F	2. Government Accession No.	3. Recipient's Catalog No.
4. Title and Subtitle Wheat Signature Modeling and Analysis for Improved Training Statistics		5. Report Date May 1976 6. Performing Organization Code
7. Author(s) W. A. Malila, R. C. Cicone, J. M. Gleason		8. Performing Organization Report No. 109600-66-F
9. Performing Organization Name and Address Environmental Research Institute of Michigan Infrared & Optics Division P. O. Box 618 Ann Arbor, Michigan 48107		10. Work Unit No. Task 17 11. Contract or Grant No. NAS9-14123
12. Sponsoring Agency Name and Address National Aeronautics & Space Administration Johnson Space Center Houston, Texas 77058		13. Type of Report and Period Covered Final Technical Report May 15, 1975 through May 14, 1976 14. Sponsoring Agency Code

15. Supplementary Notes

The work was performed for the Earth Observations Division.
Dr. Andrew Potter (TF3) was the technical monitor.

NALEPKA RICHARD F.

16. Abstract

The primary objective of this effort was to determine training data selection criteria for possible improvement of LACIE signature extraction procedures. Landsat data sets from two LACIE intensive test sites plus additional wheat agronomic data were empirically analyzed. A multispectral system simulation model also was developed, from an existing vegetation canopy reflectance model and an existing radiative transfer model, and employed to simulate Landsat wheat canopy radiances for a variety of growth stages and canopy and atmospheric conditions. Some ancillary field measurement data also were examined.

The analysis of the 1973-74 agronomic data for the Kansas ITS's indicated a number of differences which potentially could affect the spectral signatures of wheat and/or other aspects of recognition processing. Irrigation patterns varied widely within the State and many different varieties of wheat planted within the State were noted. Landsat signal statistics from data acquired over one of these sites indicated a definite correlation between irrigation practice and spectral response and also indicated that wheat variety differences produced observable spectral differences. These data also indicated that between-field differences were generally greater than within-field differences.

This same Landsat data set was classified with signatures derived from different amounts of training data. Results indicated that the amount of data used definitely affected recognition performance, both for classification of field-center pixels and for estimating the proportion of wheat in the site. The variability between signatures obtained by different draws of training data decreased as the sample size increased;

17. Key Words Landsat Data LACIE Radiative Transfer Wheat Reflectance Model Multispectral Simulation Training Procedures Recognition Performance	18. Distribution Statement Initial distribution is listed at the end of this document.

19. Security Classif. (of this report) Unclassified	20. Security Classif. (of this page) Unclassified	21. No. of Pages xi + 170	22. Price

16. Abstract (Cont'd)

the resulting signatures also became more robust and the decision threshold value became less significant. Multiclass boundary pixels and the use of too few signatures to represent the class "other" contributed heavily to observed recognition errors and proportion estimation biases.

The simulated Landsat wheat canopy radiances were qualitatively analyzed to determine the effects of the various levels of the factors which characterize the canopy and the atmospheric conditions. Variations in the canopy characteristics are most noticeable in the longer wavelength bands and variations in the atmospheric characteristics are most noticeable in the shorter wavelength bands. Brighter backgrounds increase path radiance and brighter soils increase total radiance, the amount of this latter increase depending on the particular canopy characteristics. Within a particular spectral band, the effect of variations in canopy density is determined by the relative brightness of crop and soil, and the effect of different scanner view angles is determined by the variation in path radiance and bidirectional canopy reflectance. Although a common overall trend is evident, substantial differences do exist in the temporal trajectories of the simulated radiances for various combinations of canopy density and soil brightness. All these factors can affect the multitemporal recognition of wheat.

Initial analyses of the ancillary field measurement data indicated that the measured optical thicknesses of the atmosphere were nearly all thinner than those used in the simulation, and that these thicknesses exhibited substantial temporal changes, both short-term and long-term. Also, the spectral patterns of wheat reflectances were consistent with those obtained by simulation, on a qualitative basis.

PREFACE

This document reports processing and analysis efforts on one task of a comprehensive and continuing program of research in multispectral remote sensing of the environment. The research is being carried out for NASA's Lyndon B. Johnson Space Center, Houston, Texas, by the Environmental Research Institute of Michigan (ERIM). The basic objective of this program is to develop remote sensing as a practical tool for obtaining extensive environmental information quickly and economically.

The specific focus of the work reported herein was the modeling and analysis of the wheat signatures for purposes of establishing improved training statistics for the inventory of wheat and of providing insight for other improvements of recognition procedures.

The research covered in this report was performed under Contract NAS9-14123 during the period 15 May 1975 to 14 May 1976. Dr. Andrew Potter (TF3) served as the NASA Contract Technical Monitor. At ERIM, work was performed within the Infrared and Optics Division, headed by Richard R. Legault, Vice-President of ERIM, in the Information Systems and Analysis Department, headed by Dr. Jon D. Erickson. Mr. Richard F. Nalepka, Head of the Multispectral Analysis Section served as Principal Investigator.

The authors wish to acknowledge the assistance of other members of the ERIM staff in addition to those cited above. Dr. R. E. Turner was consulted on the adaptation and use of his atmosphere radiative transfer model, and contributed the analysis of optical thickness measurements presented in Sec. 7.1. Dr. G. H. Suits was consulted on the adaptation and use of his vegetation bidirectional reflectance model. R. J. Kauth assisted in the specification of simulation parameters. Dr. J. E. Colwell provided measurements of wheat-component reflectance and transmittance spectra and assisted in defining the wheat canopy characteristics for the various stages of growth. A. P. Pentland implemented our suggested modifications of his multispectral data clustering program. Others provided assistance during various stages of the analysis and report preparation, including E. R. Kent and R. A. DeBacker. We especially wish to acknowledge Miss Darlene Dickerson who ably and steadfastly typed and prepared this report and earlier materials.

CONTENTS

CONTENTS (Cont'd)

FIGURES

FIGURES (Cont'd)

FIGURES (Cont'd)

FIGURES (Cont'd)

TABLES

1
SUMMARY, CONCLUSIONS, AND RECOMMENDATIONS

In this investigation, the spectral, spatial, and temporal characteristics of wheat and other signatures in Landsat multispectral scanner data were examined through empirical analysis and simulation. Several agronomic characteristics which influence winter wheat reflectances were established through analysis and comparison of spectral signatures from fields with known characteristics in two LACIE (Large Area Crop Inventory Experiment) intensive test sites (ITS's) in Kansas; data sets acquired in May and June 1974 were analyzed. The objective of these efforts was to gain sufficient understanding of the spectral and physical characteristics and variability of the populations that are being recognized spectrally in LACIE, so that improved criteria could be established for determining the amount and type of data required for training recognition computers for the inventory of wheat.

The selection of training data is a sampling process. An empirical study was made to determine the effects of varied training sample size on wheat recognition performance. Landsat data acquired 26 May 74 over the Finney Kansas test site were classified with signatures derived from different amounts of training data. An attempt was made to incorporate LACIE Analyst-Interpreter constraints and procedures into the three selection rules examined.

A major simulation effort then was undertaken to generate an extensive and consistent set of synthetic spectral radiance data for a variety of winter wheat fields (63 in number) at seven different stages of growth, as observed under a variety of observation conditions representative of Landsat. Effective inband radiance was computed for each Landsat spectral band, as well as calculations of inband reflectance, atmospheric transmittance and path radiance, and irradiance values. The results are concisely summarized and briefly analyzed in this report and are presented in full in a limited-distribution supplement [1]. These calculations are intended for general use by LACIE investigators.

The limited amount of data from the LACIE Field Measurement Project which was made available for analysis during the performance period of this investigation was examined and initial comparisons made with the simulated data.

1.1 CONCLUSIONS

(1) An analysis of 1973-74 agronomic data for the Kansas ITS's indicated a number of differences which potentially could affect the spectral signatures of wheat and/or other aspects of recognition processing:

(a) Irrigation patterns varied widely within the State and among ITS's; 88% of wheat acreage in the Finney ITS was irrigated and 24% in the Morton ITS, as opposed to less than 3% for the western 2/3 of Kansas.

(b) Many different wheat varieties are planted in the State, and different ones predominated in the various ITS's.

(c) Field size limitations were not a major problem in the Kansas sites; average field sizes for wheat were large, averaging 40 acres or more for the Finney and Ellis ITS's; other fields were somewhat smaller on the average.

(d) In other regions with smaller fields, the necessity of moving pixel selection lines inward from field boundaries could create a serious problem because it precludes the selection of pixels from many fields; also, the number of multiclass pixels would be greater.

(2) An analysis of Landsat signal statistics (from data acquired over the Finney ITS, 26 May 74) and their relationship to agronomic factors showed that:

(a) the irrigation practice was definitely correlated with the observed spectral response,

(b) wheat variety differences produced observable spectral differences due to leaf coloration and different dates of maturation,

(c) between-field differences were generally greater than within-field differences, and

(d) boundary pixels produced spectral features distinct from those within field centers.

(3) The amount of data used for training definitely affected recognition performance, both for classification of field-center pixels and for estimating the proportion of wheat in the site analyzed (Finney ITS, 26 May 74):

(a) Multiclass boundary pixels contributed much of the observed bias in proportion estimates.

(b) Multimodal class signatures were required, and use of too few signatures to represent class 'other' contributed to the observed recognition errors; it is important to obtain a good representation of those specific other crops which can be confused with wheat.

(c) The variability between signatures obtained by different draws of training data decreased as the sample size became larger; also, the resulting signatures became more robust and the particular decision threshold value became less important.

(4) The qualitative analysis of the simulated Landsat wheat canopy radiances has revealed that:

(a) the effects of variations in the canopy characteristics are most noticeable in the longer-wavelength bands and the effects of variations in the atmospheric characteristics are most noticeable in the shorter-wavelength bands,

(b) the effect of variations in atmosphere visibility in any spectral band is determined mainly by the relative changes in atmospheric transmittance and path radiance in that band,

(c) the effect of a brighter background is to increase the path radiance component,

(d) the effect of a brighter soil in the wheat canopy is to increase radiance, the exact amount depending on the canopy density and leaf transmittance, the latter being a function of spectral band,

(e) the effect of different scanner view angles is determined in any spectral band by the variations in path radiance and bidirectional canopy reflectance,

(f) the effect of variations in canopy density is determined in any particular spectral band by the relative brightness of crop and soil, and

(g) although a common overall trend is evident, substantial differences do exist in the temporal trajectories of the simulated radiances for various combinations of canopy density and soil brightness, which will affect results obtained with multitemporal processing techniques.

(5) Initial analyses of the ancillary field measurement data that were available for analysis during the performance period of this investigation showed that:

(a) despite calibration uncertainties, the atmosphere optical thicknesses measured were nearly all thinner (exhibited greater visibility) than those simulated,

(b) substantial temporal changes in optical thickness were noted on both a short-term (diurnal) and a long-term (day-to-day and month-to-month) basis,

(c) measured ratios of diffuse to total irradiance supported conclusion 5(a), and

(d) spectral patterns of field measurements of wheat reflectances were consistent with patterns of computed reflectances, on a qualitative basis.

(6) Data processing and analysis procedures developed during the course of this investigation have been incorporated into other investigations and efforts carried out at ERIM under the parent contract.

1.2 RECOMMENDATIONS

(1) Based on the analyses of agronomic factors and/or associated spectral characteristics, it is recommended that:

(a) agronomic factors, such as planting, irrigation, and fertilization practices be examined in regions of interest to LACIE,

(b) field size and shape distributions and field-center pixel availability be investigated in these same regions,

(c) further analyses be carried out to better identify and establish more quantitative relationships between the agronomic and spectral characteristics of wheat fields, including analyses of field measurement and simulated data.

(2) Based on the work that was completed on the influence of the amount of training data on recognition performance, it is recommended that:

(a) the joint effects of decision threshold and signature robustness (sample size) on recognition performance be examined,

(b) methods for insuring that analyst-interpreters obtain a representative sample of other (non-wheat) classes in the scene be investigated.,

(c) additional sites and multiple time periods be considered, and

(d) spectral displays, e.g., two-channel ellipse plots, be used where analyst interaction is required.

(3) Based on the simulation effort conducted, it is recommended that additional simulations and analyses of Landsat wheat canopy radiances be conducted.

(a) A quantitative analysis of the existing data should be conducted as a follow-up to the qualitative analysis already undertaken.

(b) Additional data should be generated for more levels of the various factors investigated (particularly clearer atmospheres); effects of changing wheat component reflectances and transmittances should also be examined.

(c) Calibration factors should be determined to convert the simulated radiances to their equivalent Landsat data values.

(d) The simulated data should be compared in more detail to actual Landsat data and field measurement data to evaluate their accuracy.

(e) Similar simulations should be undertaken for spring wheat and other crops which compete with it in recognition processing.

(4) To facilitate the efforts in (3) and enable other analysis efforts, it is recommended that improvements be made to the simulation model to make it more general and readily useable.

(a) The capability for generating a covariance matrix for a particular set of canopy and atmospheric conditions should be added to the model.

(b) The capability for equating the background reflectance spectrum to the actual canopy reflectance spectrum should be added.

(c) The capability for generating an entire simulated data set given a particular field pattern and set of conditions for each field should be developed using the model as a basic tool.

(5) Analyses of field measurement spectral reflectance data are recommended as soon as these data become available; intercomparisons between simulated and measured data are strongly recommended as an aid to analyses of these types individually, as well as collectively.

(6) Generalized models of wheat and other signatures should be developed, incorporating ancillary parameters describing both environmental and ground scene conditions.

2
INTRODUCTION

A key step in the successful use of computer-processed remote sensor data for agricultural inventories and other applications is the establishment of signatures to be used by recognition processors. A signature is a statistical description (mean vector and variance-covariance matrix) of signals from a class or subclass of the scene being studied. As such, the set of signatures employed must adequately represent both the range and variability of signals from the scene of interest, if satisfactory recognition performance is to be achieved.

Problems that have received considerable attention under LACIE SR&T investigations are those of extending signatures from one area to another and defining regional partitions within which this extension can take place most easily. There still remains a considerable problem in extracting adequate signatures for use both locally and in the nonlocal areas through signature extension procedures. The amount of training data required to establish signatures for recognition processing directly affects the costs (for both computer and personnel) of training the processor, whether these fields be identified by direct ground observation, by image interpretation, by computer analysis, or by a combination of these.

A major objective of the effort reported herein was to establish criteria for determining the amount and type of training data required for sufficient Landsat training statistics and signatures for computer inventory of wheat. A supporting objective, which was upgraded in emphasis, scope, and schedule midway in the contract year, was to simulate Landsat radiances and signals for wheat fields under a variety of conditions, for use in this and other investigations.

The overall approach taken toward this investigation was based on viewing the selection of training data as a sampling problem. Initial efforts, therefore, were directed at gaining an understanding of the spectral and physical characteristics and variability of the populations that are being sampled, especially the wheat fields and their Landsat signals.

Table 1 lists the major factors that enter into the determination of multispectral signatures for use in recognition. As indicated in Table 2, these include the biological and agricultural conditions which may be observed and described in varying degrees of detail by ground observers and/or photointerpreters. Also important are the actual physical characteristics of the ground cover and soil which interact with the incident radiation to produce the observed radiation; these quantities include those needed for modeling the spectral reflectance of vegetation canopies. Finally, Table 2 also lists the observation conditions which play an important role in determining the mean signals observed.

It is not sufficient to describe the mean signal levels from various scene classes for recognition purposes. The within-class variability is another important factor in determining their separability. Table 3 lists several different ground-related, atmosphere-related, and sensor-related factors which contribute to the variability in Landsat signals.

Agronomic data acquired for LACIE within the five LACIE Intensive Test Sites in the State of Kansas were analyzed thoroughly as a first step in understanding winter wheat and other classes and their variability (See Sec. 3). Actual Landsat data acquired from two of these test sites were analyzed in several ways (See Sec. 4). First, statistics (field signatures) were extracted from every field of sufficient size in the sites. Then the wheat field signatures were grouped according to their spectral similarities and these groupings correlated with the agronomic data. Next, for one site, all field-center pixels were clustered in a supervised mode and all boundary pixels

TABLE 1. ELEMENTS OF SIGNATURE DEFINITION

- FACTORS DETERMINING MEAN SIGNALS
  - BIOLOGICAL/AGRICULTURAL CONDITIONS
  - RADIATION/PHYSICAL INTERFACE CHARACTERISTICS
  - OBSERVATION CONDITIONS
- SOURCES OF VARIABILITY IN LANDSAT SIGNATURES
  - GROUND-RELATED
  - ATMOSPHERE-RELATED
  - SENSOR-RELATED
  - SAMPLING ERRORS

TABLE 2. DESCRIPTORS OF FACTORS DETERMINING MEAN SIGNALS

A. DESCRIPTORS OF BIOLOGICAL/AGRICULTURAL CONDITIONS

- CROP SPECIES AND VARIETY
- MATURITY OR GROWTH STAGE
- VIGOR
- CONDITION
  - MOISTURE LEVEL
  - INFESTATION
- PERCENT COVER
- LEAF AREA INDEX
- YIELD
- BIOMASS
- SOIL TYPE AND TEXTURE
- FARMING PRACTICE

B. DESCRIPTORS OF RADIATION/PHYSICAL INTERFACE CHARACTERISTICS

PHYSICAL STRUCTURE OF VEGETATION CANOPY

- DISTRIBUTION OF SIZE, SHAPE, LOCATION, AND ORIENTATION FOR EACH COMPONENT PART
- PLANT DENSITY AND PLANTING PATTERN
- TEXTURE AND MOISTURE CONTENT OF SOIL

COLOR OR SPECTRAL PROPERTIES OF VEGETATION CANOPY

- OVERALL COLOR OR SPECTRAL RADIANCE
- OVERALL DIRECTIONAL SPECTRAL REFLECTANCE
- REFLECTANCE OF EACH COMPONENT
- TRANSMITTANCE OF EACH COMPONENT
- SOIL REFLECTANCE

FIELD SIZES, SHAPES, AND PATTERNS

C. DESCRIPTORS OF OBSERVATION CONDITIONS

- DATE OF YEAR
- TIME OF DAY
- SOLAR ANGLES
- SCAN ANGLE
- METEOROLOGICAL CONDITIONS
- ATMOSPHERIC STATE
  - HAZE OR OPTICAL THICKNESS
  - CLOUDS
- SPECTRAL BAND
- SPATIAL RESOLUTION

TABLE 3. SOURCES OF VARIABILITY IN LANDSAT SIGNATURES

A. GROUND-RELATED FACTORS

- LOCAL GROWTH CALENDAR AND VARIATIONS IN MATURITY
- CROP CONDITION
- PLANTING PRACTICE
  - DENSITY OF PLANTS
  - FIELD PATTERNS AND SIZES
  - CROP VARIETY
- SOIL TYPE AND MOISTURE LEVEL
- LOCAL METEOROLOGICAL CONDITIONS, PAST AND PRESENT
- MANAGEMENT PRACTICE
  - IRRIGATION
  - FERTILIZATION
  - CULTIVATION
  - GRAZING

B. ATMOSPHERE-RELATED FACTORS

- HAZE LEVEL OR OPTICAL THICKNESS OF ATMOSPHERE
- METEOROLOGICAL STATE OF ATMOSPHERE
- CLOUDS

C. SENSOR-RELATED FACTORS

- LATITUDE/LONGITUDE OF SENSOR } Determine Sun Angles,
- TIME AND DATE OF OBSERVATION } Among Other Variables
- SENSOR SCAN ANGLE
- SENSOR NOISE
  - STRIPING, BANDING (Within-Frame Calibration)
  - RANDOM NOISE
  - BETWEEN-FRAME CALIBRATION

clustered in an unsupervised mode. Intercomparisons of the various spectral groupings were made.

Next, a test was carried out to explore the effects of varied amounts of training data on recognition performance (See Sec. 5). An attempt was made to incorporate LACIE Analyst-Interpreter (AI) constraints into the three data selection rules employed. Three independent data selections were made using each rule; signatures were established and used to classify the data; and recognition performances were evaluated and compared. Additional planned testing of this type was postponed due to an increased emphasis and priority on the theoretical simulations of multitemporal wheat signatures which are discussed next.

NASA has recognized the need for a consistent and extensive set of synthetic spectral radiance and LANDSAT data for use in LACIE investigations. Therefore, a set of parametric calculations of inband Landsat radiances from wheat fields at seven stages of growth was made using the ERIM Multispectral System Simulation Model (See Sec. 6). A total of 3400 combinations of wheat field characteristics, viewing geometries, and atmospheric conditions were simulated to explore the sensitivity of the received radiances to the various factors (approximately eight in number). The total inband radiances were computed by integrating spectral radiances formed by multiplying the product of reflectance, irradiance, and atmospheric transmittance spectra (after adding the appropriate path radiance spectrum) by the Landsat spectral response functions. Similarly, effective inband values of the component reflectances and the atmospheric features, were calculated as well. These calculations are concisely summarized and briefly analyzed in this report and presented in full in a limited-distribution supplement to this report [1].

The final source of data on wheat signature characteristics considered in this report was the LACIE field measurement program for wheat. Unfortunately, the major measurements, i.e., the spectral measurements of reflectance made by the field vans and the helicopter-borne spectrometer were not reduced and distributed for analysis during the contract period. Some analyses of ground observation data were carried out.

3
WHEAT AGRONOMIC DATA AND LANDSAT PIXEL AVAILABILITY FOR LACIE INTENSIVE TEST SITES IN KANSAS

During the 1973-74 growing season (as well as succeeding years) the U.S. Department of Agriculture's Agricultural Stabilization and Conservation Service (USDA/ASCS) conducted field observations and interviews with farmers within the LACIE Intensive Test Sites. Several types of useful agronomic data were compiled for the wheat fields present in the sites. Data were recorded concerning wheat variety planted, irrigation and fertilization practices, and field size. Much of the same information was obtained for other crops as well. The compiled statistics from these field visits were provided to LACIE project personnel. The major use of these data has been for the purpose of identifying the crop types present in fields to be used for training recognition processors and evaluating their subsequent performance.

More extensive use and analysis of these data were made in this investigation in an attempt to correlate the characteristics of Landsat spectral signals with these agronomic factors. The agronomic data were summarized for each of the five intensive test sites in the state of Kansas. These were compared among one another, with supplementary data summarizing planting conditions and characteristics in their respective crop reporting districts, and with statewide agricultural planting and harvesting patterns. These comparisons are presented in Sec. 3.1.

Another important factor in recognition processing of Landsat data is the proportion of single-class (field-center) pixels in the scene. As examined more fully under another task [2] of this contract, the proportion of field-center pixels depends on the field sizes and shapes relative to the ground resolution size of a pixel. The presence of a high proportion of multiclass pixels (those which cross field boundaries) can deleteriously affect crop proportion estimation accuracy. A summary was made of the average field sizes for two of the five intensive test sites, Finney and Ellis. These data and their possible influence on the accuracy of classification processors is discussed in Sec. 3.2.

3.1 ANALYSIS OF AGRONOMIC DATA FOR WINTER WHEAT

The agronomic practices which most affect the vigor and density of wheat stands could be expected to have the greatest influence on spectral characteristics observable by Landsat In Kansas, water availability is perhaps the major factor limiting growth, especially in the semi-arid Southwest Crop Reporting District (CRD). Therefore, irrigation should be important to the spectral characteristics of a wheat field.

Statistics were extracted from USDA/ASCS 1973-74 observations to describe the moisture supply practices (e.g., irrigation) in the five LACIE Intensive Test Sites (ITS's) which were located in two of Kansas' nine crop reporting districts, the Southwest and the Central. These statistics are presented, in Table 4, along with values for the county, crop reporting district and the western two-thirds of the state (the six western-most CRD's). It is immediately evident that there are substantial variations in these practices throughout the state. The majority of wheat in the western two-thirds of the state was planted on summer fallowed land, 36% on continuous-cropped dry land, and less than 3% on irrigated land. The Central CRD had essentially no wheat on irrigated land, with 58% on continuous-cropped dry land. The Southwest CRD, on the other hand, had 10% on irrigated land and less than that on continuous-cropped dry land, with 81% on summer fallowed land. These patterns are related to the local amounts of rainfall, and differ more widely on a county-by-county basis.

Finally, we see that the Finney Intensive Test Site for 1973-74 was preponderantly (88%) irrigated, a very anomalous area for the state

TABLE 4. IRRIGATION AND FERTILIZATION PRACTICES ON KANSAS SITES

FARMING PRACTICE	PERCENT OF WHEAT ACREAGE															
	FINNEY			ELLIS			MORTON			RICE			SALINE			WESTERN TWO-THIRDS OF STATE OF KANSAS†
	ITS*	CO†	CRD†	ITS	CO	CRD	ITS	CO	CRD	ITS	CO	CRD	ITS	CO	CRD	
1. Moisture Supply			(SW)			(C)			(SW)			(C)			(C)	
(a) Irrigated	88	13.8	10.1	0	0	0.1	24	13.2	10.1	0	0	0.1	0	0	0.1	2.8
(b) Summer Fallowed		82.3	81.3		81.7	41.4		84.9	81.3		39.7	41.4		22.7	41.4	61.2
(c) Continuous-Cropped Dry Land		3.9	8.6		18.3	58.5		1.9	8.6		60.3	58.5		77.3	58.5	36.0
2. Fertilized	78			26			26			100			100			
3. Neither Irrigated Nor Fertilized	10			74			74			0			0			
4. Both Irrigated and Fertilized	76			0			23			0			0			

*For 1973-74 Crop in LACIE ITS (Intensive Test Site), from USDA/ASCS Observations.

†For 1972-73 Crop in CRD (Crop Reporting Districts) and Western 2/3 of State [3].
SW = Southwest CRD and C = Central CRD

of Kansas. It is primarily for this reason that the location of the Finney ITS was changed for the 1975-76 growing season. Even in the Morton ITS, nearly twice as high a percentage of wheat was irrigated (24%) as was in the county (13%). There was no irrigation in other test sites or counties.

Statistics on fertilization practices, as extracted from the USDA/ASCS records, also are presented in Table 4 for the five sites. These indicate that 100% of wheat acreage in Rice and Saline counties was fertilized, while the value was 78% in Finney and only 26% in Ellis. In the Finney ITS, nearly all wheat fertilized was also irrigated, and only 10% was neither fertilized nor irrigated. In the Morton ITS, on the other hand, nearly all wheat irrigated also was fertilized but 74% of the wheat acres were neither irrigated nor fertilized. Thus, although the percent irrigated varies, there is a high probability that a fertilizer was applied wherever there was irrigation. Adequate amounts of fertilizer should enable vigorous growth with accompanying healthy colors of the wheat vegetation.

More than 15 varieties of winter wheat were planted in Kansas during the 1973-74 growing season. The varieties planted and the relative amounts of each change from year to year. Most common in 1973-74 was the Scout variety, as it had been for the preceding four years or more. However, the percentage of acreage seeded to Scout (36.5%) was 10% less than the previous year, with most of the increase being in the Eagle variety (up to 17.8%). Each other variety contributed less than 10% of the total for the state.

Table 5 summarizes the percentage of each variety of wheat planted in the five Kansas intensive test sites during the 1973-74 growing season. Six varieties were identified in the USDA/ASCS field observation data, in addition to a general non-specific category which happened to be the only one identified for the Saline segment. Percentages are noted both for the State and for the crop reporting

TABLE 5. APPORTIONMENT OF WHEAT ACREAGE AMONG WHEAT VARIETIES (KANSAS, 1973-74)

		PERCENT OF TOTAL WHEAT ACREAGE											
		FINNEY		ELLIS		MORTON		RICE		SALINE		STATE OF KANSAS†	
CROP CODE	WHEAT VARIETY	ITS*	CRD†	ITS	CRD	ITS	CRD	ITS	CRD	ITS	CRD	PERCENT	RANK
			(SW)		(C)		(SW)		(C)		(C)		
402	Scout	20.2 (21.2)**	58.0	82.7 (90.0)	21.7	36.9 (51.9)	58.0	44.6 (51.7)	21.7		21.7	36.5	1
404	Eagle	1.0 (1.1)	18.1	9.2 (10.0)	25.8	17.9 (25.3)	18.1	10.4 (12.0)	25.8		25.8	17.8	2
407	Satanta	56.1 (59.0)	6.5		4.6	1.1 (1.5)	6.5	3.8 (4.4)	4.6		4.6	4.7	6
408	Centurk	0.7 (0.7)	6.6		11.9	10.9 (15.3)	6.6	27.5 (31.9)	11.9		11.9	9.5	3
409	Bison	5.7 (6.0)	3.5		0.7	4.3 (6.0)	3.5					1.2	10
424	††Eagle Scout	11.4 (12.0)											
400	Unknown	4.9 (-)		8.1		28.9 (-)		13.7 (-)		100.			
	Other Var.		7.3		35.3		7.3		35.3		35.3	30.3	

*ITS denotes LACIE Intensive Test Site.

**( ) Denotes apportioning Code 400 proportionally among other varieties.

†CRD denotes Crop Reporting District; SW = Southwest and C = Central; Values are for 1974 Crop [2].

††USDA Agricultural Experiment Station personnel in Garden City, Kansas, have indicated that there is no "Eagle Scout" variety; these are most likely of the Eagle variety.

district (CRD) containing each segment [3]. Percentages on the CRD level are seen to depart substantially from the state-wide averages -- the Southwest CRD more so than the Central CRD. The Southwest CRD had about 58% Scout, 18% Eagle, 7% Centurk, and 7% Satanta, while the Central CRD had about 22% Scout, 26% Eagle, 12% Centurk, and 5% Satanta.

The percentages of the different wheat varieties for the intensive test sites departed from the patterns for both state and district. Finney ITS, for example, has 56% Satanta wheat with only 20% Scout and 1% Eagle (although the 11% called Eagle Scout, a non-existent variety, is most likely of the Eagle variety). Ellis ITS on the other hand, with no Satanta, had 83% Scout and 9% Eagle. Morton ITS came closest to matching its district. The patterns for the other sites are less clear because of greater amounts of "unknown" variety.

Reasons for the variation observed in the patterns of wheat varieties planted may lie in topographic, soil, and weather conditions, in irrigation and fertilization practices, in differences in the speed with which newer varieties gain acceptance by the growers, and/or in combinations of these factors. Wheat variety might affect the observable multitemporal multispectral characteristics of wheat due to different maturation dates, different spectral reflectances and transmittances of components at comparable stages of development, different growth forms and habits, and different densities. Several of these effects were observed and are discussed in Sec. 4.

3.2 FIELD SIZE AND LANDSAT PIXEL AVAILABILITY

For training, it is usual to use only field-center pixels so as to avoid contamination of pure crop signatures by pixels which cross field boundaries and therefore contain mixtures of two or more materials. Hence, field size is another variable which can have an important effect on recognition performance. LACIE AI's attempt to select only field-center pixels for training, with a minimum of four field-center pixels per selected field [4]. In recognition, mixture pixels can cause problems because they frequently may be misclassified. The larger the average field size in the segment, the smaller the proportion of mixture pixels that will exist [2].

A detailed analysis of field sizes was made for two ITS's, Finney and Ellis. Fig. 1 presents histograms of the number of fields in these ITS's as a function of the field size. Different vertical scales are used because the overall size of the Finney ITS is larger (30 sections) than that of the Ellis ITS (9 sections). The fields tabulated are for all LACIE ground truth codes except 800, non-agricultural. Overall, the Ellis ITS tends to have smaller fields than the Finney ITS. The predominance in Ellis of small "other" fields in the category 10 acres or less is notable. The mean and median wheat fields in the Finney ITS are both about 44 acres whereas in the Ellis ITS the mean is about 40 acres but the median is only about 30 acres. Also in the Ellis ITS, the mean "other" field size is about 18 acres while the median is about 25 acres. In the Finney ITS, on the other hand, the mean "other" field size is just over 40 acres while the median is about 35 acres.

The distribution of field sizes does not fully indicate the way in which wheat acreage is found in the sites. Fig. 2 presents cumulative distributions of wheat and "other" acreages as functions of field size. These curves show that roughly 25% of the wheat acreage is in fields of 80 acres or more in size, 50% in fields of 55 acres or more, and 75% in fields of just under 40 acres or larger. The distributions for wheat are much more similar between the two sites than for "other", where the effect of the smaller fields in the Ellis ITS are more evident.

Part of the job of preparing Landsat data for the analyses which were performed was the designation of field-center pixels in the data sets. Data preparation was performed jointly by several Tasks under this contract. A semi-automated procedure, which had been previously developed [5] and later employed in part of the CITARS data preparations [6], was refined and used in LACIE data set preparations.

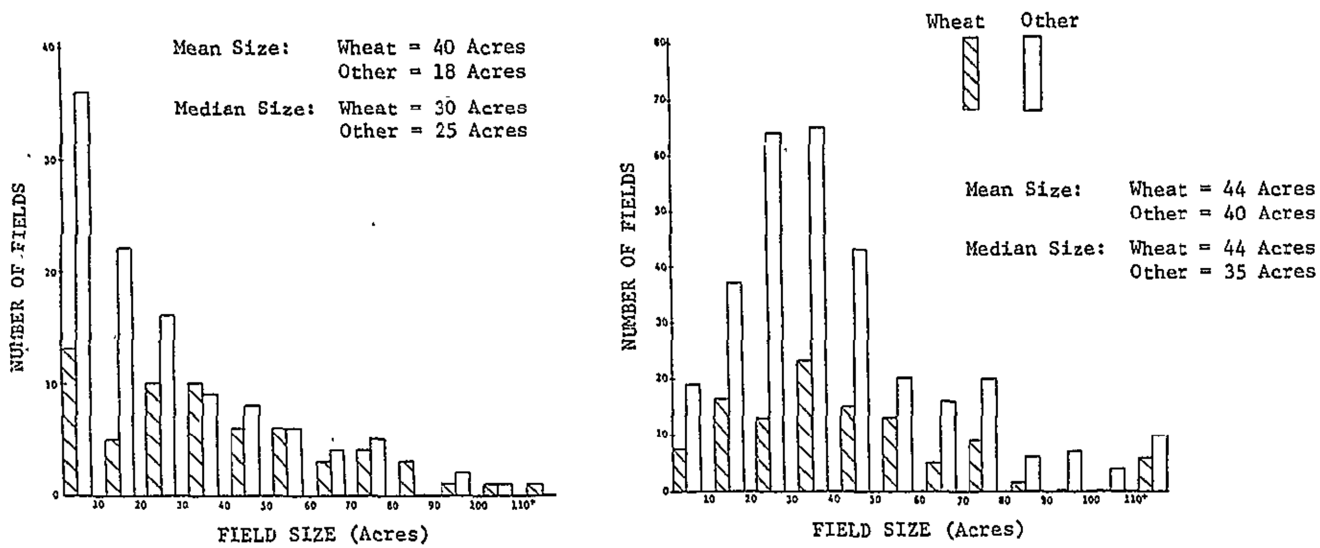

(a) Ellis (Kansas) Intensive Test Site, 1973-74

(b) Finney (Kansas) Intensive Test Site

FIGURE 1. DISTRIBUTION OF FIELD SIZES

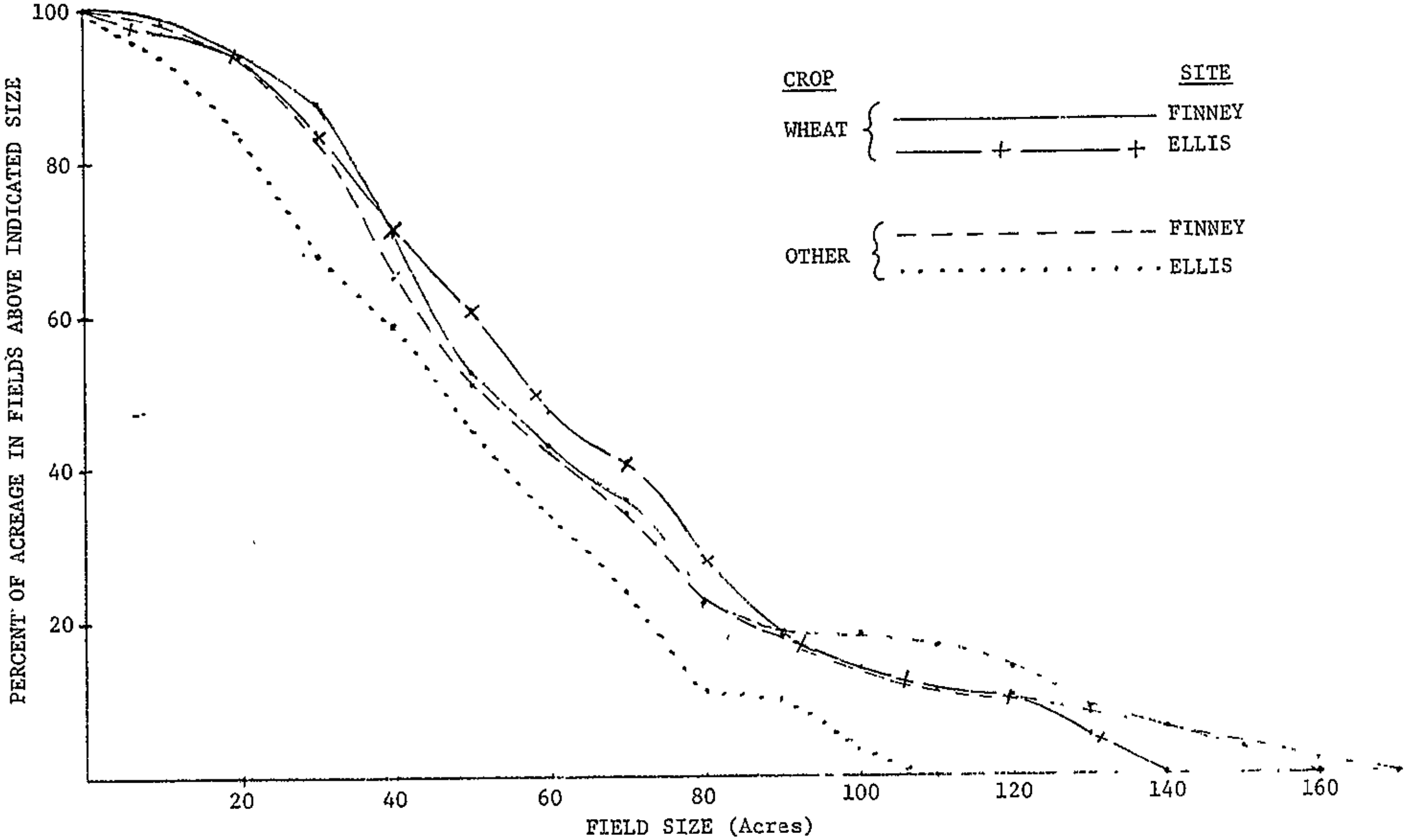

FIGURE 2. DEPENDENCE OF DISTRIBUTION OF CROP ACREAGES ON FIELD SIZE; KANSAS 1973-74

Coordinates of every field vertex in the intensive study sites analyzed were digitized from the rectified aerial photomaps provided by NASA/JSC. At the same time, coordinates were digitized for control points which could be located in digital line-printer 'graymaps' of the Landsat data. Regression techniques were then used on the control points to determine a transformation to convert the photo coordinates of all the field vertices to Landsat data coordinates. These Landsat coordinates then could be used to extract signatures and perform other analyses of the Landsat data. Computer plots of the field patterns were also drawn to scale to be overlayed on computer graymaps.

Each field was defined by a polygon described by its vertices. A feature of the ERIM multispectral processing programs is a capability to specify an inset distance from field boundaries to insure the selection of only field-center pixels, by eliminating those pixels close enough to the boundary to be mixture pixels. Typically, allowance was made for a complete-pixel guard row around the periphery of each field (i.e., an inset parameter of 1.5 pixels). This also would seem to be a reasonable criterion for the LACIE analyst-interpreters to follow.

A surprisingly small number of field-center pixels are present in a Landsat data set. Summary statistics were computed for field-center pixels selected in the Finney ITS (with the 1.5 pixel inset). Fig. 3 presents the average field size (in acres) for the given numbers of field-center pixels selected. The average size of fields containing <u>one</u> pure field-center pixel was over 30 acres and for <u>four</u> pixels (the LACIE minimum) fields of over 40 acres were required. These are large fields in comparison to the size of a Landsat pixel, which is approximately 1.1 acres. The average size of fields for which <u>no</u> field-center pixels were available was over 20 acres, and more than half the fields in the segment fell into this category. Fig. 4 presents a plot of the number of fields for which various numbers of field-center pixels were available. After a large peak of 240 fields with no pixels, to 23 fields

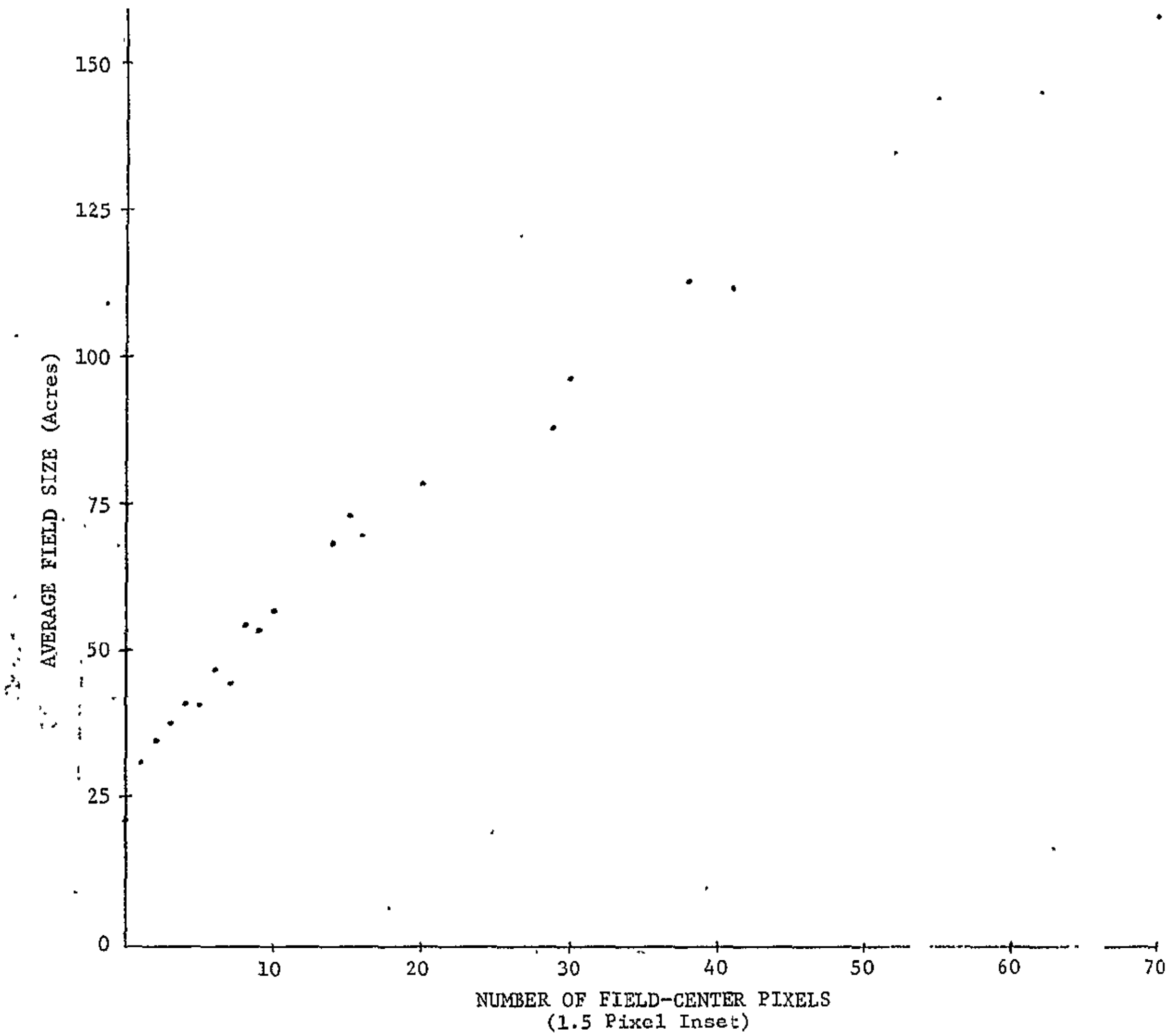

FIGURE 3. RELATIONSHIP BETWEEN AVERAGE FIELD SIZE AND NUMBER OF FIELD-CENTER PIXELS (FINNEY ITS)

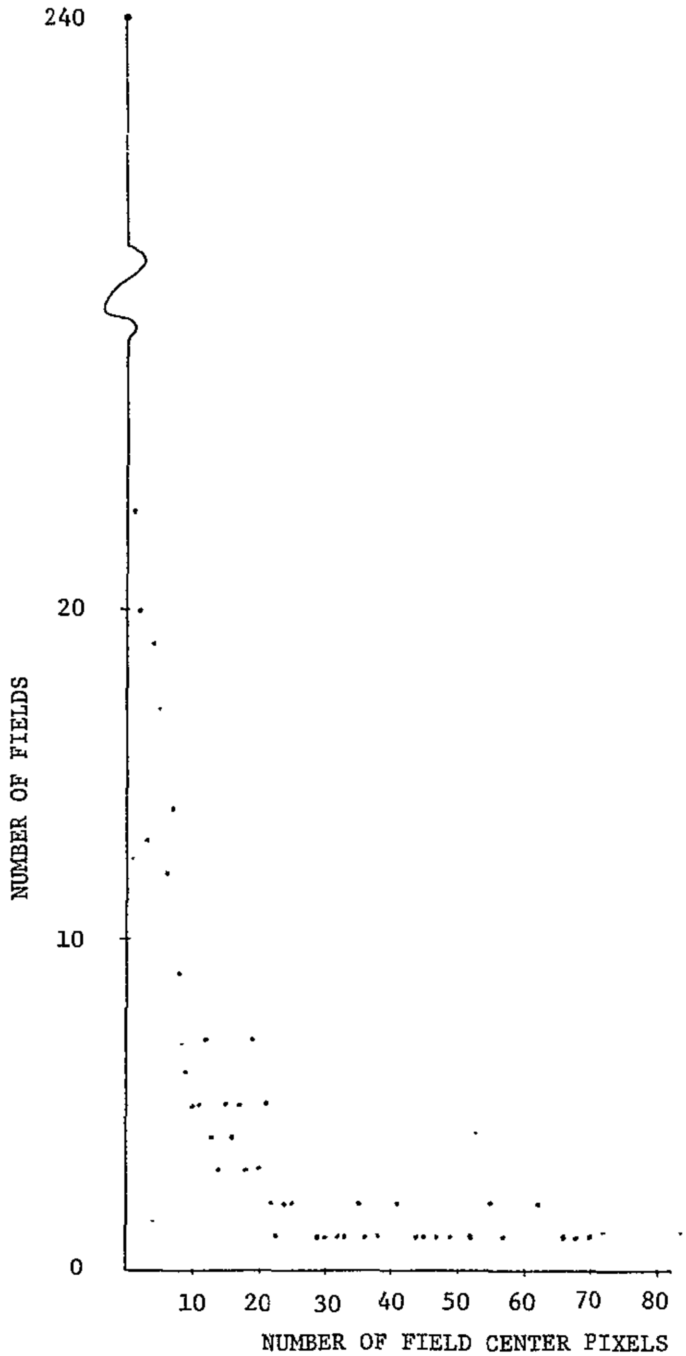

FIGURE 4. DISTRIBUTION OF FIELD-CENTER SIZES (IN PIXELS), FINNEY ITS, 26 MAY 74

with one pixel, the number of fields falls off almost exponentially to only one or two fields for pixel numbers greater than 20, with a maximum of 70 pixels (for one 160-acre field). Figs. 3 and 4 include both wheat and "other" fields.

For wheat specifically, Fig. 5 presents a cumulative distribution of field-center wheat pixels selected as a function of the number of pixels in a field, for the Finney ITS. From this graph it can be seen that 25% of the field-center wheat pixels are from fields yielding 45 or more pixels each, with 50% of pixels from fields with 22 or more pixels each, and 75% from fields with 12 or more field-center pixels. These results show an even greater concentration of wheat field-center pixels in the larger fields than was observed in the preceding graphs for wheat acreage. Fig. 5 also includes a curve giving the cumulative percent of wheat fields as a function of the number of field-center pixels selected in each.

3.3 DISCUSSION

A thorough examination of the agronomic data from the Kansas LACIE ITS's has shown a wide variation in the characteristics of wheat fields. This variation potentially could lead to spectral differences between fields and variability within fields which would be evident in their Landsat signals. In the next section, the extent of such ground-related spectral differences in Landsat data will be examined.

The major difference found among the sites was the 88% irrigation of wheat fields in the Finney ITS, compared with 24% in Morton, and 0% in the other three sites. Fertilizer usually was applied whenever there was irrigation. The percentages of the different wheat varieties planted were also found to differ from site to site and from CRD to CRD.

To summarize the observations regarding field-center pixels, we note that LACIE AI's, for the most part, will be selecting training data from among fields of 40 acres or more in size, with their requirement for a minimum of four field-center pixels per field. For the

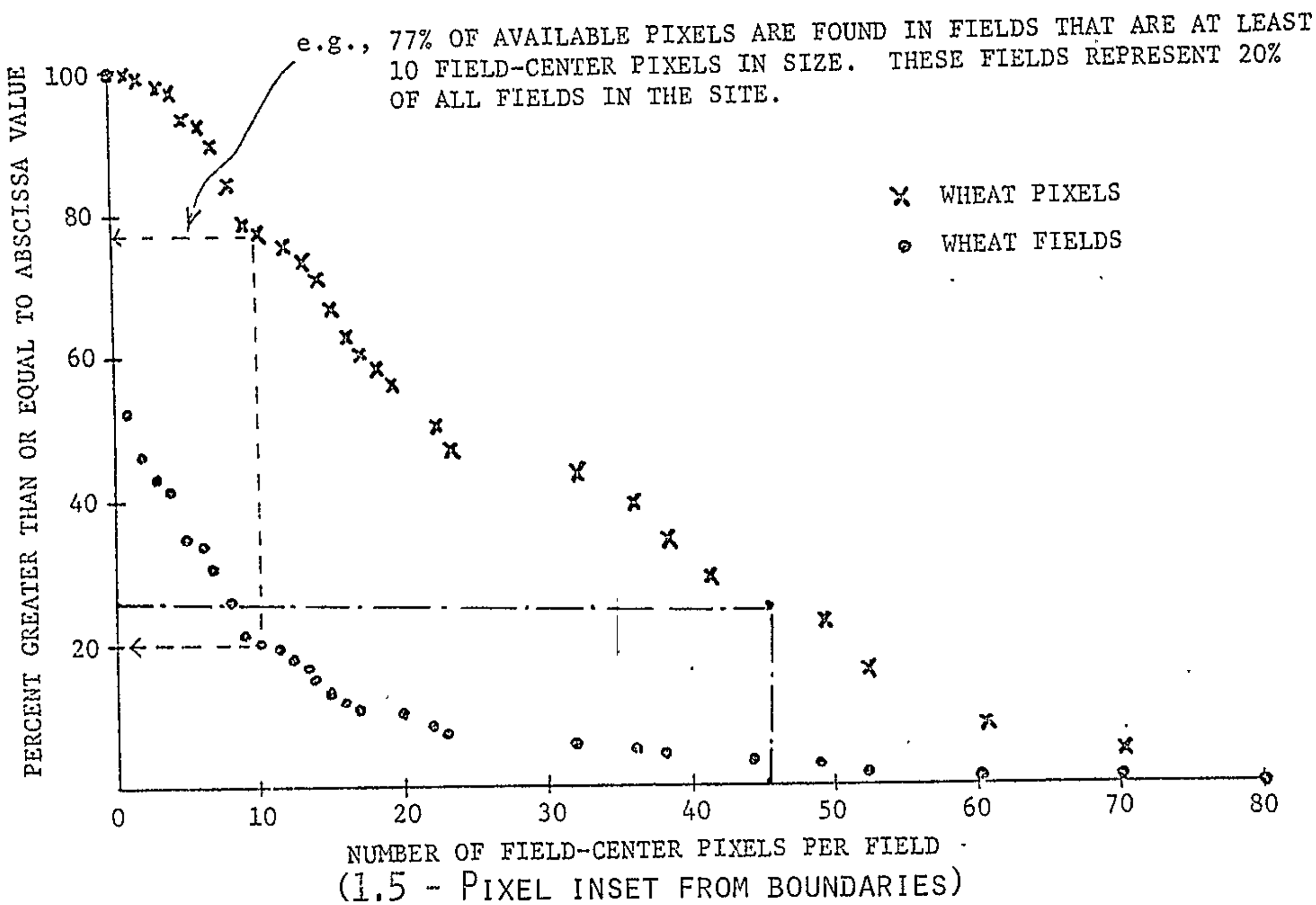

FIGURE 5. CUMULATIVE DISTRIBUTIONS OF FIELDS AND FIELD CENTER PIXELS
FINNEY INTENSIVE TEST SITE (1973-74)

Finney and Ellis ITS's, this corresponds to sampling from about 75% of the wheat acreage but only about 40% of the individual wheat fields; 77% of wheat field-center pixels (1.5-pixel inset) in the Finney ITS were in 20% of the total number of wheat fields. Also noted are the different average field sizes between the Finney and Ellis ITS's and the fact that the average size of wheat fields was greater than that of other fields.

The distributions of field sizes in the Finney and Ellis ITS's in Kansas are such that AI's should have no difficulty selecting a sufficient number of training fields and training pixels, although as noted above 60% of the individual wheat fields will not be sampled. The problem of finding sufficient training data could become severe in areas where average field sizes are smaller and/or field shapes tend to be long and narrow rather than more like squares. Planting patterns (i.e., field size and shape distributions) and field-center pixel availability in other areas of interest to LACIE should be examined.

4
LANDSAT SIGNAL STATISTICS AND THEIR RELATIONSHIP TO AGRONOMIC FACTORS

Having determined the major agronomic differences between winter wheat fields in the intensive test sites, attention was directed toward determining whether or not spectral manifestations of those or other differences existed in Landsat signals. First, signal statistics were extracted from each individual field of sufficient size in two Kansas intensive test sites and analyzed, as discussed in Sec. 4.1. Then, multispectral clustering procedures were applied, as described in Sec. 4.2. The results are discussed in Sec. 4.3.

4.1 ANALYSIS OF LANDSAT SIGNAL STATISTICS FROM INDIVIDUAL FIELD CENTERS

Signal statistics were extracted from Landsat data for every field for which field-center pixels could be identified. Such individual 'field signatures' were selected for the Finney 26 May 74 and Ellis 12 June 74 data sets.

A total of 57 wheat fields and 161 other fields were analyzed for the 5x6-mi Finney ITS. Ellipse plots were made for various pairs of Landsat bands for three groups of fields -- those with 1-4 pixels, those with 5-12 pixels, and those with 13 or more pixels. The plots of Channels 3 vs 2 (Landsat Bands 6 vs 5, i.e., 0.7-0.8 μm vs 0.6-0.7 μm) for wheat are presented in Fig. 6(a), (b), and (c). Each ellipse represents the contour for a χ^2 value of 1.0, i.e., approximately 40% of the pixels in the distribution would fall within the ellipse in the two-dimensional case. The major concentration of wheat for each set of pixel sizes is in the same spectral location on these graphs; however, some small and large fields have ellipses with larger Channel 3 values than the middle-sized fields.

In the Ellis ITS, which was smaller (only 3x3 mi), statistics were extracted for a total of 25 wheat fields and 32 other fields.

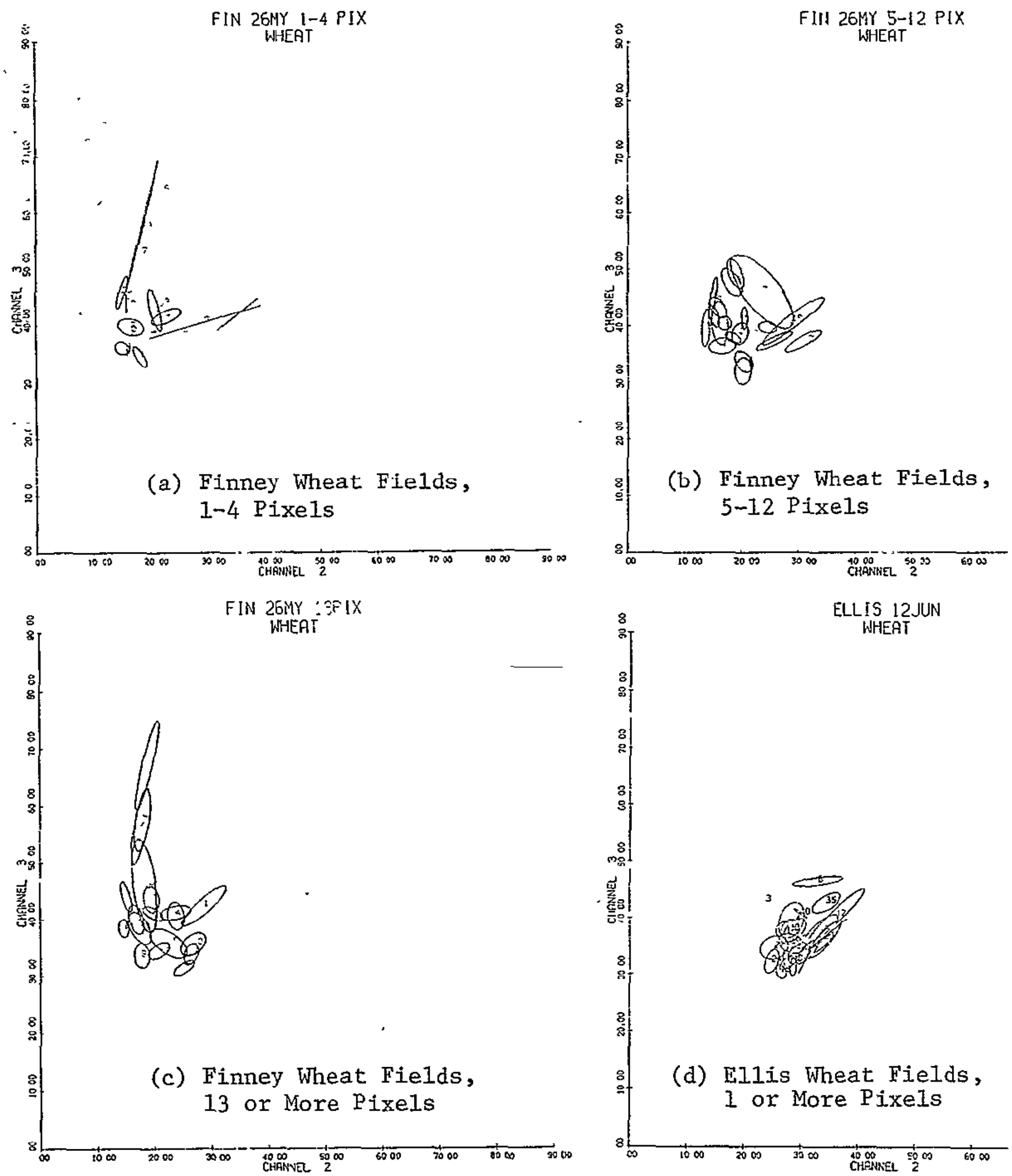

FIGURE 6. WHEAT FIELD SIGNATURE DISTRIBUTIONS AND INFLUENCE OF FIELD SIZE

These wheat signatures were more tightly bunched spectrally than the Finney fields and had a slightly different spectral location, as shown in Fig. 6(d).

Next, a computer analysis was performed on the statistics from the 38 wheat and 105 "other" fields in the Finney ITS which had five or more field-center pixels. To examine the spectral similarities and dissimilarities of these fields, a new signature-combination program, GROUP, was employed [7]. First, it was necessary to reduce the number of individual field signatures to a practical level, so the cluster-combining feature of the ERIM data clustering program [8] was applied to each major ground-truth class of fields. (This program computes the Mahalanobis distance between signatures as the combining criterion.) A total of 34 individual or combined field signatures (11 wheat and 23 other) were developed to input to program GROUP. Program GROUP successively combines the pair of remaining signatures which best satisfies a user-specified weighting of rankings according to five criteria: (1) resultant combined determinant, (2) resultant combined trace, (3) the between-signature Bhattacharyya distance, (4) between-signature probability of misclassification, and (5) resultant average pairwise probability of misclassification between the classes wheat and other. For the results presented here, the weightings applied were 1, 1, 1, 0, and 3, respectively, for the five criteria, giving greatest weight to the probability of misclassification between wheat and other.

Fig. 7(a) displays ellipse plots of the 34 Finney combined signatures which were the input groups to program GROUP; the plots again are for Channels 3 vs 2. Ellis signature groups are shown in Fig. 7(b). From the spectral standpoint, the Finney wheat groups exhibit substantial variety while, for the most part, being distinct from the other signatures. Therefore, further analysis was performed to see if these groups could be characterized according to agricultural characteristics of the fields which made them up.

The makeup of the 11 Finney wheat groups is summarized in Table 6.

(a) Finney ITS, 26 May 74

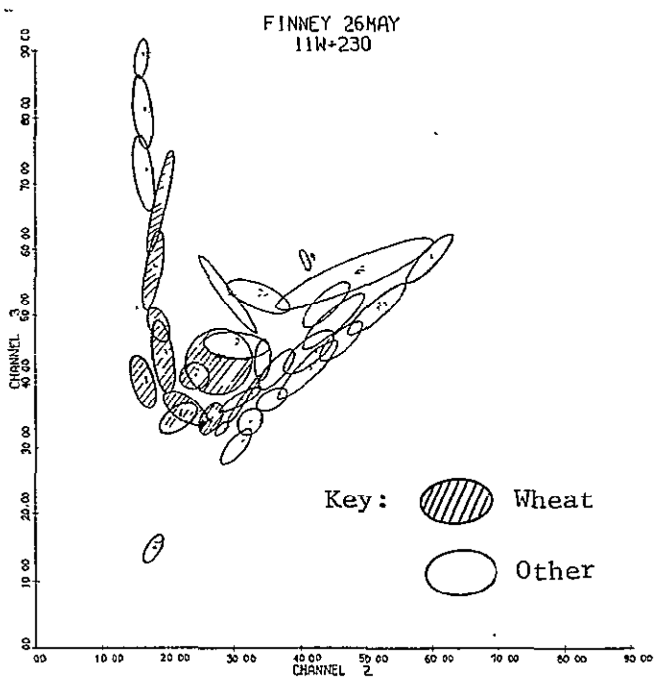

(b) Ellis ITS, 12 Jun 74

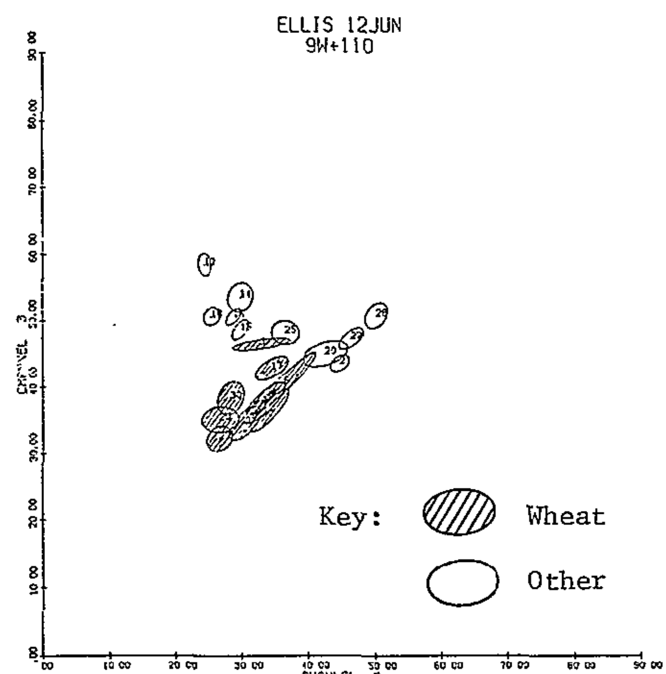

FIGURE 7. INTERMEDIATE SPECTRAL GROUPINGS OF INDIVIDUAL FIELD SIGNATURES

TABLE 6. CHARACTERISTICS OF WHEAT SIGNATURE GROUPS, FINNEY 26 MAY

WHEAT GROUP NUMBER	NO. OF PIXELS	NO. OF FIELDS	NO. FIELDS, BY VARIETY 402	404	407	408	409	424	400	IRRIGATED	FERTILIZED
1	186	13	1		12					13/13	9/13
2	53	3	2					1		3/3	3/3
3	113	5	1		2		1	1		5/5	5/5
4	43	4			4					4/4	4/4
5	8	1	1							0/1	0/1
6	11	2			1			1		2/2	2/2
7	31	3	1		1				1	3/3	2/3
8	31	2					1	1		2/2	1/2
9	15	1					1			1/1	1/1
10	122	3	2		1					0/3	0/3
11	52	1	1							1/1	0/1

Three of these groups contain only one field, while the largest (Group 1) contains 13. It is interesting to note that the non-irrigated fields are all in Groups 5 or 10. When program GROUP was used to successively combine wheat groups until just one average group remained, Groups 5 and 10 were paired before they were combined with any others. The full combination tree for the 11 wheat groups is presented in Fig. 8.

Spectrally, it can be seen in Fig. 9 that Groups 5 and 10 have among the highest Channel 2 (0.6 - 0.7 μm) signals of the wheats and among the lowest Channel 3 (0.7 - 0.8 μm) signals. This would indicate advanced growth stage, dryness, and/or more exposed soil, all compatible with a non-irrigated condition.

At the other extreme are Groups 8 and 9 which spectrally appear to be immature and still green, 9 more so than 8. In fact, their signals in the "green" channel, Channel 1 (0.5 - 0.6 μm), were found to be relatively greater than for the other wheats. Group 6 appears to be a little less green and more senescent than Groups 8 and 9, with Group 3 closer matching the remaining groups.

There is an indication of correlation between immaturity or greenness and variety, although one cannot be completely definite from this example. That is, two of the three fields in Groups 8 and 9 are Variety 409 (Bison) and the other field of this variety is in Group 3. The third field in Groups 8 and 9 is Variety 424 (Eagle (Scout)) and two of the other three fields of this variety were found in Groups 6 and 3. It also is of interest to see that 16 of the 20 fields of the most common variety (407, Satanta) are found in Groups 1 and 4, along with only one field of another variety. The fields of Variety 402 (Scout) tend to be lighter in both Bands 2 and 3, compared to Variety 407 (Satanta).

Another factor which should be considered in this analysis of wheat spectral characteristics and agronomic factors is the spatial distribution of the features and characteristics. Fig. 10 presents

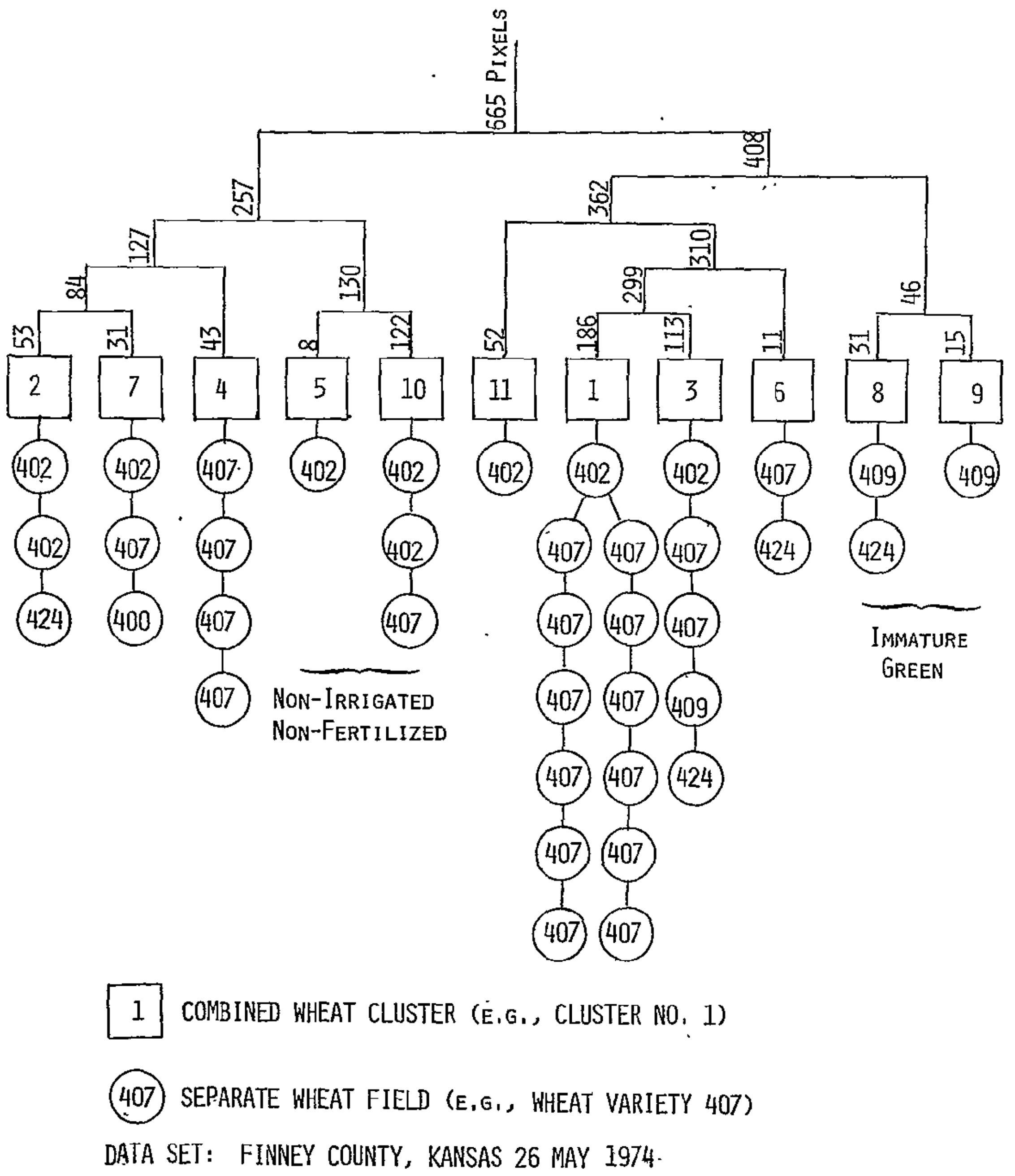

FIGURE 8. WHEAT FIELD SPECTRAL COMBINATION TREE WITH ASSOCIATED AGRICULTURAL CHARACTERISTICS; FINNEY ITS, 26 MAY 74

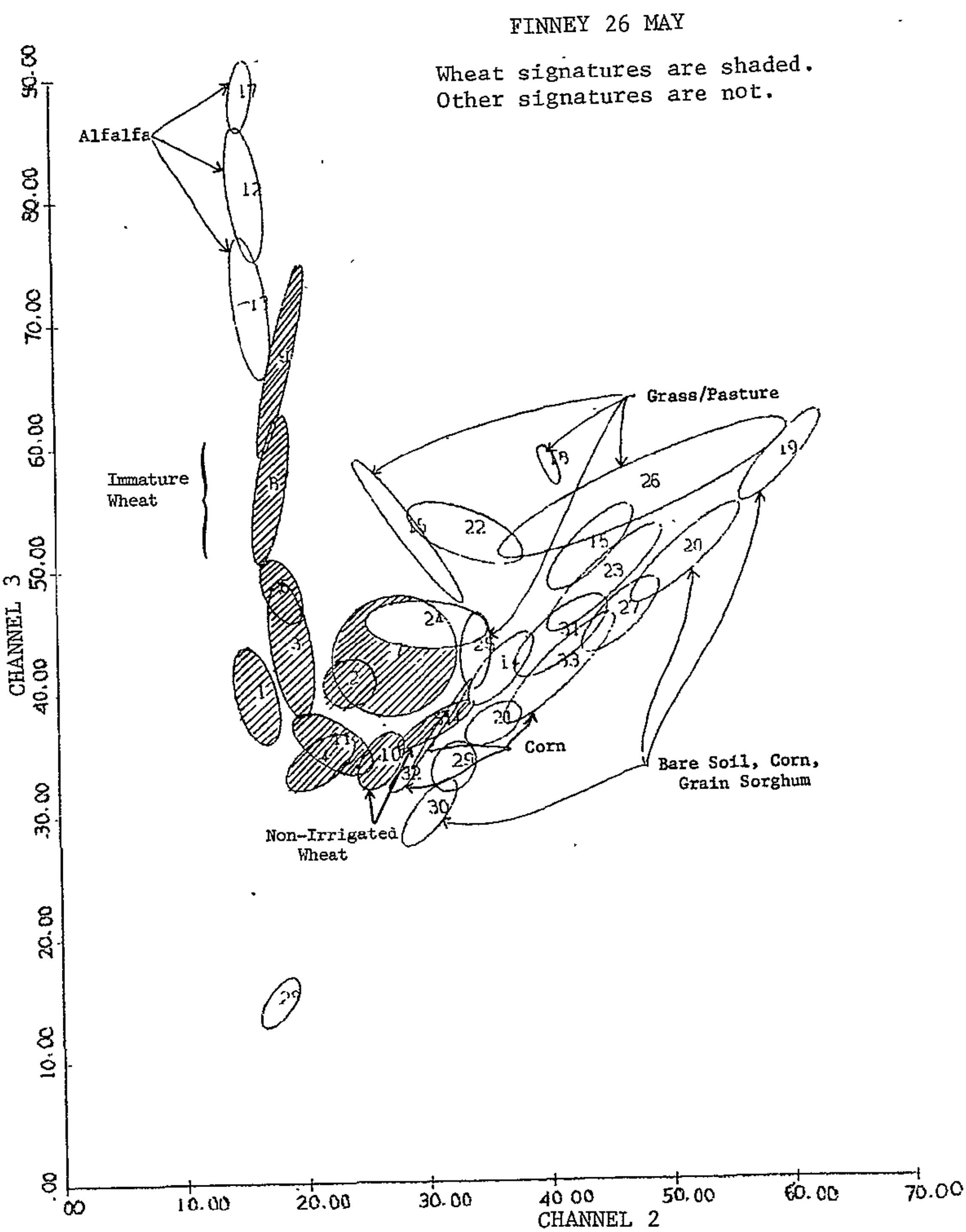

FIGURE 9. SPECTRAL GROUPINGS OF WHEAT AND OTHER SIGNATURES

(a) Distribution of Spectral Groups

Group(s)	Description
1	Major Group, Primarily Satanta
9,8,6,3	Groups Listed in Order of Greenness
5,10	Non-Irrigated, Non-Fertilized

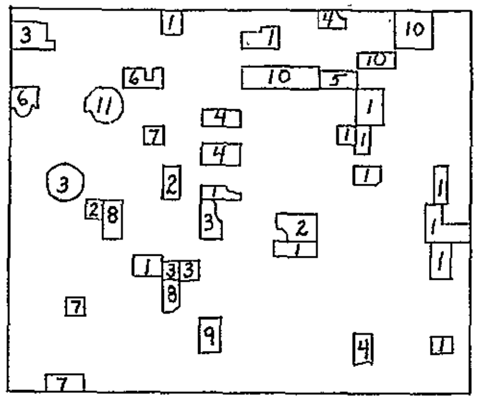

(b) Distribution of Wheat Varieties

Key: Symbol	Variety
2	402 Scout
7	407 Satanta
9	409 Bison
24	424 Eagle 'Scout'
0	400 Unknown

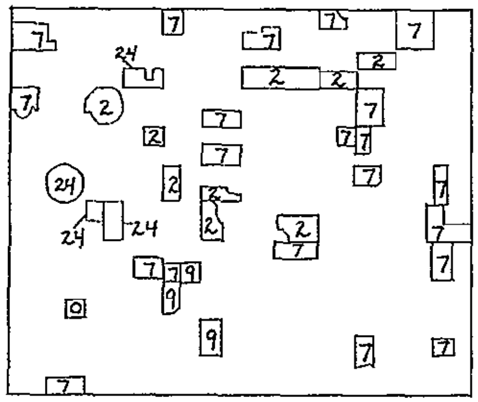

(c) Distribution of Irrigation and Fertilization Practices

Key:
- Non-Fertilized
- Non-Fertilized and Non-Irrigated
- Fertilized and Irrigated

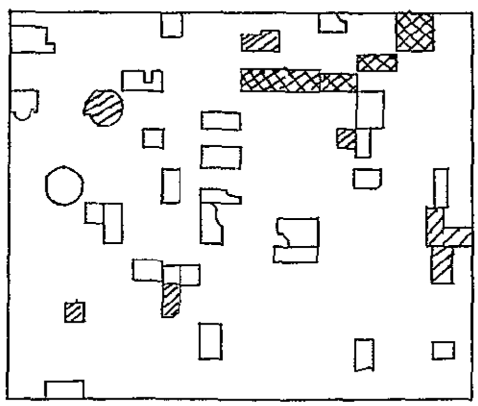

FIGURE 10. SPATIAL DISTRIBUTION OF SPECTRAL GROUPS AND AGRONOMIC FACTORS, FINNEY ITS. Wheat fields containing field-center pixels (1.5 inset)

maps of the wheat fields analyzed in the Finney ITS. Part (a) indicates the spectral group to which each field was assigned, while Part (b) indicates the wheat variety for each field, and Part (c) the irrigation and fertilization practices. Some patterns are evident. The non-irrigated fields found in spectral Groups 5 and 10 are in the upper righthand corner. The greener fields of spectral Groups 8 and 9 are just to the left and below the site center and the fields of the other green-tending groups (3 and 6) extend from there up to the upper lefthand corner. It is along this swath and the non-irrigated fields in the upper right where varieties other than the most common 407 (Satanta) are planted (See Fig. 10(b)). There was no clear association of these planting patterns with soil maps for the area.

The spectral pattern found for wheat in the Ellis ITS differs from that just discussed for the Finney ITS, referring again to Fig. 6. There are at least two possible explanations for these differences. One reason is the 18-day interval between acquisition dates, allowing the Ellis wheat fields additional time to senesce or ripen. Second, the Ellis fields were not irrigated and were predominantly of the Scout variety which exhibited different spectral characteristics than the majority of the Finney fields which were irrigated and of the Satanta variety. In this regard, the fields of Ellis are more typical of those in the State of Kansas than are the fields of Finney. Affecting the overall patterns in the two sites are the atmospheric conditions at the times of acquisition which could have been different.

A major observation that can be made regarding the preceding analysis of wheat signatures is that, in general, the variability of Landsat signals is greater between fields than within fields. Two main sources of this between-field variability were determined for the data sets analyzed in the Finney ITS. First, irrigation, or the lack of it, was definitely correlated with the observed spectral responses. Second, spectral differences could be associated with wheat variety on the site. Variety 409 (Bison) was greenest, 407 (Satanta) was darkest, and 402 (Scout) was lighter than 407. These observations were checked against the experience and knowledge of USDA personnel at the USDA Agricultural Experiment Station near Garden City, Kansas, and were found to be consistent. The Bison variety is the slowest to mature of the varieties planted in the area, Satanta has a dense canopy with dark leaf color, and Scout tends to be lighter with spotted or streaky leaf coloration. Both the planting density and the actual density of wheat on irrigated fields is greater than that on non-irrigated fields. For example, row spacing tends to be greater on the non-irrigated fields.

Further analyses are needed to better identify and establish more quantitative relationships between agricultural and spectral characteristics of wheat fields. Once field measurement data become available, they should form a major source for such analyses. The modeling capability and results described in Sec. 6 can provide a complementary analysis data base and an analysis tool.

4.2 MULTISPECTRAL DATA CLUSTERING ANALYSES

In the preceding section, the signal statistics analyzed were generated using pixels from spatially distinctive groups, i.e., from the centers of individual fields. Another mode of spectral data analysis, called clustering, associates pixels according to their spectral similarity and generates signal statistics or signatures from the members of the resultant clusters. Two different modes of clustering procedures that were used are (a) supervised clustering, in which the true class of each pixel is known and labels are assigned and used in the calculations, i.e., each cluster can contain pixels of only one labeled class, and (b) unsupervised clustering, in which no prior information regarding the true class is used.

Supervised clustering of the field-center pixels in the Finney 26 May 74 data set was performed to provide results that could be directly compared with the individual-field results of Sec. 4.1. Next, unsupervised clustering was performed on those pixels which included field boundaries, i.e., those which contained mixtures of two or more ground covers. Finally, unsupervised clustering was performed on all pixels in the segment.

In addition to providing additional insight into the spectral character and variability of Landsat data from the Finney ITS, the results of these clustering procedures were used in the analysis discussed in Sec. 5 of the influence of the quantity of training data on recognition performance.

The clustering algorithm employed [8] forms an estimate of the spectral distributions in the scene by using multivariate normal distributions with diagonal variance-covariance matrices as basis elements. Pixel assignments are made using a quadratic decision rule, allowing for different variances in the different channels. A new cluster is formed when the current pixel is not within a threshold distance from one of the previously formed clusters.

In order to efficiently carry out the separate clusterings of field-center and boundary pixels, a feature was added to the basic clustering program to enable it to readily distinguish between various groups of pixels. In essence, it was the capability to extract and use, for control, information contained in channels added to the normal data channels. For the analyses here, three additional channels were created using field polygon cards describing the vertices of each field in the site; they were: (1) a fifth channel containing the field number from the ground truth forms, (2) a sixth channel containing the ground truth crop code, and (3) a seventh channel giving the distance, in pixel units, of each pixel center from the nearest boundary of the field within which it was located.

This use of additional channels is an extension of their development and previous uses which, at ERIM, began with the creation of new data features which were linear combinations of the original data channels [9]. The introduction of polygonal field coordinate descriptors and boundary inset parameters was done to facilitate analyses of Landsat data and the accurate identification of field-center pixels for training and evaluation of recognition performance [5]; procedures employing them were used extensively in the CITARS project [6] and have since been refined. These and the feature described in the preceding paragraph have recently been incorporated as an integral part of the ERIM PROtotype Classification And Mensuration System (PROCAMS) [10] and used by other tasks of this contract [7,12].

The three specific spectral cluster analyses carried out on the Finney 26 May 74 data set were as follows:

(1) All pixels inset by 1.5 or more pixel units, as designated in Channel 7, were defined to be single-class field-center pixels and were clustered in a supervised fashion. Using the crop code information in Channel 6 as labels, wheat pixels were clustered only with other wheat pixels and all 'other' crop pixels were clustered among themselves. Fig. 11(c) displays ellipse plots for Landsat Channels 3 vs. 2 for the resultant 47 clusters.

(2) All pixels within 0.5 or less pixel units from the nearest boundary were included in the set of multiclass boundary pixels clustered in an unsupervised fashion. The resultant clusters are displayed in Fig. 11(b).

(3) All pixels within the 5x6-mi Finney ITS were also clustered in an unsupervised fashion, with results as shown in Fig. 11(a).

Several interesting points can be observed in these cluster plots. The clusters formed from the whole area quite completely fill a triangular region of spectral space in Fig. 11(a). However, the field-center clusters form more of a "V" shaped pattern in which both ground truth information here and past experience have shown that bare soil

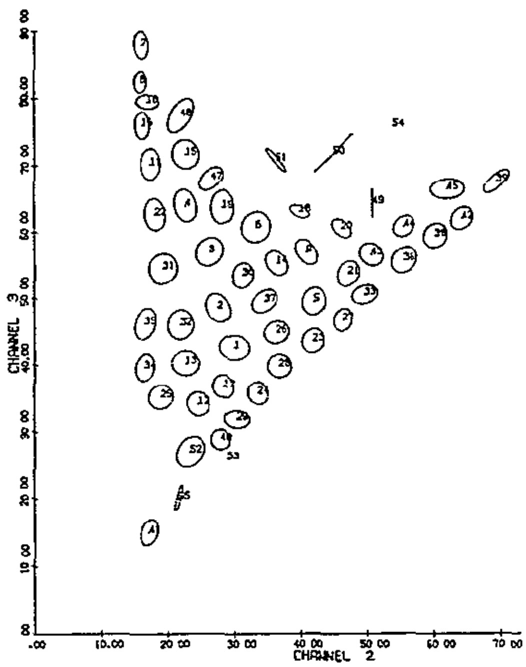

(a) Finney Whole Area Clusters

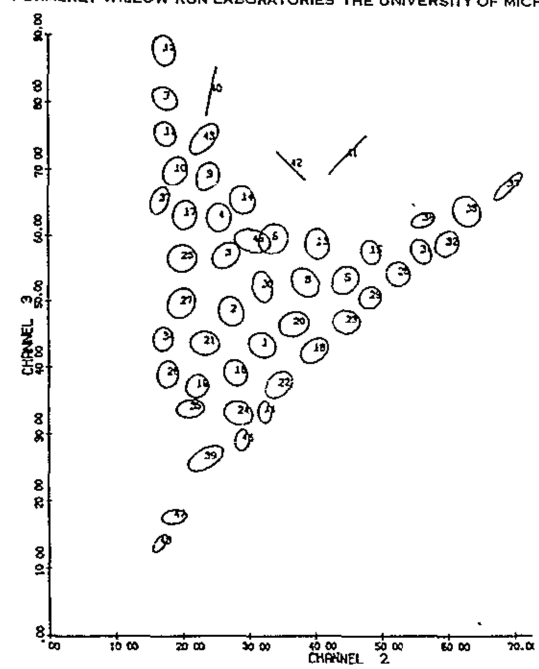

(b) Finney Boundary Clusters
(≤ 0.5 Pixel from Boundaries)

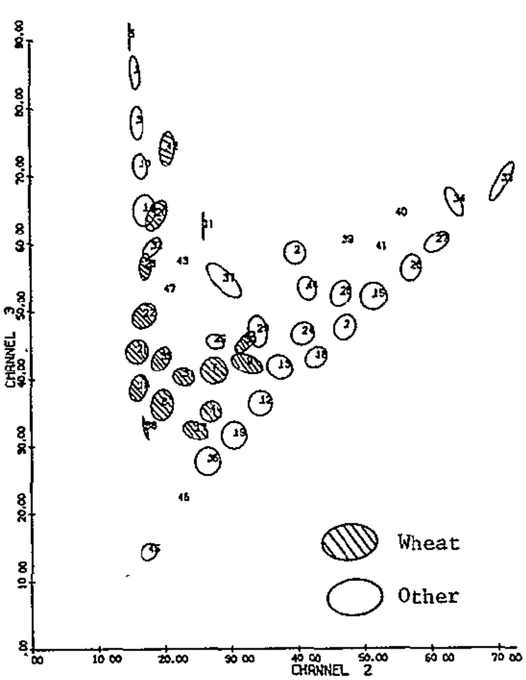

(c) Finney Field-Center Clusters
(1.5-Pixel Inset)

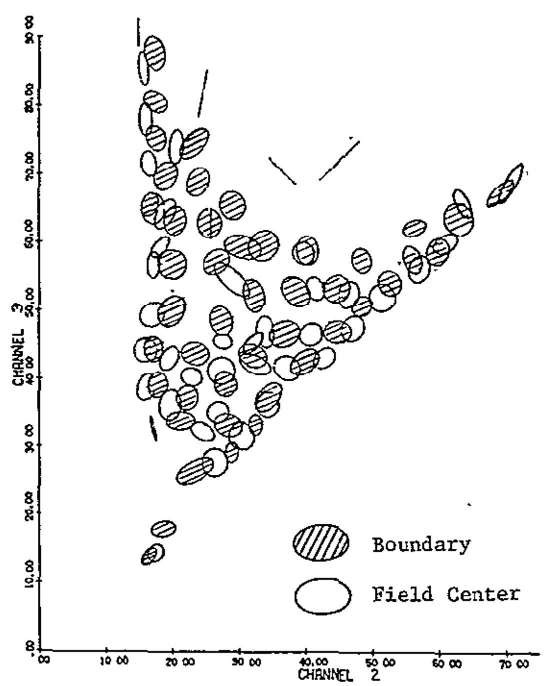

(d) Comparison of Field-Center and Boundary Clusters

FIGURE 11. COMPARISON OF DATA CLUSTERING RESULTS FOR THE FINNEY KANSAS ITS, 26 MAY 74

fields tend to lie along the righthand arm of the "V", water and other "dark" scene elements at its apex, and healthy green vegetation at the top of the lefthand arm. From Fig. 11(b), it can be seen that the upper center portion of the "V" is filled primarily by clusters of the boundary pixels. For example, signals representing mixtures of a healthy green crop (such as alfalfa) and bare soil would fall in this region.

Finer distinctions can be drawn between the field-center and boundary pixel clusters when their cluster plots are overlaid. Fig. 11(d) displays the field-center clusters as open ellipses and the boundary clusters as shaded ellipses. Note how the boundary pixel clusters tend to fall in the spectral space between field-center clusters.

4.3 DISCUSSION

Upon comparing the field-center clusters of Fig. 11(c) with the individual field signatures of Fig. 6 and Fig. 7 (the latter of which includes some combining of field signatures), the earlier conclusion that between-field spectral differences for wheat generally are greater than within-field differences is confirmed for the Finney 26 May 74 data. Obviously when there is just one other class, between-field differences predominate in that class as well.

An important result of the separate clusterings of field-center and boundary pixels was the verification of different spectral patterns in the two cases. First, spectral features were found among the boundary pixels which did not exist within the field-centers. Second, the spectral locations of the boundary pixel clusters usually were between the field-center clusters.

5
INFLUENCE OF TRAINING DATA AMOUNT ON RECOGNITION PERFORMANCE

Multispectral signatures used in recognition processing are intended to describe, in an adequate statistical fashion, the characteristics of remote sensor signals from the particular scene classes they represent. More than one signature may be needed for an individual class, and signatures for all classes which may become confused with the classes of interest should be included in the set used for processing. The usual assumption made is that the signal distributions for classes or subclasses are sufficiently described by multivariate normal (Gaussian) distributions. One of the major problems faced in the training process is that of determining how many fields should be selected for use in training to establish the signatures. This problem cannot readily be addressed separately from considerations of both the spectral characteristics of the relevant scene classes and the amount of information available and procedures used to select the training fields.

If the scene classes are relatively homogeneous within and between fields, the sampling approach can be much simpler and require fewer samples to adequately describe the signature means and dispersion volumes than for a scene with non-homogeneous classes. The preceding sections have shown that wheat fields had widely differing spectral characteristics in the Finney ITS on 26 May 74, due to differing varieties, maturation stages, and irrigation practices. These variations would not be satisfactorily represented by a single signature for wheat, necessitating sub-class signatures to describe the various modes.

The procedure by which training fields are identified also enters in. If, for example, one were to ask a ground observer to select fields at random for identification, the number of fields required to obtain representatives of all modes would be much larger than if the observer were asked to obtain a certain number from each combination of the key factors affecting spectral response, such as irrigation practice and variety. In LACIE, there are no ground observers to provide identification information, except for development and evaluation purposes. Thus, the manner in which AI's (Analyst-Interpreters) operate must be considered. Since AI's use Landsat imagery which has inherent spectral characteristics they can and do make use of these characteristics in selecting training fields.

5.1 APPROACH

The previously described analyses of wheat populations in the Finney, Kansas, ITS were made largely in support of the analysis, reported in this section, of the effects of varied sample size on recognition performance.

Two sampling parameters are of concern in LACIE: (1) the number of fields chosen for training and (2) the total number of pixels chosen. Our best information as to the LACIE AI procedures and constraints current at the time this analysis was started was used as a guide in devising and implementing the analysis. AI selection of the eight or ten most different spectral classes in a scene was simulated through the spectral cluster analysis and subsequent grouping of spectrally similar clusters to reduce the number of spectral classes to four wheat and four "other". Each field in the site was assigned to one of these eight groups, by majority vote of a "baseline" classification of its pixels.

Training fields then were selected from within each group by random draws made with probability of selection proportional to field size. Three different data selection rules, resulting in different quantities of training data (i.e., different numbers of fields and/or pixels), were specified and used. Three different draws were made using each rule. The individual signatures previously extracted for the selected fields in each group were combined with equal weights to form signatures for use in recognition.

Nine separate recognition runs were made using the resultant signature sets. Recognition performance was evaluated with regard to the accuracy of both classification of field-center pixels and the estimated proportion of wheat in the site. The nine sets of results were compared to one another and to the baseline result. The baseline result was obtained by using all available (at a 1.5-pixel inset) data for training and establishing a less constraining number of recognition signatures (seven wheat and ten other).

5.2 SIMULATION OF VARIOUS AI TRAINING DATA SELECTION RULES

In choosing representative training statistics for LACIE segments, the AI has at his or her disposal multitemporal false color imagery of the test site of interest. The number of distinguishable classes present is determined first, simply by identifying and distinguishing colors that are visible to the eye. Then each color class is photo-interpreted to be 'wheat' or 'other'. From each class, then, enough fields are delineated to meet minimum requirements on the number of fields and/or number of pixels. The minimum requirements for 'wheat' color classes are more stringent than for 'other' color classes.

The data clustering and cluster combination procedures previously described in Sec. 4 were used as a substitute for the AI's determination of spectral classes. Initially, the 47 clusters shown in Fig. 12(a) were generated, far more than the number of color classes that could be distinguished by an AI. These 47 were reduced to the intermediate eleven wheat and 23 other clusters shown in Fig. 12(b), by clustering as previously discussed. A further reduction in their number was made by grouping clusters until the four wheat signatures shown in Fig. 12(c) resulted, and the remaining other signatures were reduced to the four others shown in Fig. 12(c).

Each field of five or more pixels was then assigned to one of the eight spectral groups, to enable subsequent simulation of random selections of training data within the 'distinguishable color classes'.

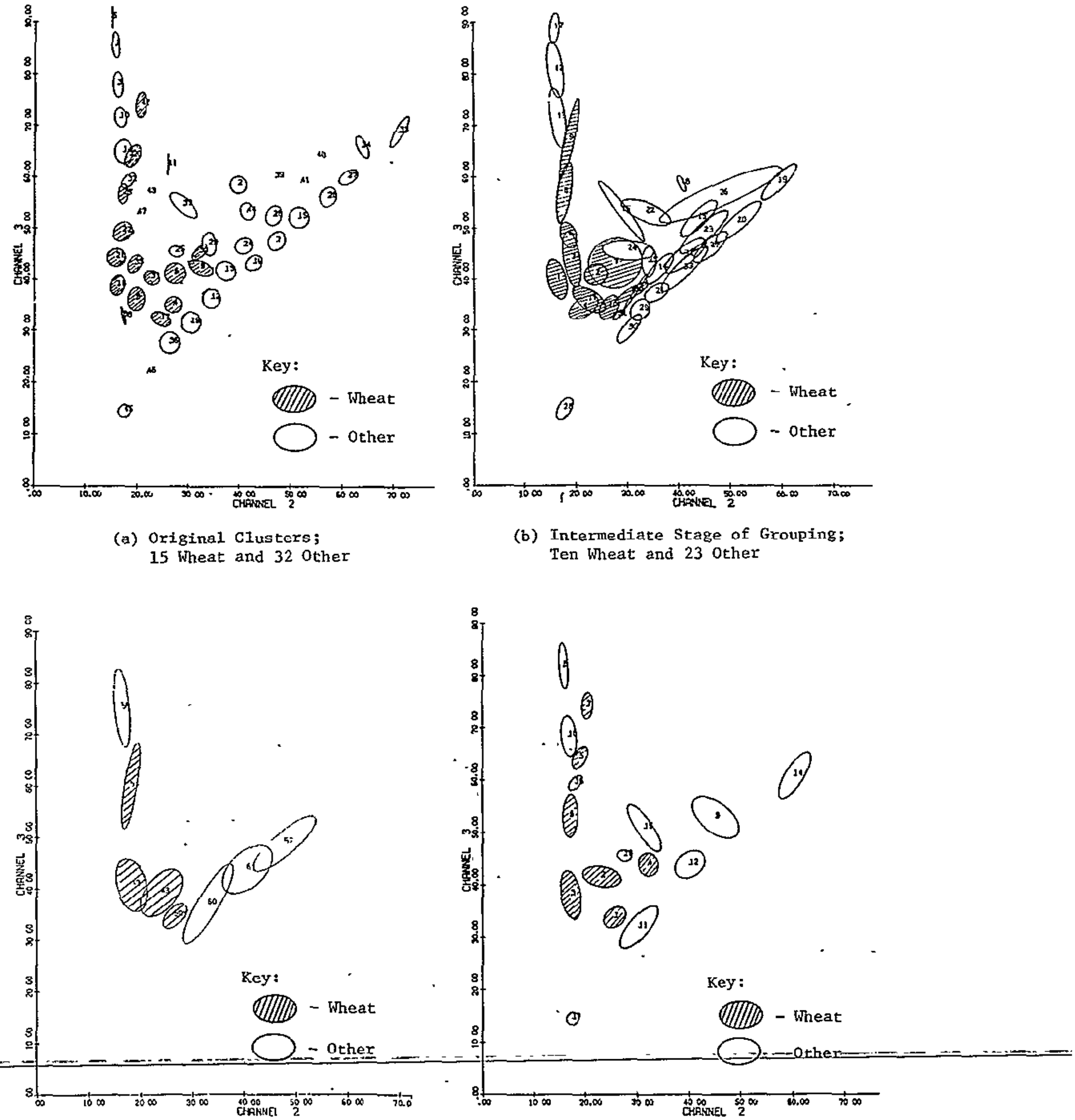

(a) Original Clusters;
15 Wheat and 32 Other

(b) Intermediate Stage of Grouping;
Ten Wheat and 23 Other

(c) Final Eight Spectral Groups Used;
Four Wheat and Four Other

(d) Baseline Signature Set;
Seven Wheat and Ten Other

FIGURE 12. ILLUSTRATION OF FIELD-CENTER SPECTRAL GROUPS AND SIGNATURE SETS, FINNEY, KANSAS, ITS, 26 MAY 74

This assignment was accomplished simply according to how the individual pixels within the given field were classified in a baseline classification run made using 17 signatures (See Fig. 12(d)). Each of the 17 signatures was associated with one of the eight spectral classes, and the predominant class recognized within a field determined the class label assigned to it.

Training fields for each of the eight classes were chosen by a random sampling procedure with probability proportional to field size (i.e., number of field-center pixels). This sampling procedure reflects our expectation that the AI would be more likely to select the larger fields because they would be easier to locate and identify and would contribute a greater number of training pixels to the total requirement.

Three sampling rules were specified with resultant sample size as the parameter being varied. The three rules generated small, medium (the one most similar to the AI implemented requirements), and large sample sizes. The three rules incorporated the following minimum requirements in field and pixel selection:

Rule A. Small Number: One field per subclass, with extra field(s) chosen if required to obtain a minimum of 80 pixels for wheat, 120 pixels for other, and at least five pixels per subclass.

Rule B. Medium Number (Most LACIE-Like): Enough fields for 160 wheat and 240 other pixels, with at least five pixels per subclass.

Rule C. Large Number: Enough fields for 320 wheat and 480 other pixels., again with at least five pixels per subclass.

Three draws of training fields for each rule were made with probability of selection proportional to field size. Table 7 summarizes the selection results. Typically, the percentage of total wheat pixels (and fields) chosen for training was higher than the percentage of other pixels (and fields) chosen, usually more than 2:1 in favor of wheat. Hence, the wheat crop tended to be more fully described than the other crops.

TABLE 7. SUMMARY OF SELECTION RESULTS

		WHEAT				OTHER			
		NO. OF PIXELS	PERCENT OF TOTAL WHEAT PIXELS	NO. OF FIELDS	PERCENT OF TOTAL WHEAT FIELDS	NO. OF PIXELS	PERCENT OF TOTAL OTHER PIXELS	NO. OF FIELDS	PERCENT OF TOTAL OTHER FIELDS
RULE A, SMALL:	DRAW 1	80	11.8	4	7.3	180	9.2	6	3.7
	DRAW 2	83	12.2	4	7.3	192	9.8	6	3.7
	DRAW 3	93	13.7	4	7.3	125	6.4	6	3.7
RULE B, MEDIUM:	DRAW 1	174	25.6	9	16.4	256	13.0	8	4.9
	DRAW 2	202	29.7	6	10.9	251	12.8	8	4.9
	DRAW 3	185	27.2	6	10.9	286	14.5	8	4.9
RULE C, LARGE:	DRAW 1	321	47.2	14	25.5	493	25.1	20	12.3
	DRAW 2	337	49.6	21	38.2	497	25.3	23	14.1
	DRAW 3	343	50.4	12	21.8	505	25.7	20	12.3
ALL FIELD CENTERS:		680	100.0	55	100.0	1967	100.0	163	100.0

Once training fields were selected, a combined signature was made for each subclass selection of fields, with equal weights being given to the training fields. These eight signatures were then used for recognition. The results from nine recognition runs, one for each of three draws of the three rules, were compared and analyzed. The analysis centered on examinations of (1) field-center classification accuracy and (2) whole area proportion estimation. Before describing the results of these runs, the recognition signature patterns will be examined.

5.3 EXAMINATION OF THE SELECTED SIGNATURE SETS

One would expect that the variability between corresponding signatures of the three draws within a rule would diminish as the sample size became larger. Fig. 13 illustrates that this was found to be the case; signatures from two draws are displayed for each of the three selection rules, again with Channel 3 plotted versus Channel 2.

Another observation that can be made is that the wheat signatures become more robust as the sample size increases. The wheat signatures in Fig. 13(f) compare well with the wheat signatures in Fig. 12, and Fig. 13(e) is quite similar. The wheat signal space is more fully represented here than in the other cases with smaller sample sizes.

Comparing draws within each rule, one finds that in Rule A (compare Figs. 13(a) and 13(b)) both means and variances for a given spectral class differ dramatically from draw to draw. The conclusion drawn is that the sample size of Rule A was insufficient to accurately estimate the mean and variance-covariance characteristics of each class. The signatures displayed for Rule B (compare Figs. 13(c) and 13(d)) indicate that both means and variances for corresponding signatures also differ from one another, but to a lesser degree than those of Rule A. Finally, the ellipses drawn using Rule C and pictured in Figs. 13(e) and 13(f) appear to estimate mean and variances of their corresponding classes with greater consistency than do those of the

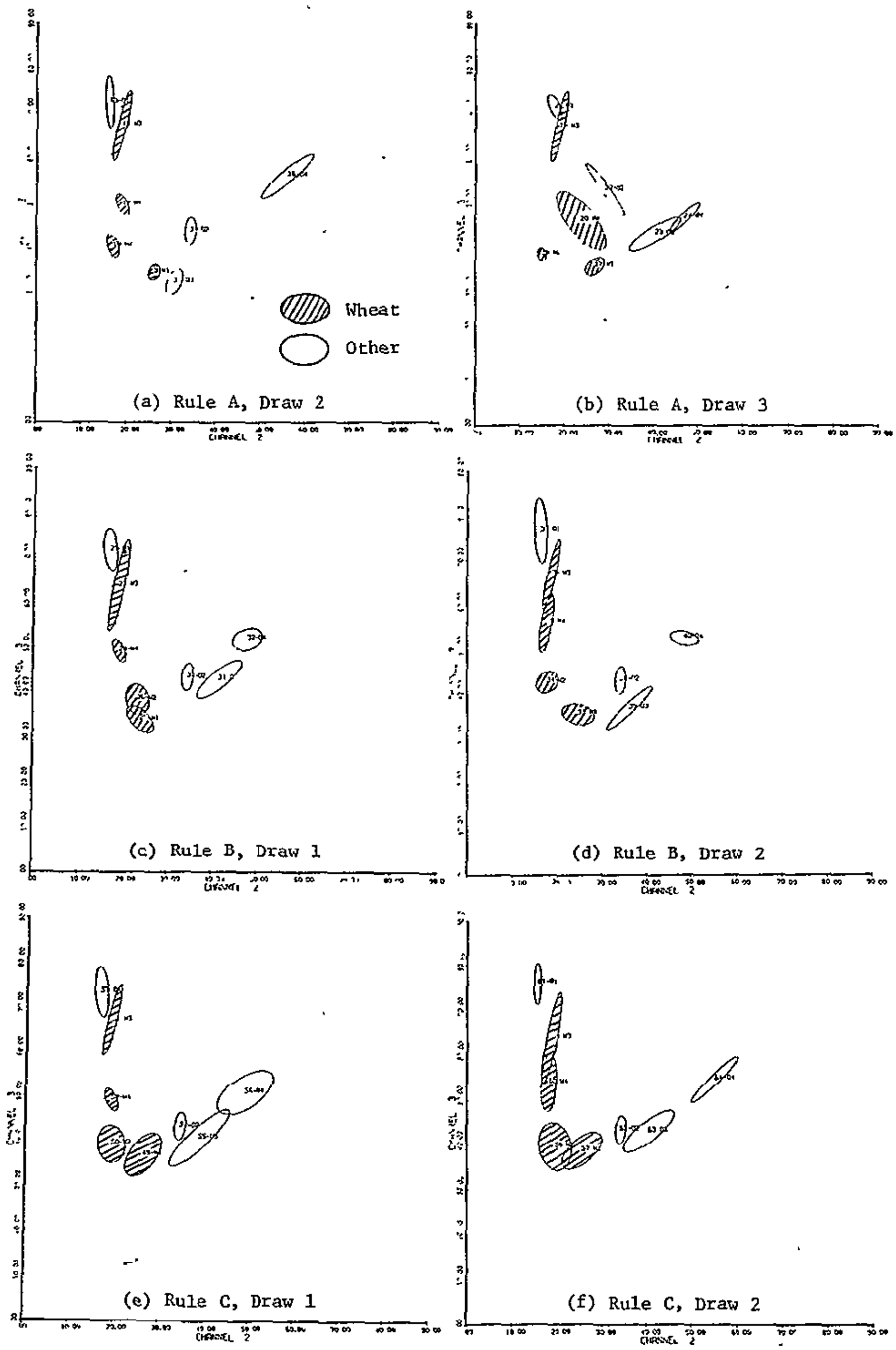

FIGURE 13. INFLUENCE OF TRAINING SAMPLE SIZE ON SIGNATURE PATTERNS

other selection rules. One would expect these facts to be reflected in the recognition results, i.e., results corresponding to Rule A should vary more between draws than those generated from Rule B and, likewise, those from Rule C should be even less variable.

This between-rule analysis suggests already that the Rule A selection criterion is inadequate. Two additional observations can be made. First of all, the boundary clusters described earlier (Sec. 4.2) that fill the center portion of the 'V' pattern in the signal space are not usually described by these signatures. This is natural since field-center spectral classes were not found in that vicinity. A related observation is that four subclasses for 'other' are probably too few to adequately describe the spectral characteristics of 'other' to the same degree of accuracy that the four wheat subclasses describe wheat signal distributions.

5.4 RECOGNITION RESULTS

Recognition runs were made using the ERIM linear decision rule [11] with a decision threshold corresponding to a 0.001 probability of false rejection (for normal distributions). Classification results are presented in Table 8 for field-center pixels defined by three different insets from the field boundaries. Both individual results for each draw and average results for each rule are included. The corresponding wheat proportion estimates for the entire site are presented in Table 9.

The field-center results indicate a sharp increase in the correct classification accuracy for wheat pixels when increased amounts of training data were used. With the 1.5-pixel inset, for example, the correct percentage increased from 74.0% with signatures based on a small amount of training data (Rule A) to 91.7% with the medium amount (Rule B). The greater amount of training data with Rule C produced another increase by 5.2 percentage points to 96.9% correct. This trend is repeated for pixel insets of both 1.0 and 0.5 pixel. Although not

TABLE 8. RESULTS OF TRAINING DATA SELECTION TEST, FINNEY 26 MAY 74, FIELD-CENTER RESULTS

TRAINING DATA SELECTION		CORRECT CLASSIFICATION PERCENTAGE FOR FIELD-CENTER PIXELS WITH:								
		1.5-PIXEL INSET			1.0-PIXEL INSET			0.5-PIXEL INSET		
Rule	Draw	Wheat	Other	Conditional Average*	Wheat	Other	Conditional Average*	Wheat	Other	Conditional Average*
A	1	69.9	93.7	81.8	65.4	92.8	79.1	59.4	92.6	76.0
	2	78.2	97.3	87.8	74.9	96.8	85.8	67.4	96.2	81.8
	3	73.8	96.4	85.1	73.1	94.6	83.8	68.9	93.8	81.3
	Avg.	74.0	95.8	84.9	71.1	94.7	82.9	65.2	94.2	79.7
B	1	83.5	96.1	89.8	80.7	94.9	87.8	78.0	93.9	85.9
	2	95.3	95.6	95.5	93.8	94.1	93.9	88.9	93.3	91.1
	3	96.3	91.7	94.0	94.2	89.4	91.8	88.3	88.6	88.4
	Avg.	91.7	94.5	93.1	89.6	92.8	91.2	85.1	91.9	88.5
C	1	96.3	96.7	96.5	95.2	95.6	95.4	91.6	94.5	93.0
	2	98.9	95.6	97.3	98.1	93.7	95.9	95.3	91.9	93.6
	3	95.6	96.4	96.0	94.6	94.3	95.5	90.8	93.3	92.1
	Avg.	96.9	96.3	96.6	96.0	94.5	95.3	92.6	93.2	92.9

*The conditional average is the average of the correct classifications of wheat (given wheat) and other (given other).

TABLE 9. RESULTS OF TRAINING DATA SELECTION TEST, FINNEY 26 MAY 74, WHEAT PROPORTION ESTIMATES

TRAINING DATA		WHEAT PROPORTION ESTIMATE
GROUND TRUTH (30 SECTIONS)		$\boxed{0.251}$
BASELINE RUN - ALL DATA		$\boxed{0.276}$
RULE A, SMALL:	DRAW 1	.181
	DRAW 2	.177
	DRAW 3	.217
	AVERAGE	$\boxed{0.192}$
RULE B, MEDIUM:	DRAW 1	.244
	DRAW 2	.268
	DRAW 3	.288
	AVERAGE	$\boxed{0.267}$
RULE C, LARGE:	DRAW 1	.288
	DRAW 2	.327
	DRAW 3	.279
	AVERAGE	$\boxed{0.298}$

shown explicitly in the table, most of the wheat pixels which were not correctly classified were thresholded, i.e., not assigned to any one of the eight signatures, and were therefore counted as 'other'. As more training fields were used, the descriptions of the wheat signal population improved, the wheat signatures became more robust, and more wheat pixels were correctly classified. Correct classifications of 'other' field-center pixels were relatively independent of the amount of training data used. Field-center accuracy also was greatest when the most stringent criterion (1.5-pixel inset) was employed to define the field centers. In other words, the closer the field boundaries were approached, the less accurate was the field-center classification performance.

The proportion of wheat recognized in the entire site also increased as the amount of training data was increased (See Table 9). However, it went from an underestimate of the wheat proportion with the small amount of training data to an overestimate with the large amount of training data. Possible explanations for these proportion estimation results are explored in the next section.

5.5 ANALYSIS OF WHEAT PROPORTION ESTIMATES

Three analyses of the proportion estimation results and possible explanations of them will be presented in this section. First, on a site-wide basis, the relative contributions of field-center and non-field-center pixels to the estimated proportions will be examined. Next, section-by-section comparisons will be made between true and estimated proportions. Finally, the crops present in those sections where wheat proportion estimates were most in error will be analyzed.

5.5.1 COMPARISON OF WHEAT PROPORTION ESTIMATES WITHIN AND OUTSIDE FIELD CENTERS

The wheat proportion estimates were based on classification results for all pixels in the site, boundary as well as field-center pixels. However, to gain insight into the observed proportion estimation performance, values were tabulated separately for pixels within and outside field centers. Table 10 presents such comparisons for the three different pixel insets. Note that less than 2/3 (0.159/0.251) of the wheat actually lies within field centers with the minimal 0.5-pixel inset, approximately 1/3 with the 1.0-pixel inset, and about 1/6 with the 1.5-pixel inset.

The numbers in Table 10 were computed using the following equation:

$$p_{FC} = \frac{A_{W,FC} * NW_{FC} + (1 - A_{O,FC}) * NO_{FC}}{N_{TOTAL}}$$

where

p_{FC} is the contribution from field centers to the estimate of wheat.

$A_{W,FC}$ is the wheat field-center classification accuracy

NW_{FC} is the number of field-center wheat pixels

$A_{O,FC}$ is the 'other' field-center classification accuracy

NO_{FC} is the number of field-center 'other' pixels

N_{TOTAL} is the total number of pixels in the scene

Upon comparing the true proportions of wheat within and outside field centers to the corresponding estimated proportions, one first finds that the absolute discrepancies are greatest, in most instances, for pixels that lie outside field centers. Second, proportion estimates for pixels outside field centers are more sensitive to the training data selection procedure than are those within field centers. For example, absolute differences between proportion estimates with Rules

TABLE 10. COMPARISON OF WHEAT PROPORTION ESTIMATION ACCURACY WITHIN AND OUTSIDE FIELD CENTERS (FINNEY INTENSIVE TEST SITE, 26 MAY 74, 30 SECTIONS)

	1.5-PIXEL INSET		1.0-PIXEL INSET		0.5-PIXEL INSET		0.0-PIXEL INSET
	WITHIN FIELD CENTERS	OUTSIDE FIELD CENTERS	WITHIN FIELD CENTERS	OUTSIDE FIELD CENTERS	WITHIN FIELD CENTERS	OUTSIDE FIELD CENTERS	FIELD CENTERS (ALL PIXELS)
GROUND TRUTH VALUES:							
(1) TOTAL NUMBER OF PIXELS							
(a) TOTAL	2,673	14,533	5,604	11,602	10,264	6,942	17,206
(b) WHEAT	707	3,612	1,504	2,815	2,739	1,580	4,319
(2) TRUE CONTRIBUTION TO WHEAT PROPORTION IN SITE	0.041	0.210	0.087	0.164	0.159	0.092	0.251
(TOTAL WHEAT = 0.251)							
ESTIMATED PROPORTION OF WHEAT IN SITE, WITH TRAINING BY:							
RULE A (AVG)(Small)	0.035	0.157	0.075	0.117	0.129	0.063	0.192
RULE B (AVG)(Medium)	0.044	0.223	0.095	0.172	0.171	0.096	0.267
RULE C (AVG)(Large)	0.044	0.254	0.097	0.201	0.177	0.121	0.298
BASELINE (All Field-Center Data)	0.044	0.232	0.096	0.180	0.168	0.108	0.276

A and C are greater for non-field-center pixels, regardless of the inset parameter and whether they were in the majority or minority of pixels.

Fig. 14 graphically illustrates the data contained in Table 10. Note that the case for field centers with a 0.0 inset is equivalent to the total estimate of wheat in the scene. The series of illustrations on either side of the graph indicate the component parts for varying pixel insets. These plots clearly show that field-center errors for Rules B and C and the baseline case are almost constant, whereas the variation among boundary pixels is much greater. The other observations drawn from Table 10 data also are clearly portrayed, e.g., the greater magnitudes of errors among boundary pixels and the underestimation with Rule A signatures.

5.5.2 SECTION-BY-SECTION ANALYSIS OF WHEAT PROPORTION ESTIMATES

Section-by-section wheat proportion estimates are compared in Fig. 15 to the actual wheat proportions, as given in ground truth data. Fig. 15(a) presents the baseline case, where all available field-center pixels were used to establish signatures. Several sections are seen to have significant overestimates of their wheat proportion, leading to an overall section-by-section rms error of 0.053 and a small positive bias in the overall wheat proportion estimate.

For examination in conjunction with the analysis of Fig. 15, Fig. 16 displays both the section-by-section rms error and the entire-site proportion-estimation bias for each signature set used in the study. Average values are presented for each data selection rule, as well as the values for each individual draw.

The section-by-section results for the three draws of training fields using data selection Rules A, B, and C are presented in Figs. 15(b), (c), and (d), respectively. With Rule A, most sections were underestimated and the rms errors were large (0.109 average for the three draws). A few sections were overestimated and it is interesting

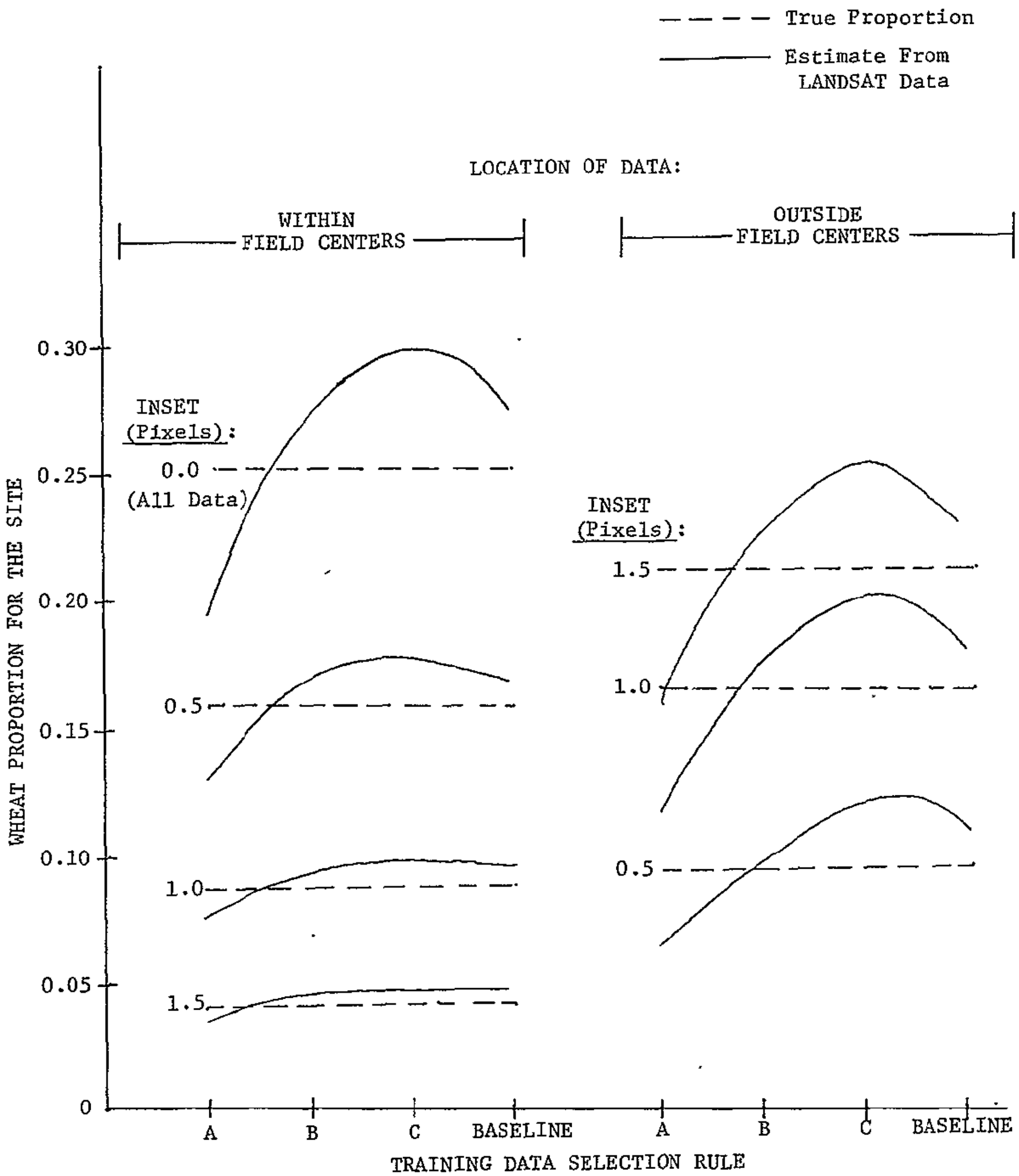

FIGURE 14. RELATIVE CONTRIBUTIONS OF PIXELS WITHIN AND OUTSIDE FIELD CENTERS TO WHEAT PROPORTION ESTIMATES; FINNEY, 26 MAY 74

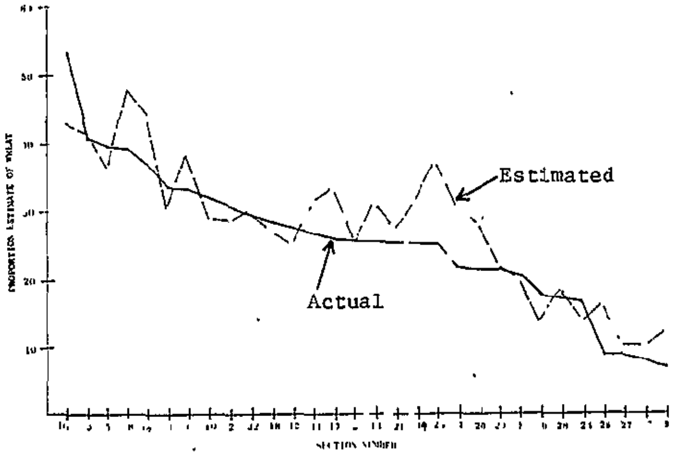

(a) Wheat Proportion Estimates Obtained
With the Baseline Signatures

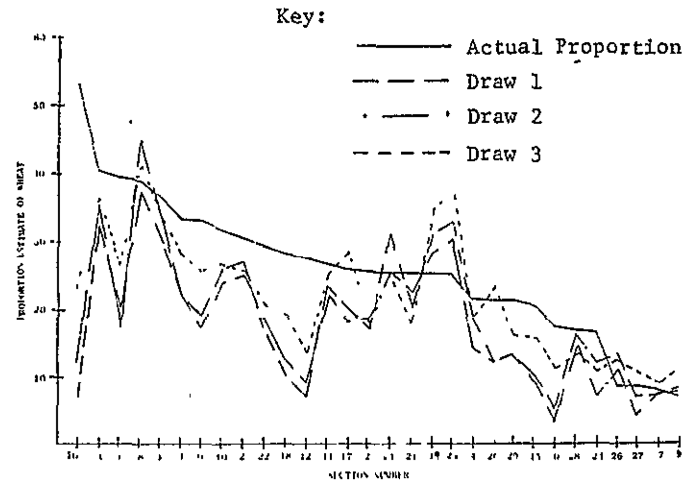

(b) Wheat Proportion Estimates Obtained
With Training Selection Rule A

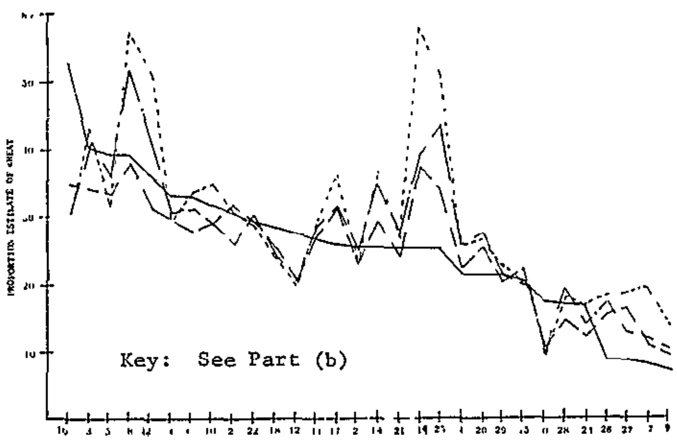

(c) Wheat Proportion Estimates Obtained
With Training Selection Rule B

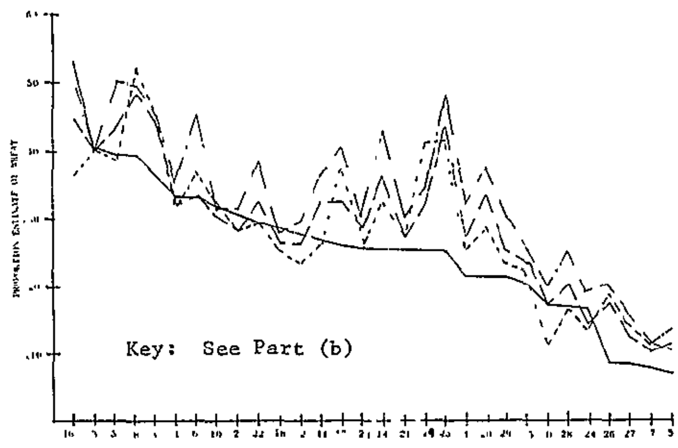

(d) Wheat Proportion Estimates Obtained
With Training Selection Rule C

FIGURE 15. SECTION-BY-SECTION COMPARISON OF ACTUAL WHEAT PROPORTIONS WITH THOSE ESTIMATED USING VARIOUS TRAINING DATA SELECTION RULES (30 Sections, Finney ITS, 26 May 74)

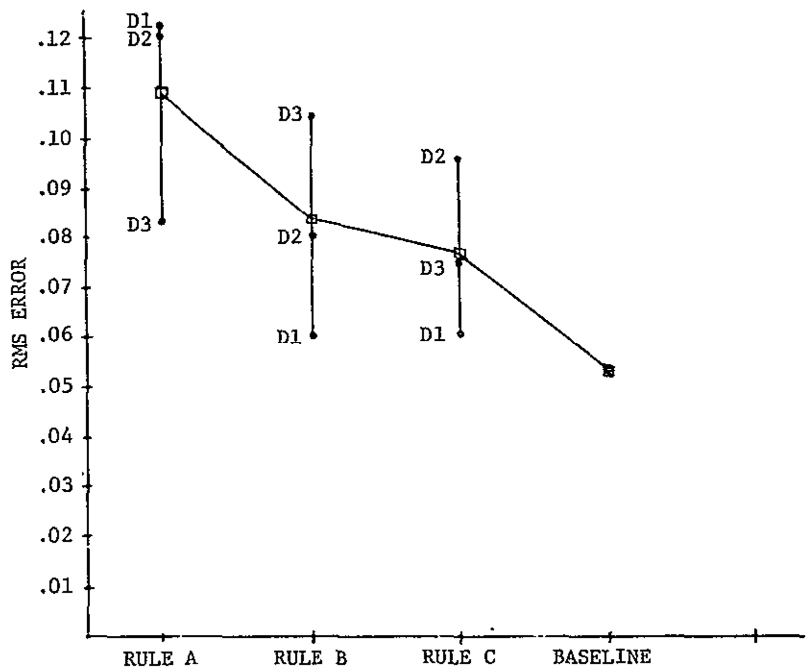

(a) Section-By-Section RMS Error

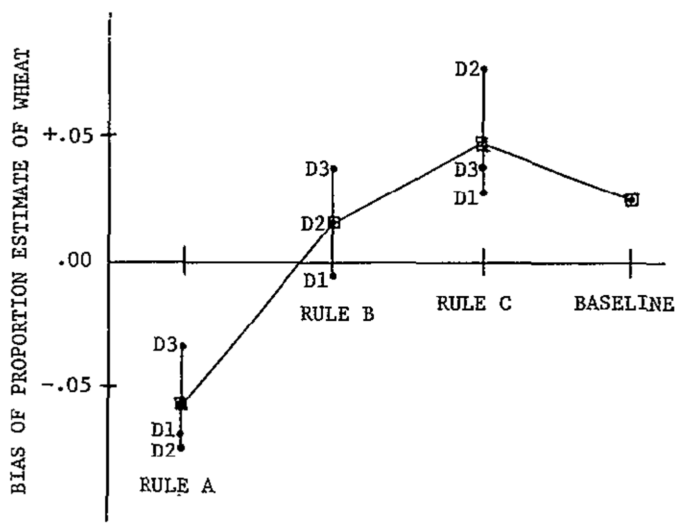

(b) Wheat Proportion Estimation Bias
for Entire Site

FIGURE 16. WHEAT PROPORTION ESTIMATION RESULTS FOR INDIVIDUAL DRAWS USING THE VARIOUS DATA SELECTION RULES; FINNEY ITS, 26 MAY 74

to note that, in every case, these sections were also overestimated by the baseline signature set and all draws using Rules B and C.

The pattern for Rule B is also variable, but the average rms error is lower (0.083). The wheat proportion estimates for most sections increased above their Rule A values, many approaching their true values but a few (notably, Sections 8, 19, and 25) being grossly overestimated for most of the draws. The average bias in proportion estimates for the site were smaller for Rule B than for either Rule A or Rule C. If it were not for the few sections with large overestimates, the site proportion estimate would have been quite accurate with Rule B.

The results with increased amounts of training data (Rule C) showed a greater tendency to overestimate the wheat proportion in each section but the estimates were more consistent and, on the average, their rms error was lower than for Rule A or B. The sections which had large overestimates with Rule B were also overestimated by Rule C. The wheat proportion bias was greater than for Rule B, presumably because of the more robust nature of the wheat field signatures in comparison to the limited scope of other class signatures.

5.5.3 ANALYSIS OF FOUR SECTIONS REPRESENTING EXTREMES OF PROPORTION ESTIMATION BIAS

Several sections were identified in which the wheat proportion was consistently overestimated by all signature sets. In addition, there were some which tended to be underestimated, especially so for Rule A. Four sections were selected for additional analysis to see if reasons for such overestimates (Sections 19 and 25) and underestimates (Sections 12 and 16) could be determined.

Table 11 presents acreages of the major crops in each of these four sections. Also listed are the average wheat proportion biases for the various rules, expressed as a percentage of the total section area. Two pertinent observations are that: (1) relatively large acreage of alfalfa and early-planted corn were found in Sections 19 and 25, where

TABLE 11. CROP DATA COMPILED FOR FOUR SECTIONS EXHIBITING WHEAT PROPORTION ESTIMATION BIASES

	ACREAGE					BIAS IN WHEAT PROPORTION ESTIMATE (Expressed as Percent of Total Section Area)			
SECTION	WHEAT	ALFALFA	CORN (April Planting)	CORN (May Planting)	BARE AND SUMMER FALLOW	RULE A	RULE B	RULE C	BASELINE
19	118.4	73.0	145.6	0.0	224.4	+5.8	+19.1	+10.5	+6.2
25	153.7	136.3	156.8	0.0	105.5	+8.1	+17.3	+18.5	+11.1
12	178.4	10.0	44.8	249.1	106.3	-17.9	-7.7	-1.5	-2.9
16	334.5	0.0	0.0	0.0	249.5	-39.2	-21.2	-10.4	-10.6

wheat was overestimated, and (2) large acreages of bare soil, summer fallow land, and/or late-planted corn were found in Sections 12 and 16, where wheat was underestimated.

The significance of these observations and their implications for multispectral recognition will be facilitated by reference to Sec. 4 in which the spectral characteristics of wheat and other signals were examined, to Fig. 13 which displays many of the signatures used to obtain the results being analyzed, and to Fig. 17 which displays the spectral signatures obtained from large fields in the Finney ITS -- wheat in Part (a), corn and grain sorghum in Part (b), and other crops in Part (c).

Healthy green alfalfa fields produce Landsat signals that are large in Channel 3 and small in Channel 2, as shown in Fig. 17(c). Fields of bare soil or recently planted corn (and grain sorghum) produce signals falling along a line as shown in Fig. 17(b). Alfalfa fields lie spectrally close to signals from immature wheat, the uppermost of the four subclasses of wheat shown in Fig. 13. If an alfalfa field were not as dense or vigorous as most, it might be misclassified as wheat by the immature wheat signature. Another possibility is that fields of bare soil or corn might lie adjacent to alfalfa fields and pixels that include these boundaries would have mixture signals that could appear more like wheat than like either of these or any other crop signature. In most of the cases portrayed in Fig. 13, many pixels falling in between the arms of the 'V' pattern would be classified as wheat by the particular signature sets used.

Another possible source of wheat false alarms lies with corn fields that are darker and fall spectrally near the lower left of the distribution of corn field signatures (Fig. 17(b)). These fields are close to the wheat subclass which represents the most senescent and/or least dense, non-irrigated wheat fields. As can be seen in Fig. 13, the signatures generated for the other classes often did not adequately

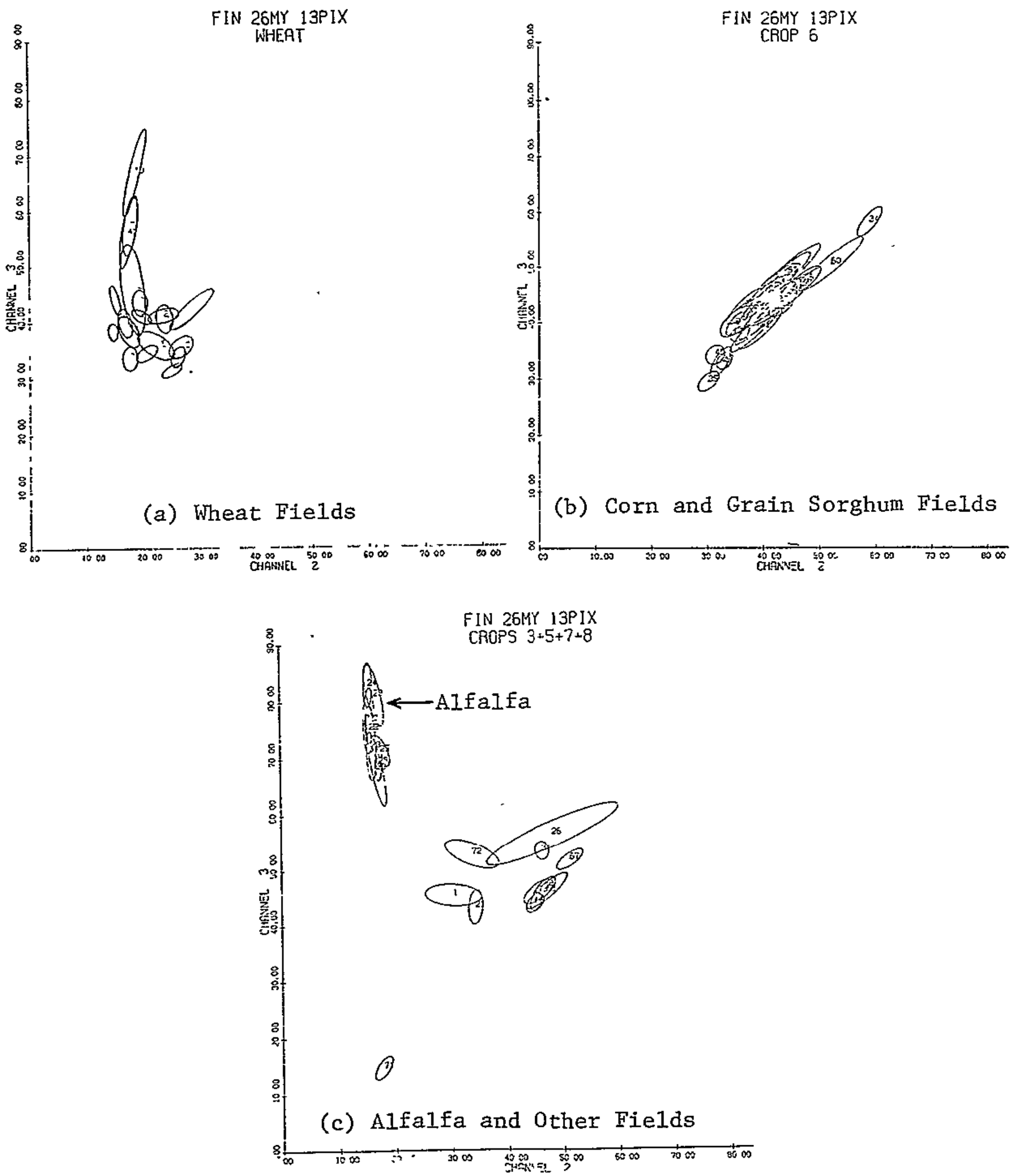

FIGURE 17. FIELD SIGNATURE PLOTS FOR VARIOUS CROPS; FINNEY ITS, 26 MAY 74

represent this region of corn's spectral response. Upon checking the individual corn fields in Sections 19 and 25, it was found that these early-planted corn fields did indeed have spectral signatures in this region.

Thus, plausible reasons for the large overestimates of wheat in Sections 19 and 25 have been advanced, namely the presence of particular multiclass boundary pixels and inadequate representation of all other-crop subclasses. Turning now to the underestimated sections (12 and 16), note that the absence of alfalfa in significant amounts precludes the existence of boundary pixels which would appear spectrally similar to wheat. Also, at the other side of the wheat spectral region, there was little or no early-planted corn to potentially be classified as wheat.

5.6 DISCUSSION

A good start was made on examining the influence of the amount of training data on winter wheat recognition performance. Additional planned effort was postponed because emphasis was shifted to the simulation modeling effort discussed in Sec. 6. However, useful results were obtained which may have practical implications either for LACIE operations or for further exploration in subsequent SR&T (Supporting Research and Technology) investigations. The results of this study and some of the procedures developed already have found applications in other tasks on this contract. For example, they were useful in the development of the training procedure used in the test and evaluation task [7] and in the development of some of the computer-aided training procedures [12].

The sampling aspect of the training problem was examined for one site and one time period. For more general applications, multiple time periods and multiple sites must be considered in the establishment of training criteria. For example, in Sec. 4, substantial differences in the spectral character of both wheat and other populations in the

Finney and Ellis ITS's were observed. The LACIE training problem is one of characterizing wheat and other spectral characteristics jointly for several segments, with a minimum requirement on AI identifications.

The amount of data used for training was shown to definitely affect both classification performance on field-center pixels and wheat proportion estimation accuracy for the entire site. It also was shown that boundary pixels contributed much of the bias in the proportion estimates. One factor which should have been examined more fully and which would affect the results in an undetermined manner is the effect of varying the detection threshold in the decision algorithm. With the fewest training fields (Rule A), the signatures tended to be compact and about one-quarter of the scene pixels were thresholded. This decreased to about one-sixth for Rule B and 6% for Rule C; only 3% of pixels were thresholded with the baseline signature set. The use of more and more training data reduced the importance of the particular decision threshold level used.

The spectral sampling of wheat pixels was more complete than that for other pixels. Perhaps twice as many other spectral classes should have been defined. The choice of four was quite arbitrary, and the results obtained indicated that it is important to adequately represent the other signals as well as those for wheat.

The study was limited in that only one site at one time of year was examined before the emphasis was shifted to other efforts. In several ways though, the Finney site was a good first choice. Although not typical of much of Kansas, because of its high percentage of irrigated fields, it nevertheless contained a variety of wheat fields which pointed out several factors which affect wheat signatures and the need to consider multimodal signatures. The availability of a rather complete set of ground truth data was very helpful in the analysis.

Spectral two-channel displays of signatures and data were found to be useful analysis tools and are recommended for use in LACIE procedures where analyst interaction is required.

The procedure of simply combining signatures from training fields in each spectral 'color' class should be compared with a spectral data clustering procedure, especially if small numbers of classes are defined.

6
THEORETICAL MODELING AND ANALYSIS OF SEASONAL AND UNITEMPORAL VARIATIONS IN WHEAT SIGNATURES

A need was recognized by NASA for an extensive and consistent set of synthetic Landsat data values and associated radiance components, for general use by members of the LACIE project team as well as this specific investigation. Such data are of potential use in the development of various remote sensing systems and information extraction techniques and in solving specific problems of LACIE. Example uses and benefits are those of enabling analysts to (1) assess the relative importance of the variety of factors affecting signals, (2) gain insight into the variability of training statistics in Landsat data, (3) improve and extend analyses of field measurement data, (4) gain insight into aspects of the signature extension problem and provide quantitative data to aid in developing solutions such as haze correction algorithms, (5) gain insight into the operation of alternative classification techniques, such as the Delta Classifier [13], and (6) gain insight and provide quantitative bases for developing data transformation procedures, such as the tasseled-cap transformation [12].

6.1 APPROACH

The capability required was that of simulating multispectral scanner signals from wheat fields for a variety of ground and observation conditions and parameters. At this initial stage, it was important to consider a wide range of conditions and generate a consistent set of the simulated values. It was deemed desirable, since the basic capability existed, to carry out calculations at a relatively fine spectral interval, multiply by the relative spectral response functions of Landsat and integrate over wavelength to obtain effective inband values, rather than approximating these by values at a single wavelength for each Landsat spectral band.

Existing computer models developed at ERIM to compute vegetation canopy bidirectional reflectance and atmospheric radiative transfer characteristics were linked and a sensor submodel was added to form the ERIM Multispectral System Simulation Model. Together, they provide a capability to compute synthetic inband radiance and data values for a sensor (with specified characteristics and locations) viewing specified surface reflectors (for which bidirectional reflectance characteristics can be computed) through homogeneous, isotropic atmospheric media of specified characteristics under specified solar illumination geometries (See Fig. 18).

Effective Landsat inband values were calculated for each of the following three groups of quantities:

(1) Inband atmospheric effects, including values representing (a) direct solar irradiance, (b) diffuse sky irradiance, (c) path transmittance, and (d) path radiance.

(2) Inband reflectances, both (a) bidirectional reflectance for reflection of direct solar radiation, and (b) diffuse reflectance for reflection of indirect solar radiation scattered by the atmosphere.

(3) Sensor inband radiances that combine the reflectance and atmospheric effects calculations.

The equations used for the simulation are discussed in Sec. 6.2, while Sec. 6.3 describes the crop canopy reflectance model and the radiative transfer model for atmospheric effects. The former section also presents the Landsat spectral characteristics which were simulated, while the latter section presents the model parameters used in simulating the signals arising from wheat fields at seven stages of growth throughout the growing season and a variety of atmospheric conditions.

6.2 SIMULATION EQUATIONS AND SENSOR RESPONSE FUNCTIONS

The basic equation used for computing the spectral radiance $L(\lambda)$ at the satellite is:

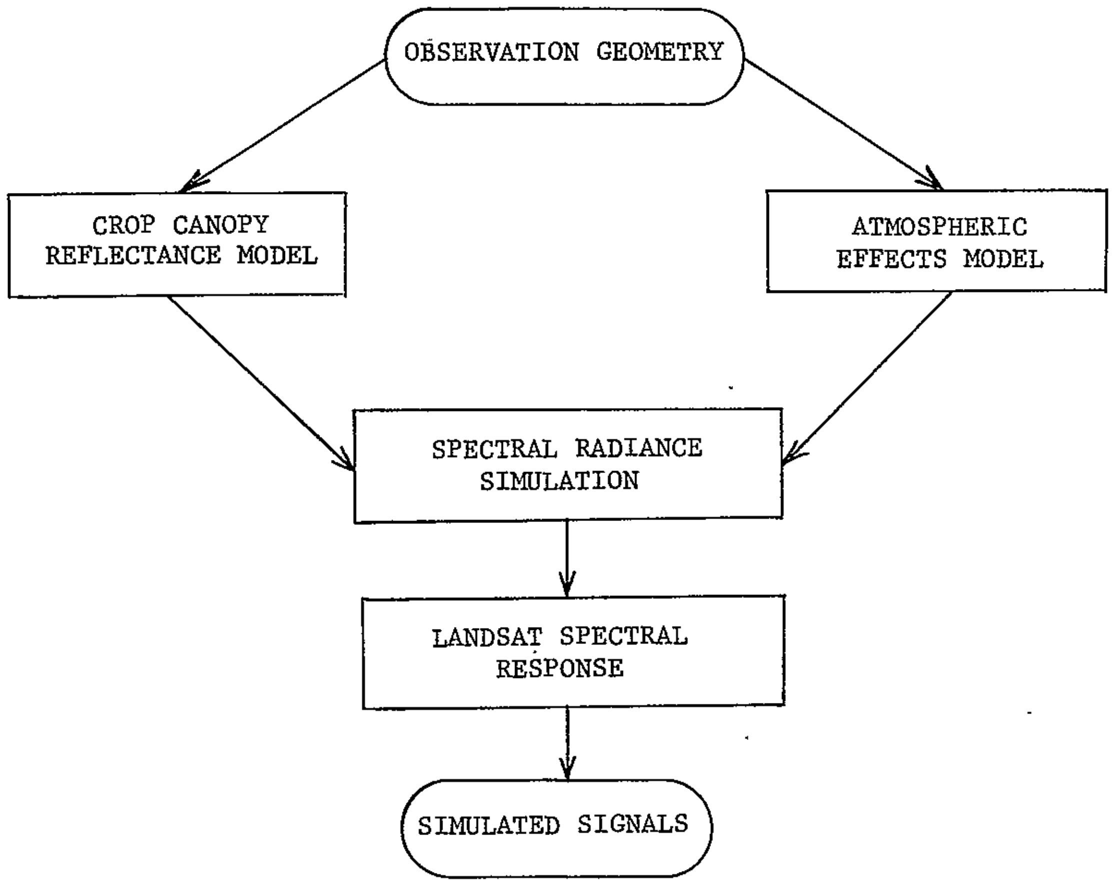

FIGURE 18. FLOW DIAGRAM FOR SIMULATION MODEL CALCULATIONS

$$L(\lambda) = \frac{1}{\pi}\left(E^{\lambda}_{Direct} \cdot \rho^{\lambda}_{Bidirect} + E^{\lambda}_{Diffuse} \cdot \rho^{\lambda}_{Diffuse}\right) T^{\lambda} + L^{\lambda}_{Path} \quad (7)$$

where E^{λ}_{Direct} is the direct (solar) spectral irradiance,

$E^{\lambda}_{Diffuse}$ is the diffuse (sky) spectral irradiance,

$\rho^{\lambda}_{Bidirect}$ is the bidirectional spectral reflectance of the surface, relative to that of a perfect Lambertian surface,

$\rho^{\lambda}_{Diffuse}$ is the Lambertian (i.e., diffuse) spectral reflectance of the surface,

T^{λ} is the spectral transmittance of the atmosphere,

and L^{λ}_{Path} is the spectral path radiance.

These individual quantities also have varying degrees of dependence on the geometry of the situation, with the radiance itself depending on both the sun and view geometries. Of the spectral quantities in Eq. (7), all were computed with the Turner Radiative Transfer Model [14], except $\rho^{\lambda}_{Bidirect}$ and $\rho^{\lambda}_{Diffuse}$ which were computed with the Suits' Canopy Reflectance Model [15]. Sec. 6.3 describes these models in greater detail.

The effective inband radiance for Landsat Band i was obtained by integration, i.e.,

$$L_i = \int R_i(\lambda) L(\lambda) d\lambda \quad (8)$$

where $R_i(\lambda)$ is the relative spectral response function for Band i. The calculations were carried out with a spectral interval of 0.01 μm and a summation of products to replace the continuous integration indicated in Eq. (8). The Landsat spectral response curves [16] displayed in Fig. 19 were digitized at the stated intervals and used in the simulation calculations.

To obtain simulated Landsat signals, V_i, one would multiply the effective inband radiance values by band calibration factors, K_i, i.e.,

$$V_i = K_i L_i \tag{9}$$

The calibration factors found in the ERTS (Landsat) Data Users Handbook [16] represent pre-launch measurements for Landsat-1. Optical changes are known to have taken place shortly after the launch of Landsat-1, but accurate measures of their effects on system calibration are not available. Since selected calculations with these standard factors did not yield values which compare well with actual Landsat data, synthetic Landsat data values were not generated for presentation in either this report or the supplement. It is recommended that more representative calibration factors be determined and applied to the radiance values presented in this report. These new calibration factors would be determined by correlating field measurement data, other data, and calculated atmospheric effects and radiance data with Landsat data values.

6.3 DESCRIPTION OF MODELS AND MODEL PARAMETERS USED IN THE SIMULATION

Calculations of wheat canopy reflectances were made using the reflectance model developed by Dr. Gwynn Suits of ERIM [15]. It was used to compute two spectral quantities. The first was the bidirectional reflectance of the canopy, expressed in dimensionless units relative to the bidirectional reflectance ($1/\pi$) of a perfect Lambertian (perfect diffuse) surface. This bidirectional reflectance applies to a surface's reflection of direct sunlight toward the sensor. The second quantity computed was the diffuse reflectance or, more precisely, the hemispherical-directional reflectance, i.e., the fraction of

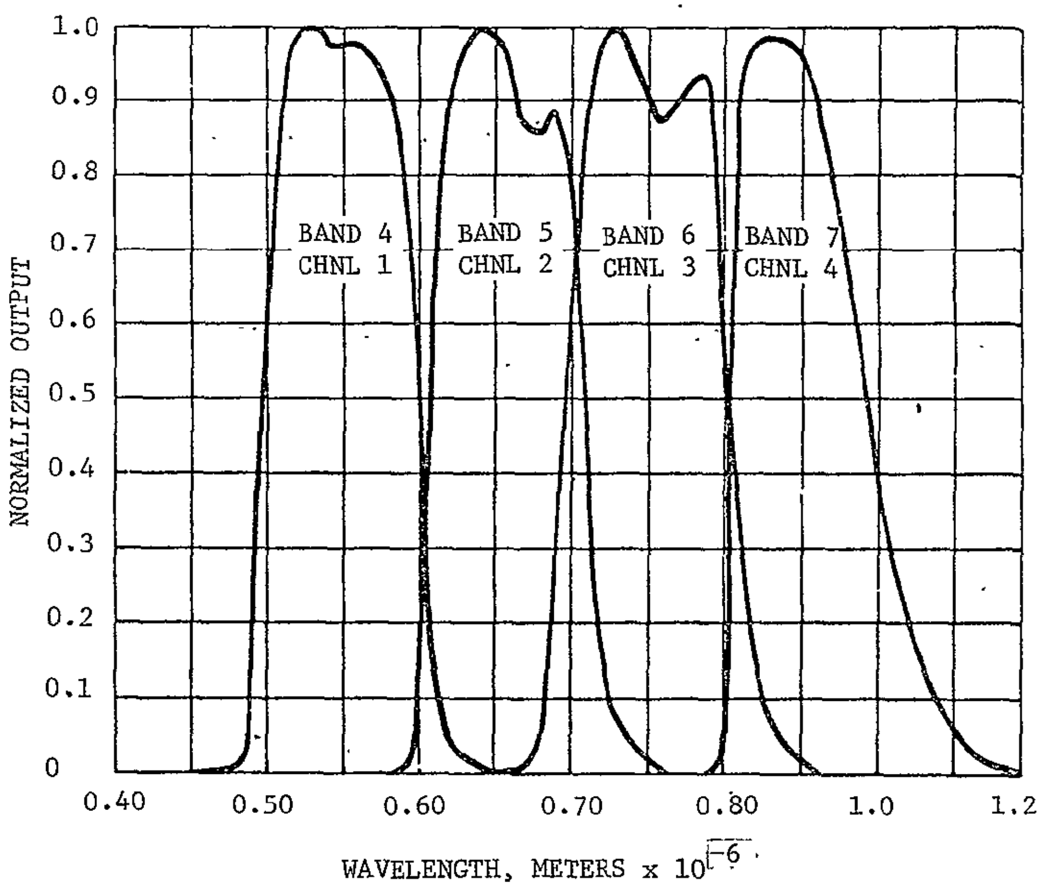

Notes: (1) All bands were normalized individually; Band 7 values were re-normalized to 1.0 at the wavelength of the peak.

(2) Abscissa scale changes for Band 7 from that used for Band 6.

FIGURE 19. LANDSAT RELATIVE SPECTRAL RESPONSE [16]

incident radiation from a uniform hemispherical source (to approximate diffuse sky irradiance) that is reflected into the view direction of the sensor by a Lambertian surface.

The overall set of factors and levels used to generate the reflectance and atmospheric quantities is presented in Table 12. The 21 wheat canopy structures simulated had physical characteristics as summarized in Table 13. In addition, three soil reflectance spectra obtained from Condit [18] were used in the calculations (See Fig. 20). These correspond to his average soil reflectance spectrum and plus and minus one standard deviation from it. View angles corresponding to the nadir and $\pm 6^{\circ}$ (toward each side of the Landsat track) were simulated, as well as sun angles for 38° and 46°N latitude for each time period. A group of 63 different canopies, each viewed under six different viewing and illumination geometries, was simulated for a total of 378 cases.

The spectral characteristics (transmittance and reflectance) of the various components of wheat (leaves, stems, and heads) were obtained from samples collected in Finney Co., Kansas, by an ERIM field team working under a Landsat follow-on contract (NAS5-22389 with the NASA Goddard Space Flight Center, Greenbelt, Md.) and measured with a laboratory instrument at ERIM. The structures assumed for the various growth stages were based largely on companion measurements by the ERIM field team, with reference being made to LACIE field measurement data. The high density canopies would be found only for the most healthy irrigated wheat fields in Kansas, while the more common, non-irrigated wheat fields would most likely fall between the low density and base density conditions.

Calculations of four atmospheric spectral properties were made with the radiative transfer model, developed by Dr. Robert Turner of ERIM [14], for sun positions and view geometries corresponding to those used for the canopy reflectance calculations. The quantities

TABLE 12. FACTORS AND LEVELS FOR SIMULATION

WHEAT CANOPY REFLECTANCE CALCULATIONS

FACTOR	NO. LEVELS	LEVELS
Stage of Maturity	7	See Table 13
Set of Spectral Properties	1	From ERIM 1975 Measurements
Soil Reflectance	3	Condit Average and ±1 Sigma
Canopy Density	3	See Table 13
Sun Positions	2	For Each Period, for 38^o and 46^oN Latitude
View Angles	3	Nadir, $\pm 6^o$

ATMOSPHERIC FEATURE CALCULATIONS

FACTOR	NO. LEVELS	LEVELS
Background Albedo Spectrum	3	Bare, Green, Brown
Haze Level	3	Hazy, Moderately Hazy, Clear
Sun Positions	2	For Each Period, for 38^o and 46^oN Latitude
View Angles	3	Nadir, $\pm 6^o$

TABLE 13. CHARACTERISTICS OF WINTER WHEAT CANOPIES

CANOPY BASE NUMBER	SIMULATION DATE	STAGE OF GROWTH	TOTAL PERCENT COVER, FOR DENSITY:			GREEN LEAF AREA INDEX, FOR DENSITY:		
			LOW	BASE	HIGH	LOW	BASE	HIGH
1	Mid November	Emergent	3	14	25	0.10	0.52	1.04
2	Mid April	Jointing	11	44	69	0.41	2.06	4.12
3	Mid May	Pre-heading (Boot)	40	79	96	1.03	3.13	6.26
4	End May	Post-heading (Green)	43	82	97	1.03	3.13	6.26
5	Early June	Senescing	27	64	84	0.28	0.92	1.61
6	Late June	Ripe	14	40	59	0	0	0
7	Early July	Harvested	7	14	23	0	0	0

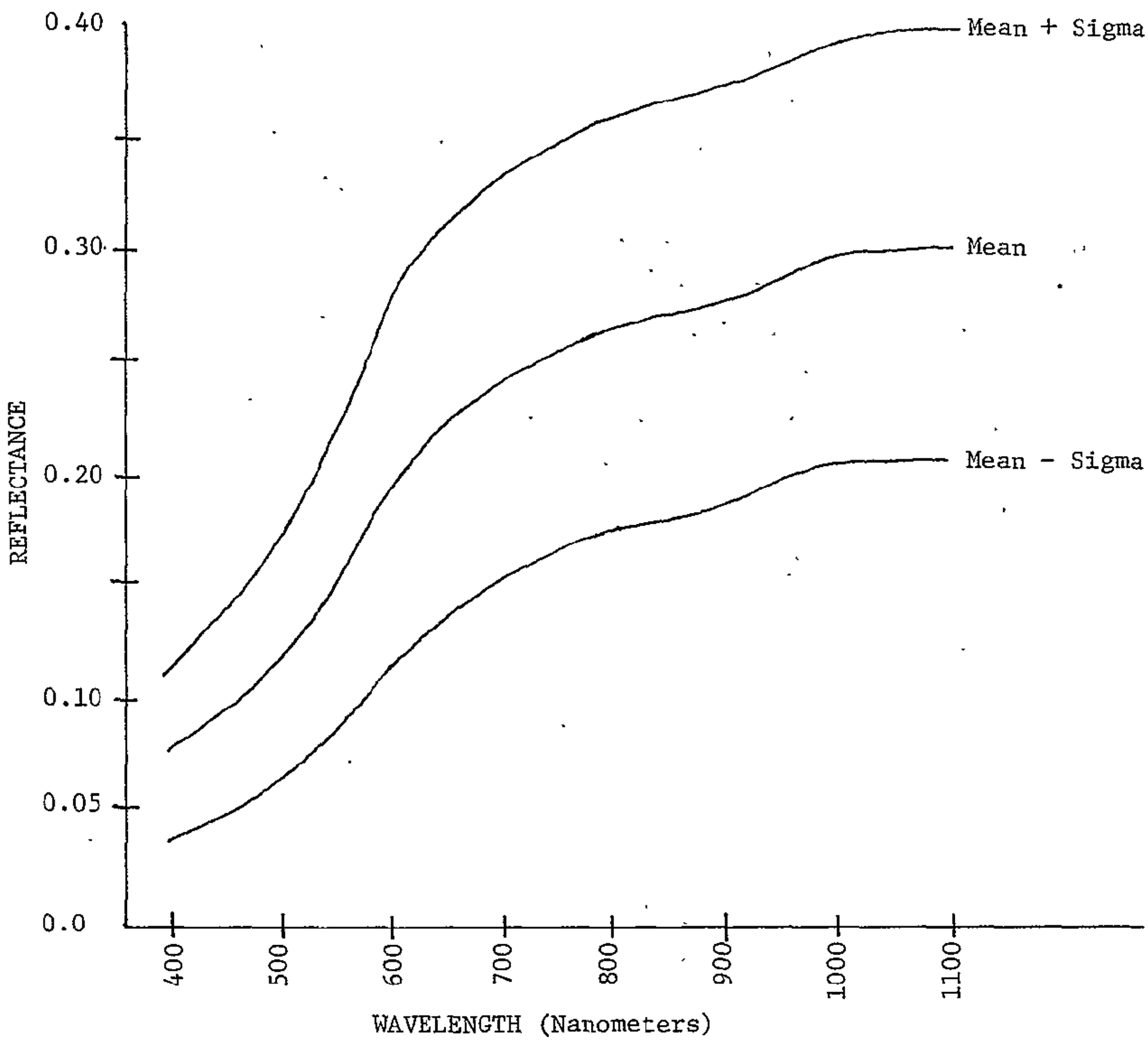

FIGURE 20. SOIL REFLECTANCE SPECTRA USED IN SIMULATION OF WHEAT CANOPY REFLECTANCES. (Soil spectra are based on the work of Condit [18].)

computed were both direct-solar and diffuse-sky spectral irradiance at the Earth's surface, path spectral transmittance from the surface to the satellite sensor, and path spectral radiance as observed by the sensor. The optical thickness spectra assumed for the atmosphere in the calculations (Table 14 and Fig. 21) were those associated with Elterman's standard atmospheres that are labeled by horizontal visual ranges of 4, 10, and 23 km for hazy, moderately hazy, and clear conditions, respectively. The three background albedo spectra used for the calculations (Table 14 and Fig. 22) are representative of bare soil (average), a green vegetation canopy, and a sparse brown (harvested wheat) vegetation canopy, respectively. Thus, for each sun position and view geometry, nine atmosphere cases were computed.

Then, the reflectance and atmospheric spectra were used with Eq. (7) to compute total radiance spectra at the satellite for 378 x 9 = 3402 cases.

Effective inband values were computed for each spectrum by multiplying it by the Landsat relative response functions and integrating over the appropriate wavelength interval. The individual inband values for reflectance, atmospheric features, and total radiance were too detailed and voluminous for general distribution in this report; however, they are available in a limited-distribution supplement to this report [1]. Concise summaries of these results and some initial analyses of them are presented in the sections that follow -- wheat reflectances in Sec. 6.4, atmospheric features in Sec. 6.5, and total radiances in Sec. 6.6.

6.4 WHEAT REFLECTANCE CALCULATIONS

Reflectance values were computed for each of the seven stages of wheat canopy growth described above. Nine different canopy conditions, corresponding to the combinations of three different densities and three different soil colors, were simulated for each growth stage, each being viewed under six different viewing and illumination geometries.

TABLE 14. BACKGROUND REFLECTANCE SPECTRA AND ATMOSPHERIC OPTICAL THICKNESS SPECTRA USED IN THE CALCULATIONS OF ATMOSPHERIC FEATURES

	BACKGROUND REFLECTANCE			OPTICAL THICKNESS (FOR INDICATED VISUAL RANGE)		
WAVELENGTH (Nanometers)	BARE	GREEN	HARVESTED	23 km	10 km	4 km
400	0.073	0.018	0.048	0.682	1.000	1.640
450	0.097	0.024	0.072	0.508	0.792	1.360
500	0.116	0.030	0.100	0.422	0.679	1.190
550	0.152	0.055	0.140	0.374	0.600	1.070
600	0.197	0.040	0.160	0.334	0.540	0.960
650	0.220	0.028	0.200	0.300	0.476	0.860
700	0.240	0.090	0.240	0.262	0.425	0.790
750	0.258	0.380	0.280	0.241	0.390	0.740
800	0.267	0.400	0.300	0.226	0.364	0.695
900	0.279	0.460	0.340	0.204	0.326	0.625
1000	0.299	0.450	0.360	0.197	0.300	0.580
1100	0.300	0.440	0.380	0.183	0.288	0.550

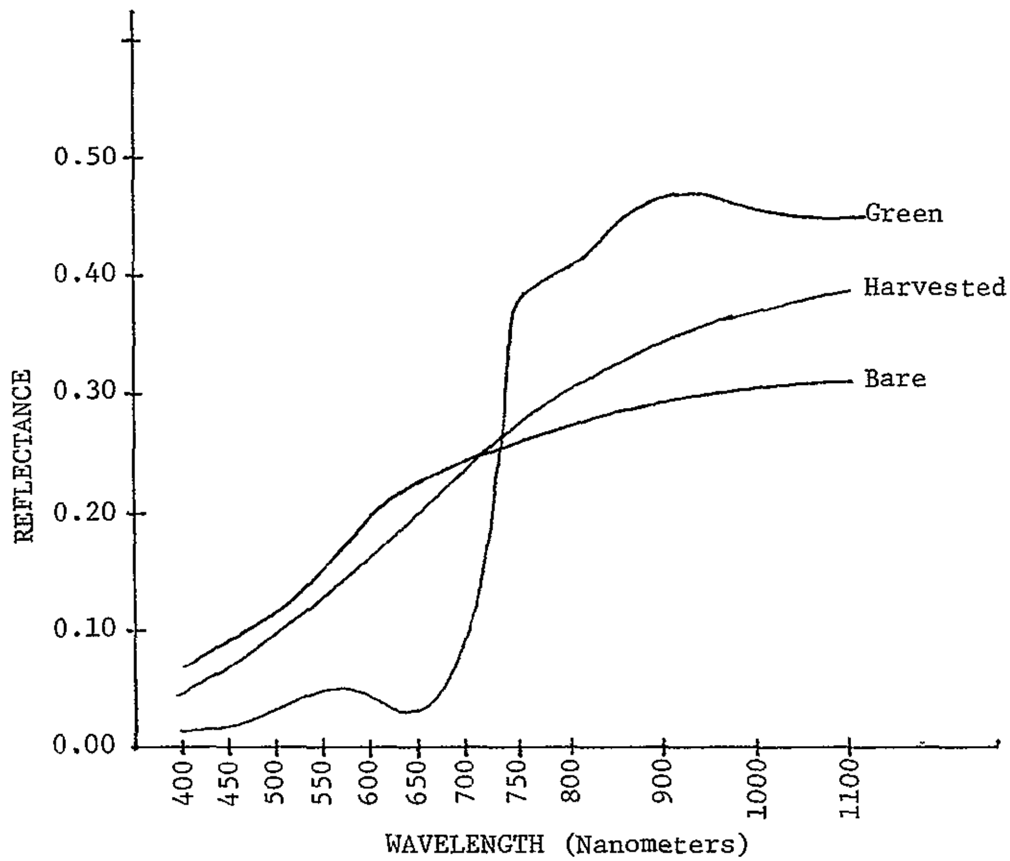

FIGURE 21. THE THREE BACKGROUND REFLECTANCE SPECTRA USED IN SIMULATING ATMOSPHERIC FEATURES

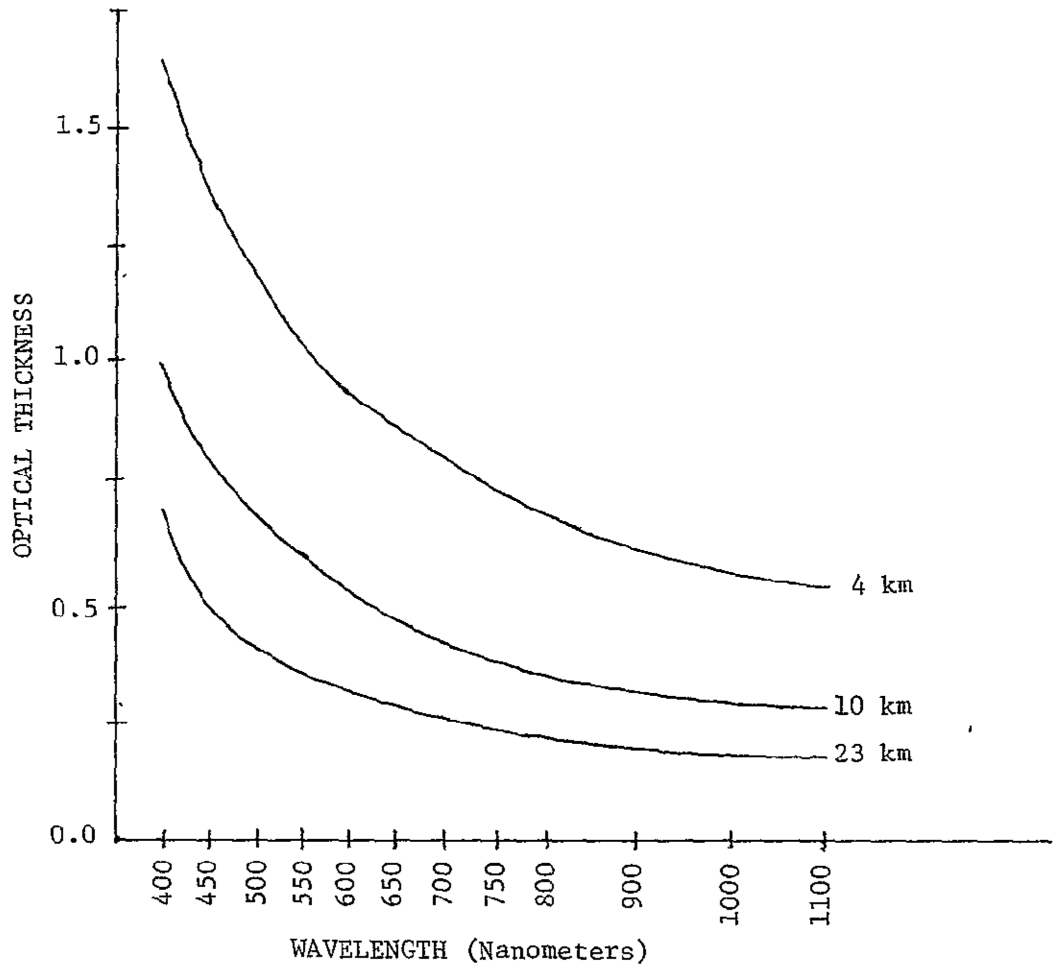

FIGURE 22. OPTICAL THICKNESS AS A FUNCTION OF WAVELENGTH FOR THE THREE MODEL ATMOSPHERES USED IN CALCULATING ATMOSPHERIC FEATURES

A wide range of resultant wheat reflectance values was obtained. For relative bidirectional reflectance, for instance, Landsat Band 4 values ranged from 0.025 to 0.198, Band 5 values from 0.033 to 0.284, Band 6 values from 0.146 to 0.356, and Band 7 values from 0.176 to 0.508 for the full range of conditions simulated.

Figs. 23 and 24 present two-band scatter diagrams which display this variation and its correlation between bands for relative bidirectional reflectance values. Effective reflectances in Band 6 are plotted vs. those in Band 5 in Fig. 23. These two bands describe most of the spectral character of Landsat scenes, because of the high degree of correlation between Bands 4 and 5 and Bands 6 and 7, as shown in Fig. 24.

A composite scatter diagram of reflectances for all seven stages of canopy growth is presented in Fig. 23, Part (a), while Parts (b) through (h) present reflectances calculated for the individual growth stages. These latter plots exhibit a substantial amount of dispersion even within individual growth stages. This is due to the combined effects of canopy density and soil color. The influence of each of these two factors is more easily distinguishable in Fig. 25 where a display of the variation of reflectance values for most of the key parameters is presented for each Landsat band.

The horizontal axis in the displays of Fig. 25 has no physical significance; it is used merely as a graphical aid. Reflectance values are displayed successively for the three soil colors within each stage of growth, with the pattern being repeated for each of the three density levels. To aid in distinguishing between growth stages, the plotting symbols for the displays are their respective growth stage numbers. It is clear that soil color has a much greater effect on reflectances from low density canopies, which may be due either to sparse growth or to early time in the growing season. The peaking and decline of green leaf area throughout the growing season is very evident in Bands 6 and 7.

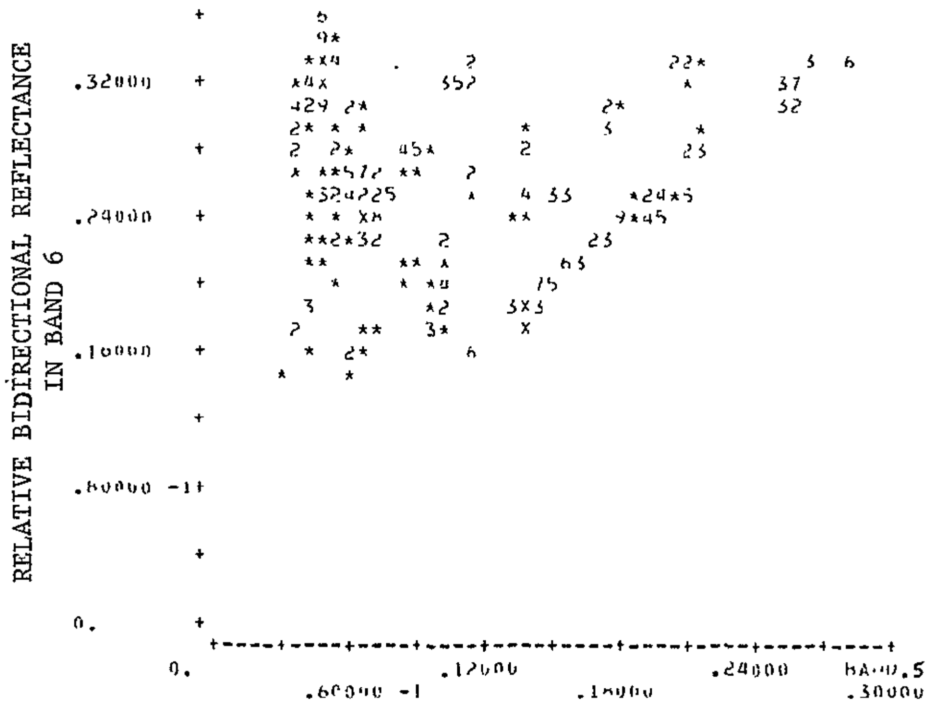

(a) Composite of All Growth Stages

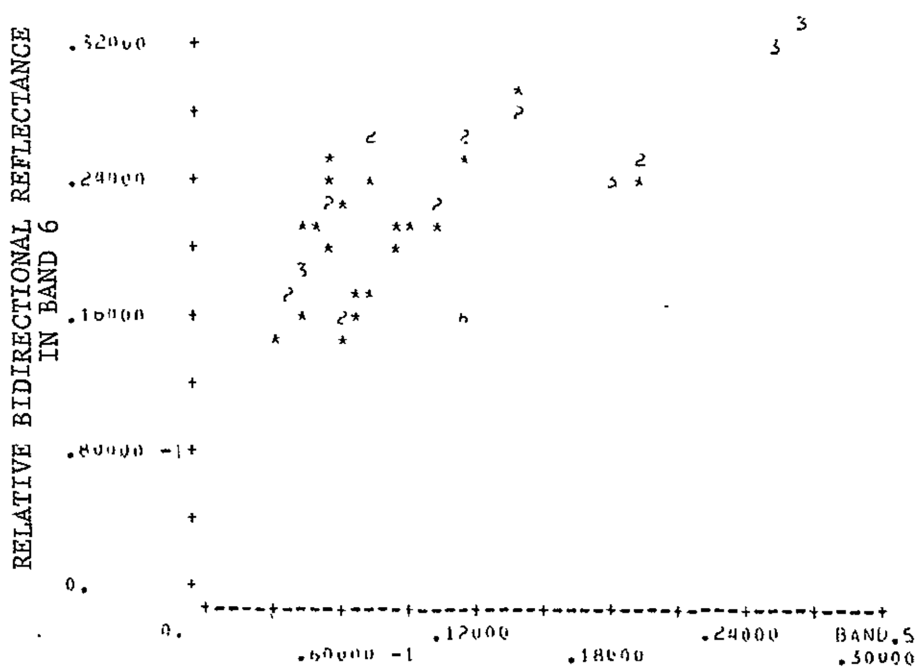

(b) Stage 1, Emergent

FIGURE 23. DEPENDENCE OF RELATIVE BIDIRECTIONAL REFLECTANCE ON CANOPY STRUCTURE AND SOIL, LANDSAT BAND 6 VS 5. (Nine Variants Present for Each Growth Stage Number) (Cont'd)

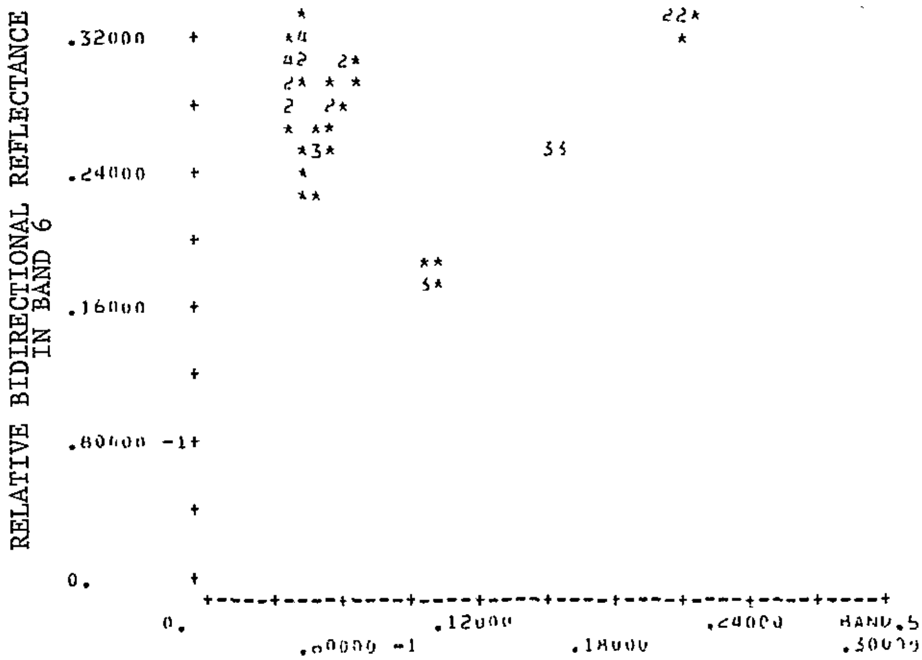

(c) Stage 2, Jointing

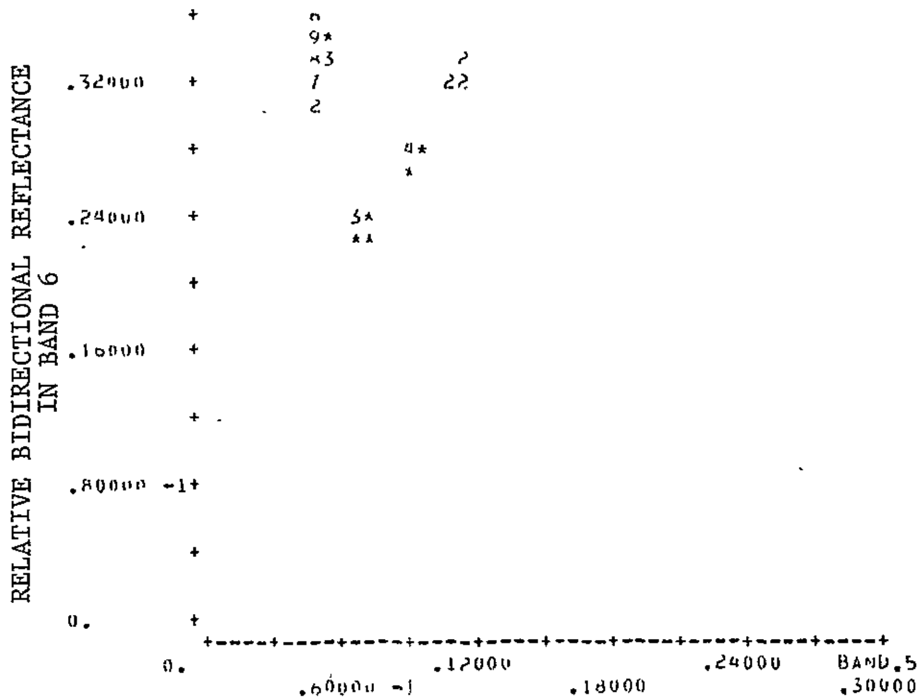

(d) Stage 3, Pre-heading

FIGURE 23. DEPENDENCE OF RELATIVE BIDIRECTIONAL REFLECTANCE ON CANOPY STRUCTURE AND SOIL, LANDSAT BAND 6 VS 5. (Nine Variants Present for Each Growth Stage Number) (Cont'd)

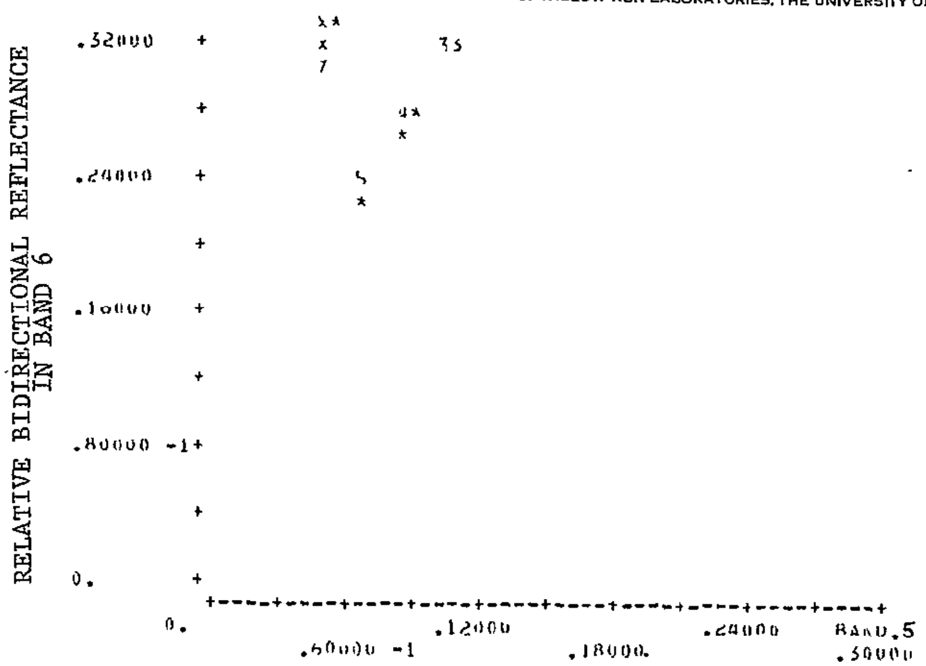

(e) Stage 4, Post-heading

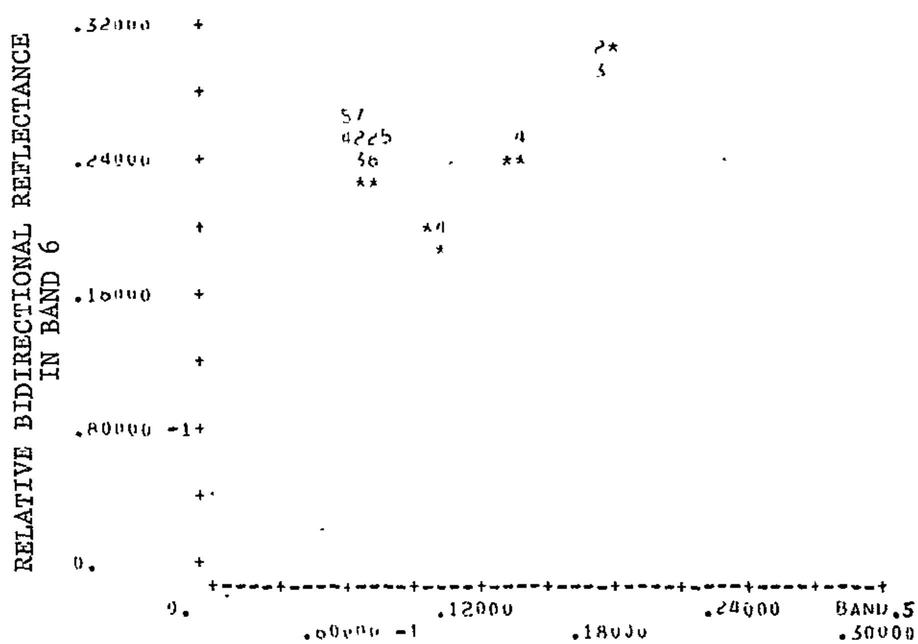

(f) Stage 5, Senescing

FIGURE 23. DEPENDENCE OF RELATIVE BIDIRECTIONAL REFLECTANCE ON CANOPY STRUCTURE AND SOIL, LANDSAT BAND 6 VS 5. (Nine Variants Present for Each Growth Stage Number) (Cont'd)

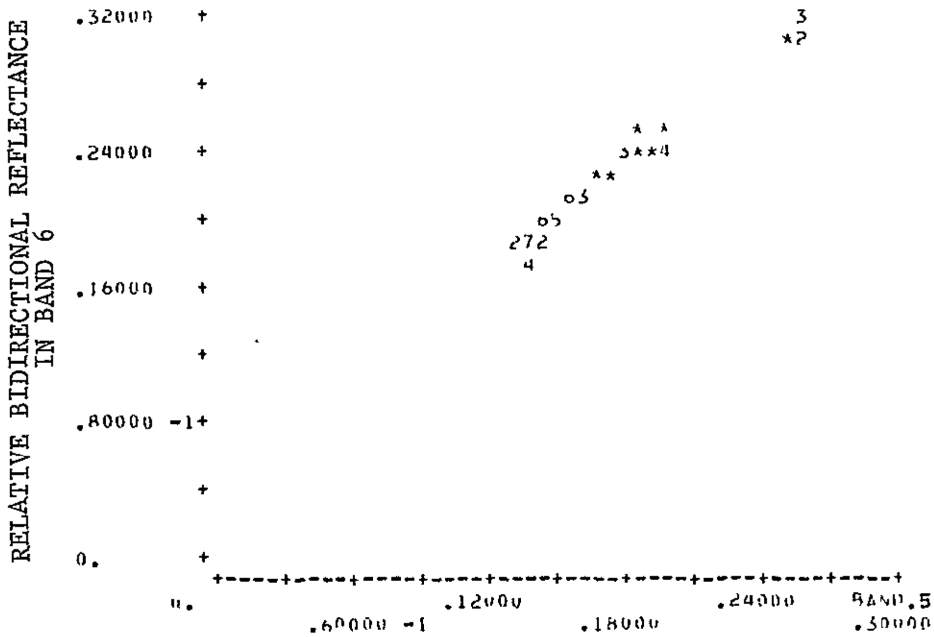

(g) Stage 6, Ripe

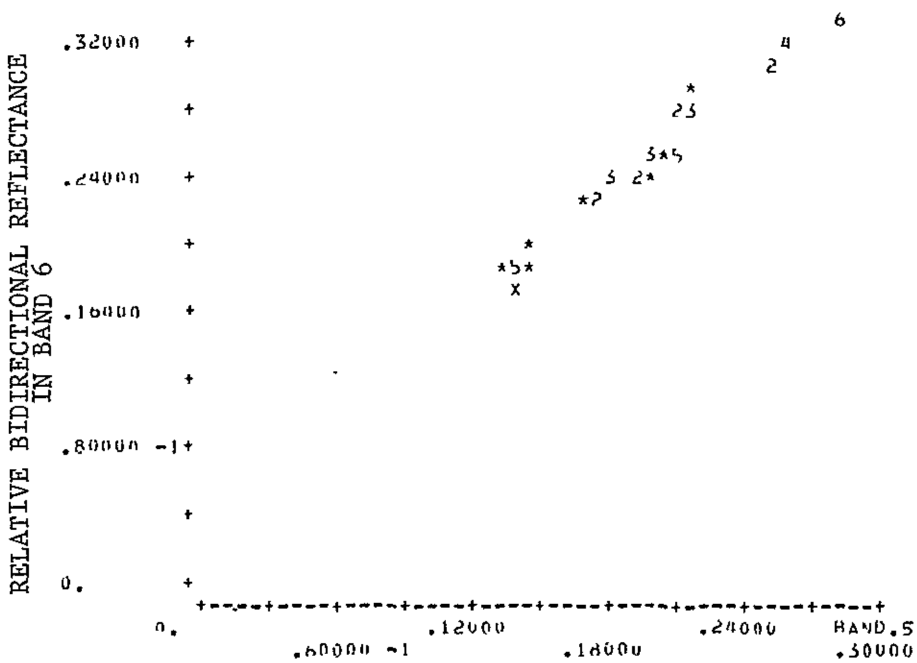

(h) Stage 7, Harvested

FIGURE 23. DEPENDENCE OF RELATIVE BIDIRECTIONAL REFLECTANCE ON CANOPY STRUCTURE AND SOIL, LANDSAT BAND 6 VS 5. (Nine Variants Present for Each Growth Stage Number) (Concluded)

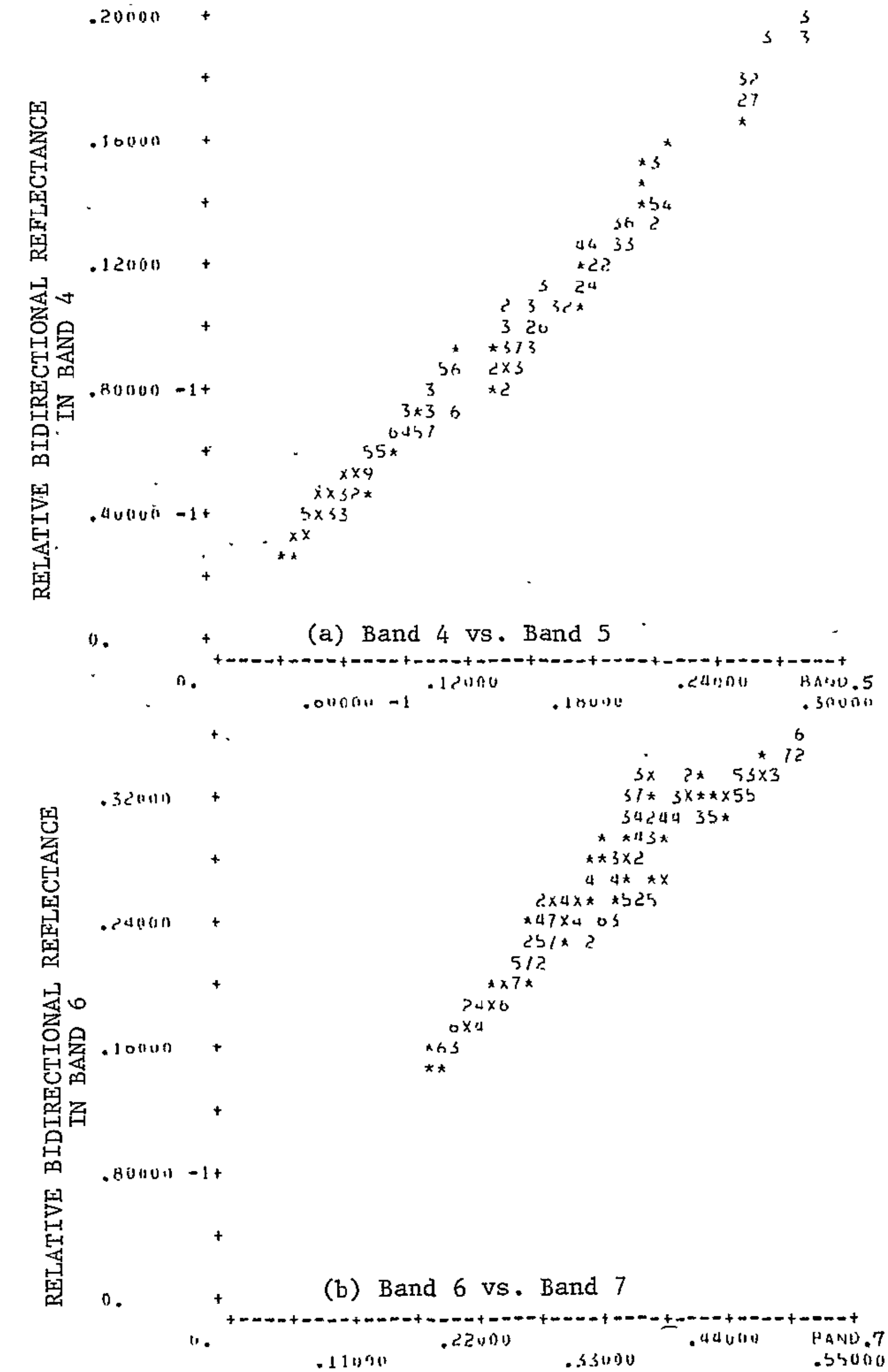

FIGURE 24. DISPLAY OF CORRELATION OF BIDIRECTIONAL REFLECTANCE BETWEEN LANDSAT BANDS 4 AND 5 AND BANDS 6 AND 7, COMPOSITE OF ALL GROWTH STAGES

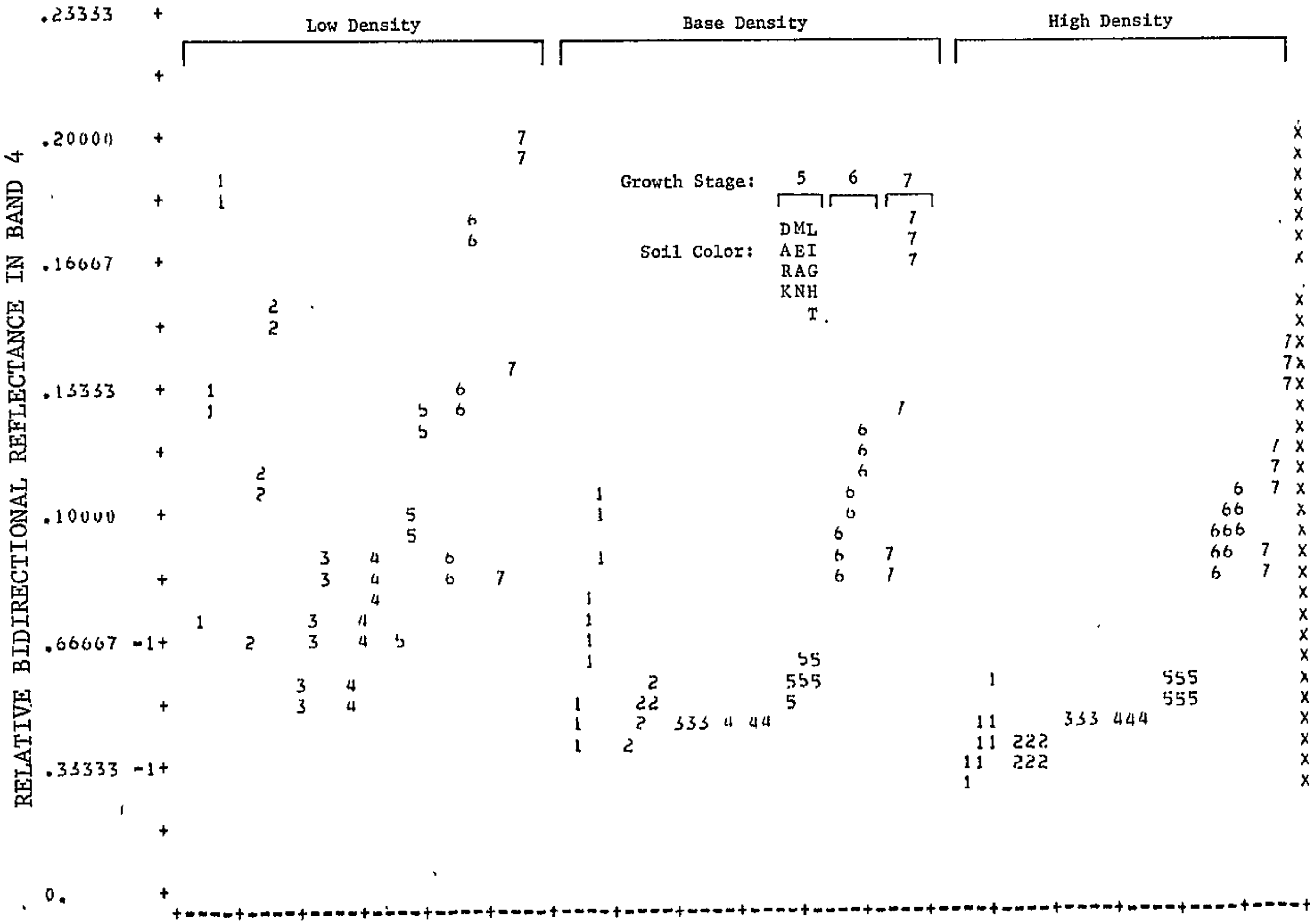

Part (a) LANDSAT Band 4, 0.5-0.6 μm

FIGURE 25. INFLUENCE OF SOIL COLOR, GROWTH STAGE, AND CANOPY DENSITY ON INBAND REFLECTANCE VALUES (Cont'd)

ORIGINAL PAGE IS OF POOR QUALITY

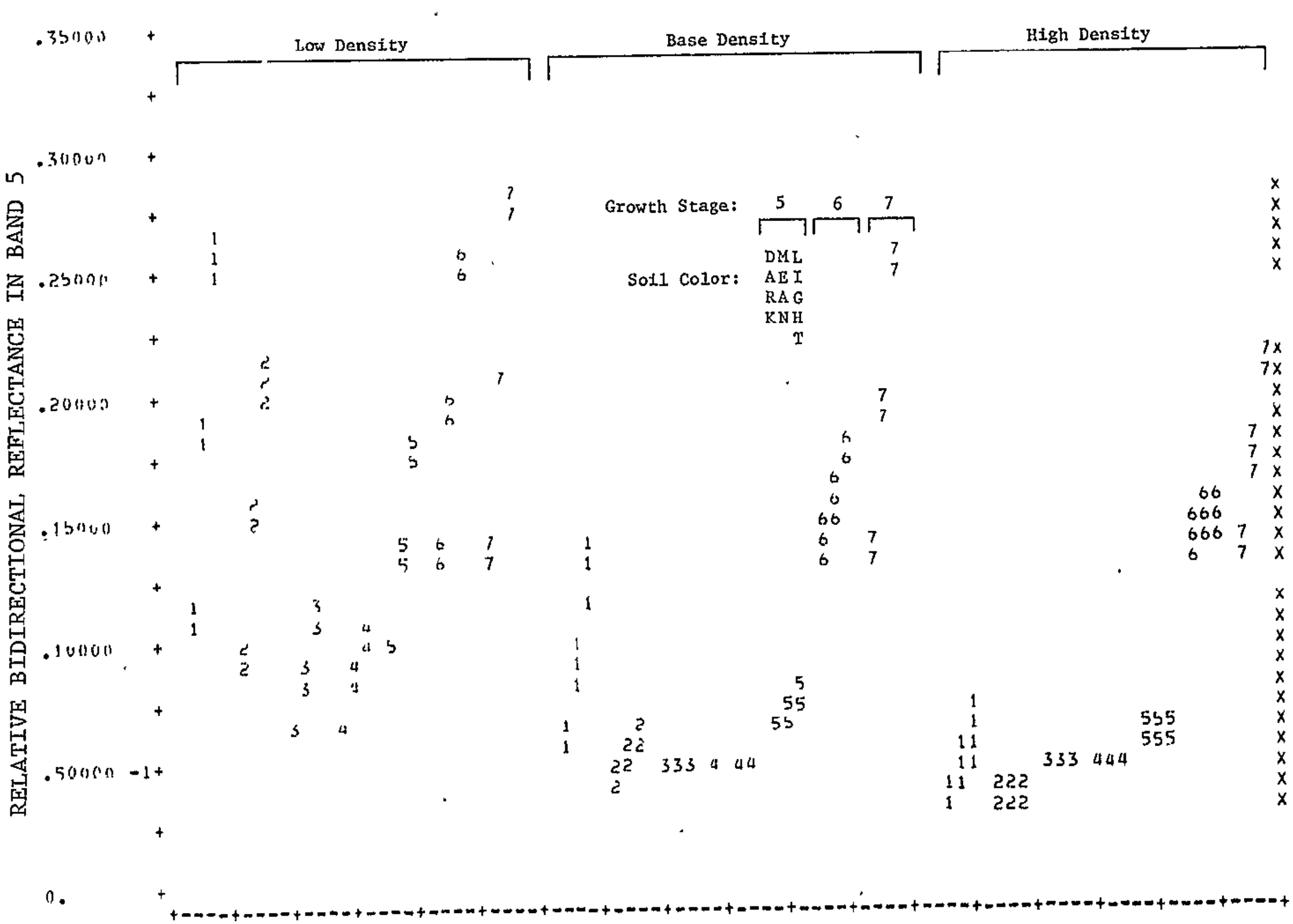

Part (b) LANDSAT Band 5, 0.6–0.7 μm

FIGURE 25. INFLUENCE OF SOIL COLOR, GROWTH STAGE, AND CANOPY DENSITY ON INBAND REFLECTANCE VALUES (Cont'd)

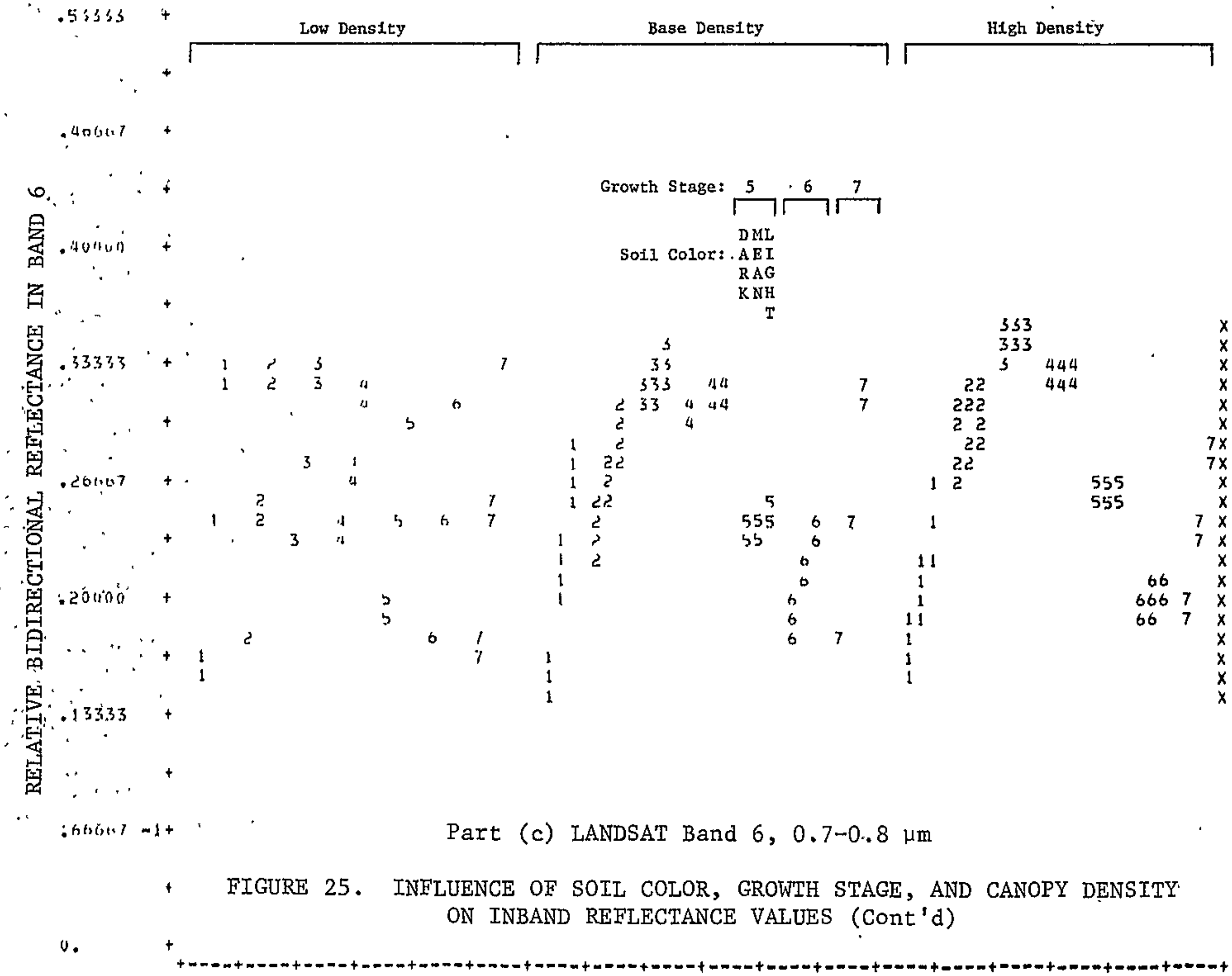

Part (c) LANDSAT Band 6, 0.7-0.8 μm

FIGURE 25. INFLUENCE OF SOIL COLOR, GROWTH STAGE, AND CANOPY DENSITY ON INBAND REFLECTANCE VALUES (Cont'd)

ORIGINAL PAGE IS
OF POOR QUALITY

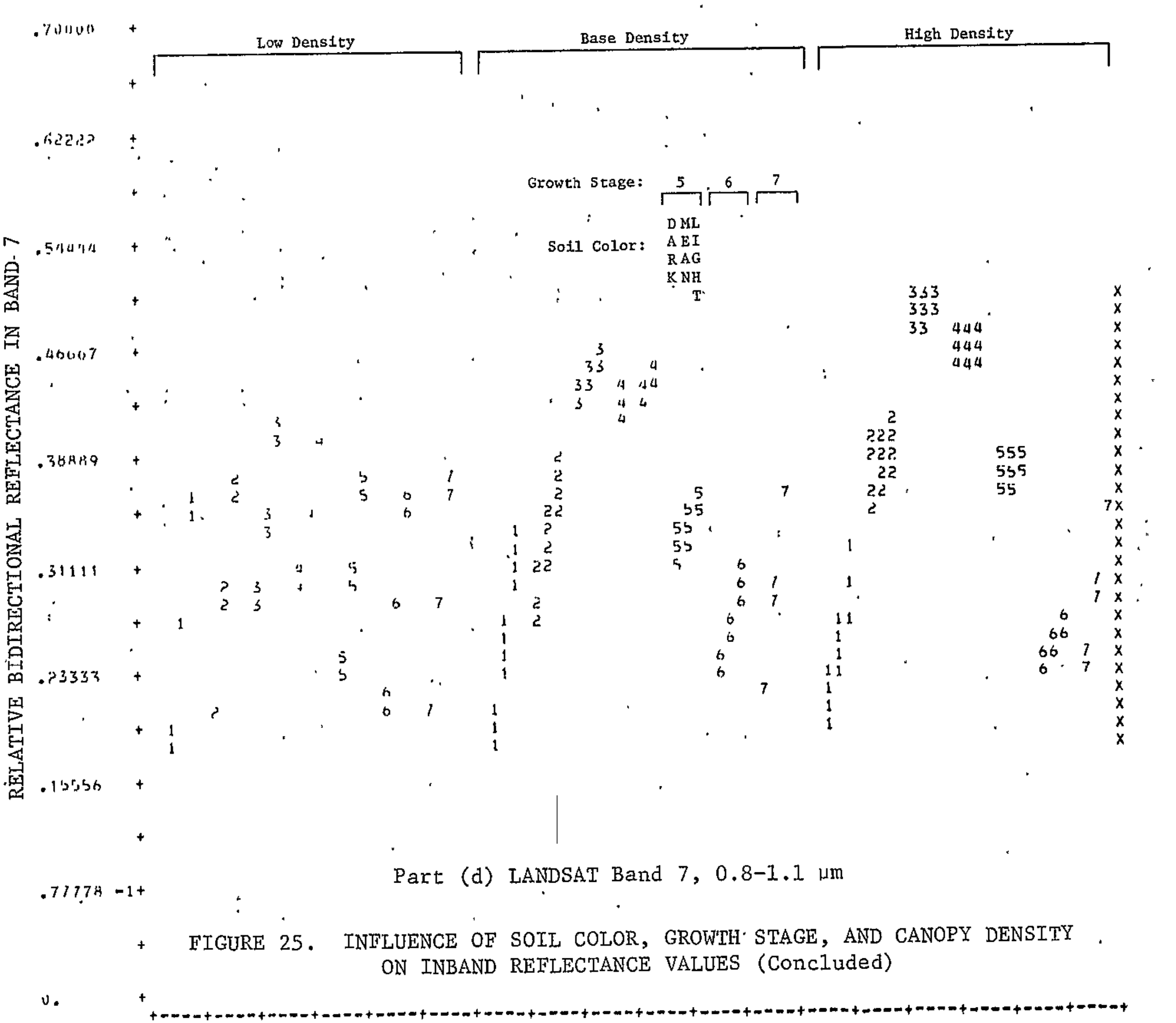

Part (d) LANDSAT Band 7, 0.8-1.1 μm

FIGURE 25. INFLUENCE OF SOIL COLOR, GROWTH STAGE, AND CANOPY DENSITY ON INBAND REFLECTANCE VALUES (Concluded)

Another observation is that the effect of heading is most noticeable in Bands 6 and 7 for high density canopies; other than that, the effect does not appear to be distinguishable.

Discussion of other important factors, such as scanner view angle, is deferred to Sec. 6.6 where the combined effects of both diffuse and bidirectional reflectance and atmospheric features are examined in the simulated total radiances.

6.5 ATMOSPHERIC FEATURE CALCULATIONS

Atmospheric feature calculations provided both irradiance spectra to represent the radiation incident on the wheat fields and transmittance and path radiance spectra to represent the atmosphere's effects on signals passing through it from the ground to the satellite sensor. The key factors are atmospheric visibility (indicated by the visual range associated with the standard atmosphere employed), background reflectance, scanner view angle, and time of year.

Figs. 26 and 27 present displays of direct and diffuse irradiances in Landsat Band 4 at 38^{o}N latitude and 10:45 AM local time for the seven times of year of interest in this study. The time of year is indicated by the brackets at the bottom of the seven groups of data points, where D1 through D7 refer to the growth stage simulation dates 1 through 7, respectively, in Table 13.

The direct irradiance in Fig. 26 is independent of scanner view angle and background reflectance but dependent on time of year and atmospheric visibility. However, the diffuse irradiance in Fig. 27 shows some variability for a fixed atmospheric visibility and time of year, due to the three different background reflectances used. Both irradiances vary in a similar manner with respect to the seven times of year but, whereas direct irradiance decreases with decreasing atmospheric visibility, the diffuse irradiance increases.

Figs. 28 and 29 present displays for Bands 4 and 6, respectively, of path radiance as a function of the three scan angles, seven times

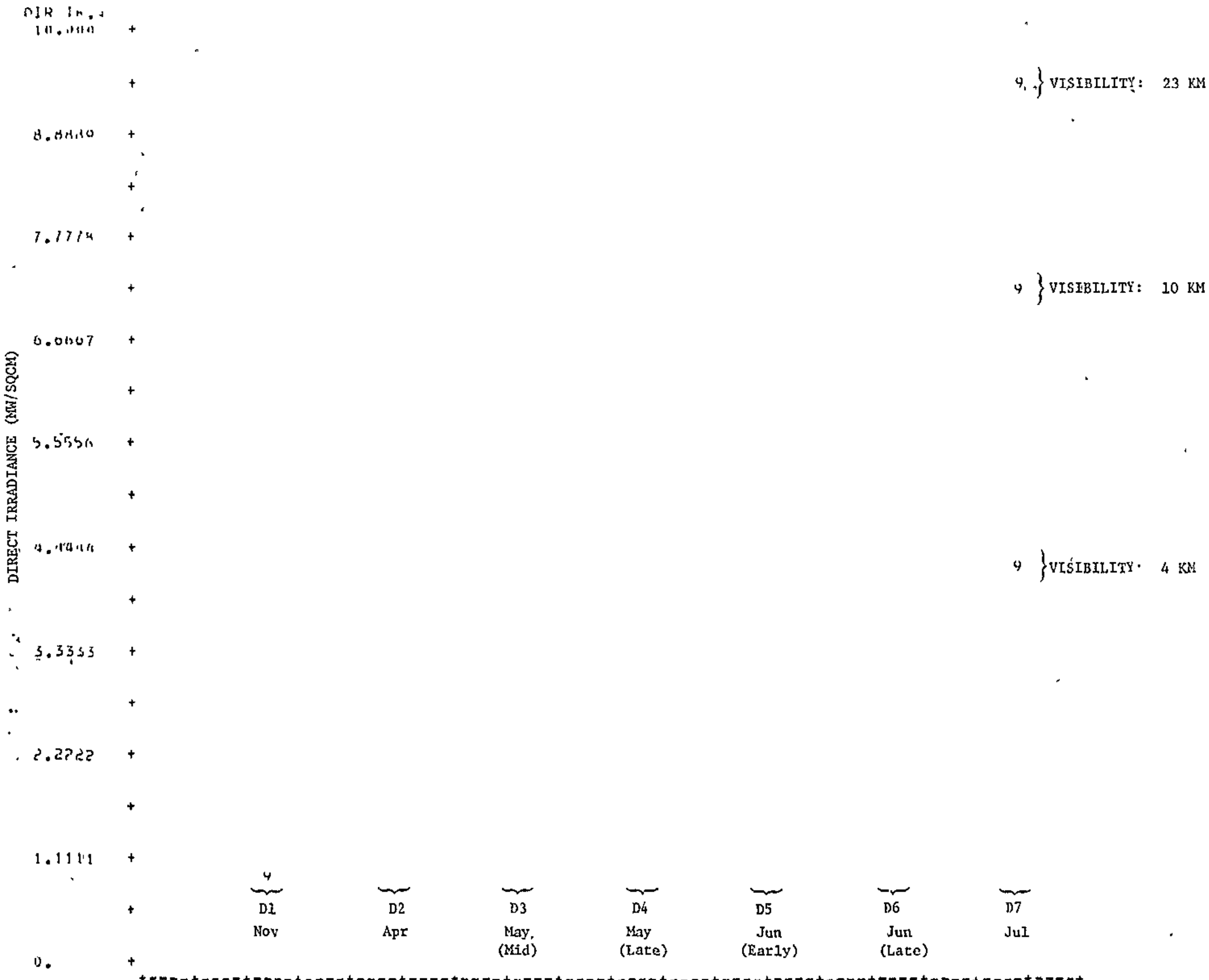

FIGURE 26. INFLUENCE OF TIME OF YEAR AND ATMOSPHERIC VISIBILITY ON INBAND DIRECT IRRADIANCE (LANDSAT BAND 4, 0.5-0.6 um)

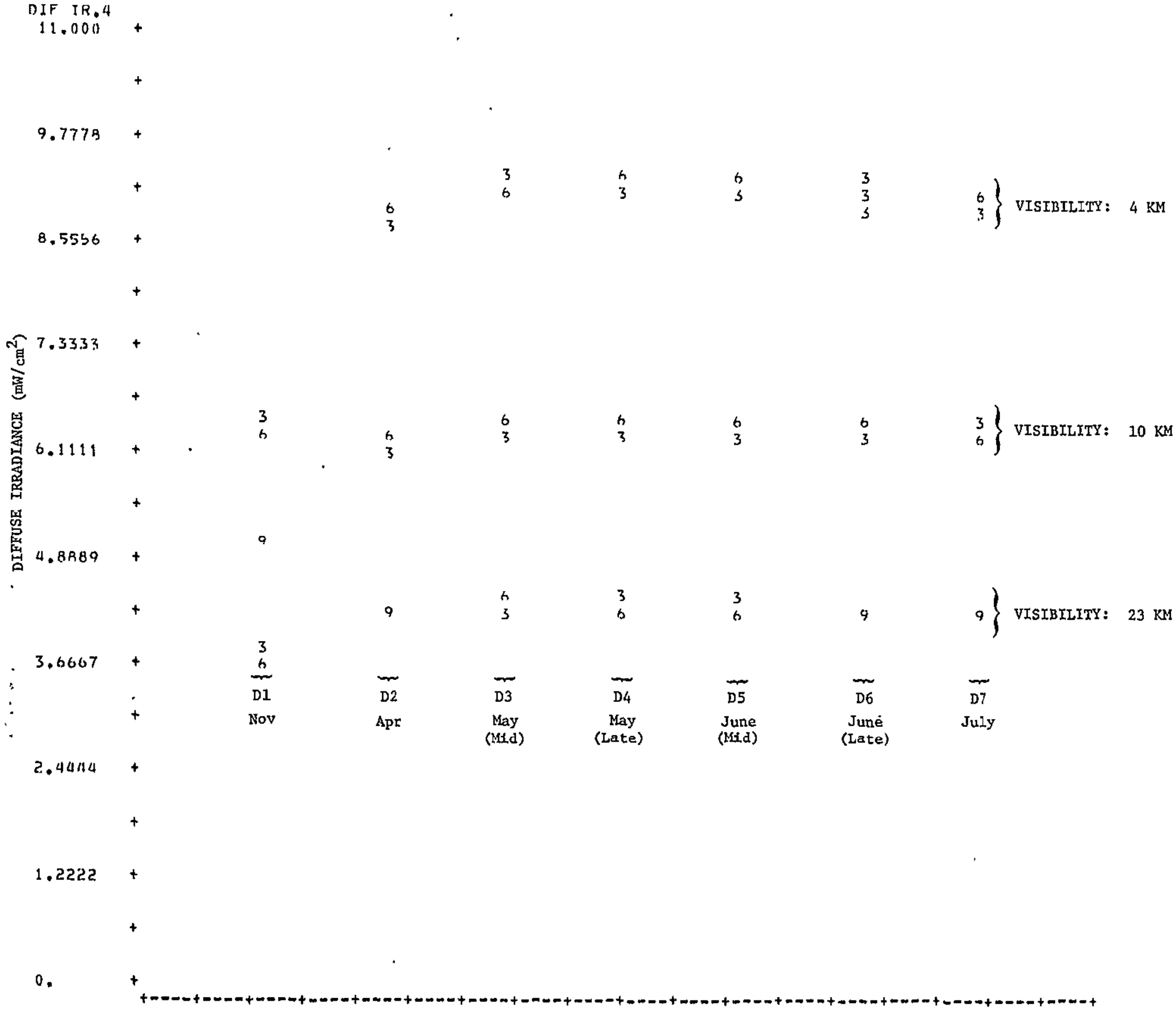

FIGURE 27. INFLUENCE OF TIME OF YEAR AND ATMOSPHERIC VISIBILITY ON INBAND DIFFUSE IRRADIANCE (LANDSAT BAND 4, 0.5-0.6 μm)

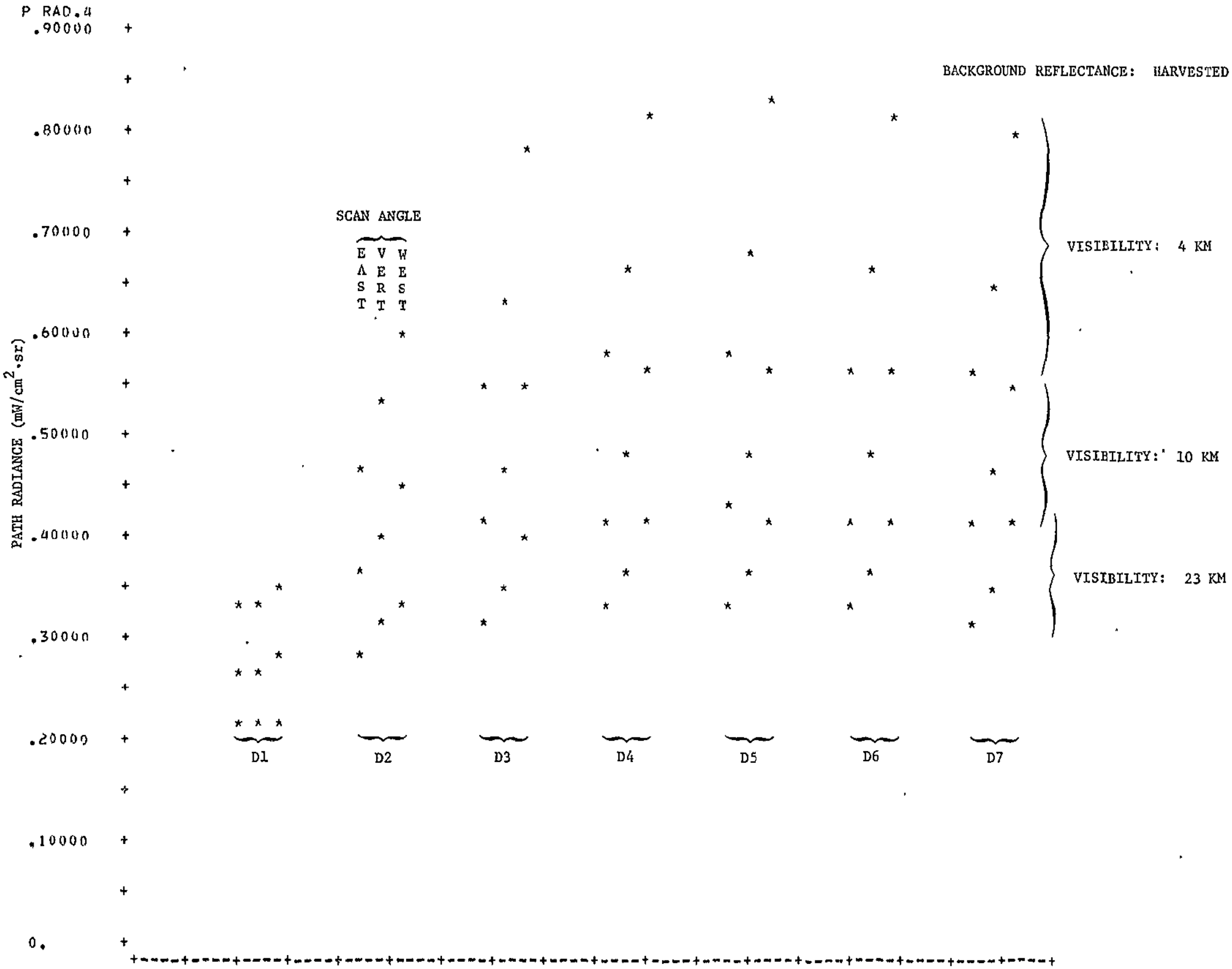

FIGURE 28. INFLUENCE OF TIME OF YEAR, SCAN ANGLE AND VISIBILITY ON INBAND PATH RADIANCE (LANDSAT BAND 4, 0.5–0.6 μm)

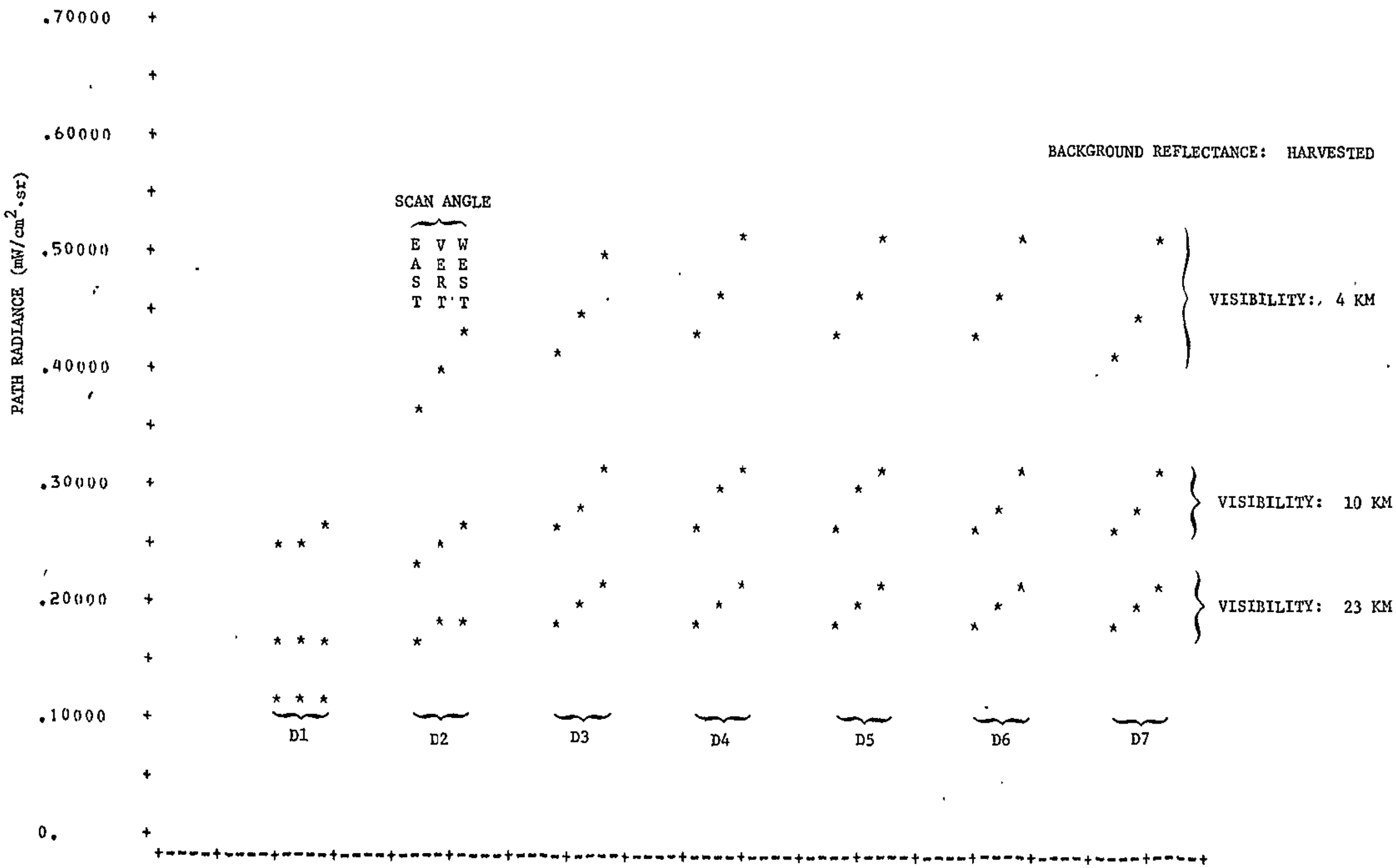

FIGURE 29. INFLUENCE OF TIME OF YEAR, SCAN ANGLE AND VISIBILITY ON INBAND PATH RADIANCE (LANDSAT BAND 6, 0.7-0.8 μm)

of year and three sets of atmospheric conditions, at 38°N latitude with background reflectance spectrum for harvested wheat. The variation of path radiance with scan angle is represented by the three successive data points associated with a particular time of year and background reflectance. From left to right these three points indicate the path radiance for scan angles of -6°, 0° and 6° along a straight line from the East toward the West. With the sun in the East, the path radiance increases for such a set of scan angles. These figures indicate the increase in path radiance to be expected as the atmospheric visibility decreases. They also indicate that the variability of the path radiance, as a function of scan angle, increases as its magnitude increases.

Figs. 30 and 31 represent scatter plots of the path radiance in Bands 4 and 6, respectively, as a function of scan angle for three sets of atmospheric conditions and three sets of background reflectances for one time of year. The figures indicate the increase in both the magnitude of the path radiance and its variability with respect to scan angle, as the atmospheric visibility decreases. These figures also indicate the extent to which path radiance depends on background reflectance.

The atmospheric transmittance in Bands 4 and 6 is displayed, respectively, in Figs. 32 and 33, as a function of scan angle and atmospheric visibility. The transmittance decreases significantly with decreasing atmospheric visibility but varies very little over the three scan angles of interest.

6.6 TOTAL INBAND (LANDSAT) RADIANCE SIMULATIONS

The wheat canopy reflectance and atmospheric effects calculations have been combined to produce simulated Landsat radiances for all combinations of levels of the various factors of interest in this investigation, as listed in Table 12. The total number of cases for which radiance values have been simulated is 3402, determined as the product of the number of levels of each factor. This large number has prevented

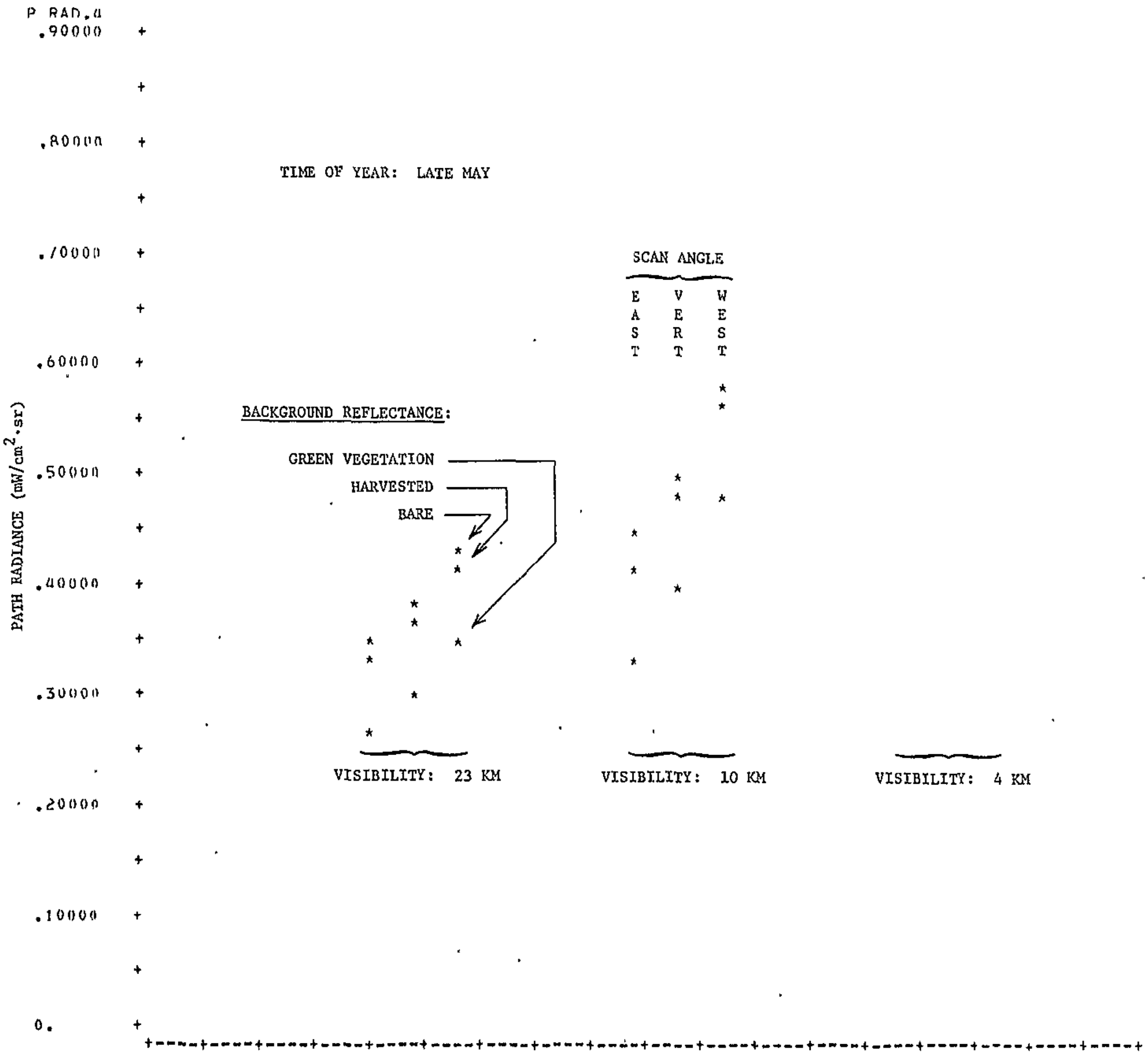

FIGURE 30. INFLUENCE OF SCAN ANGLE, ATMOSPHERIC VISIBILITY AND BACKGROUND REFLECTANCE ON INBAND PATH RADIANCE (LANDSAT BAND 4, 0.5-0.6 μm)

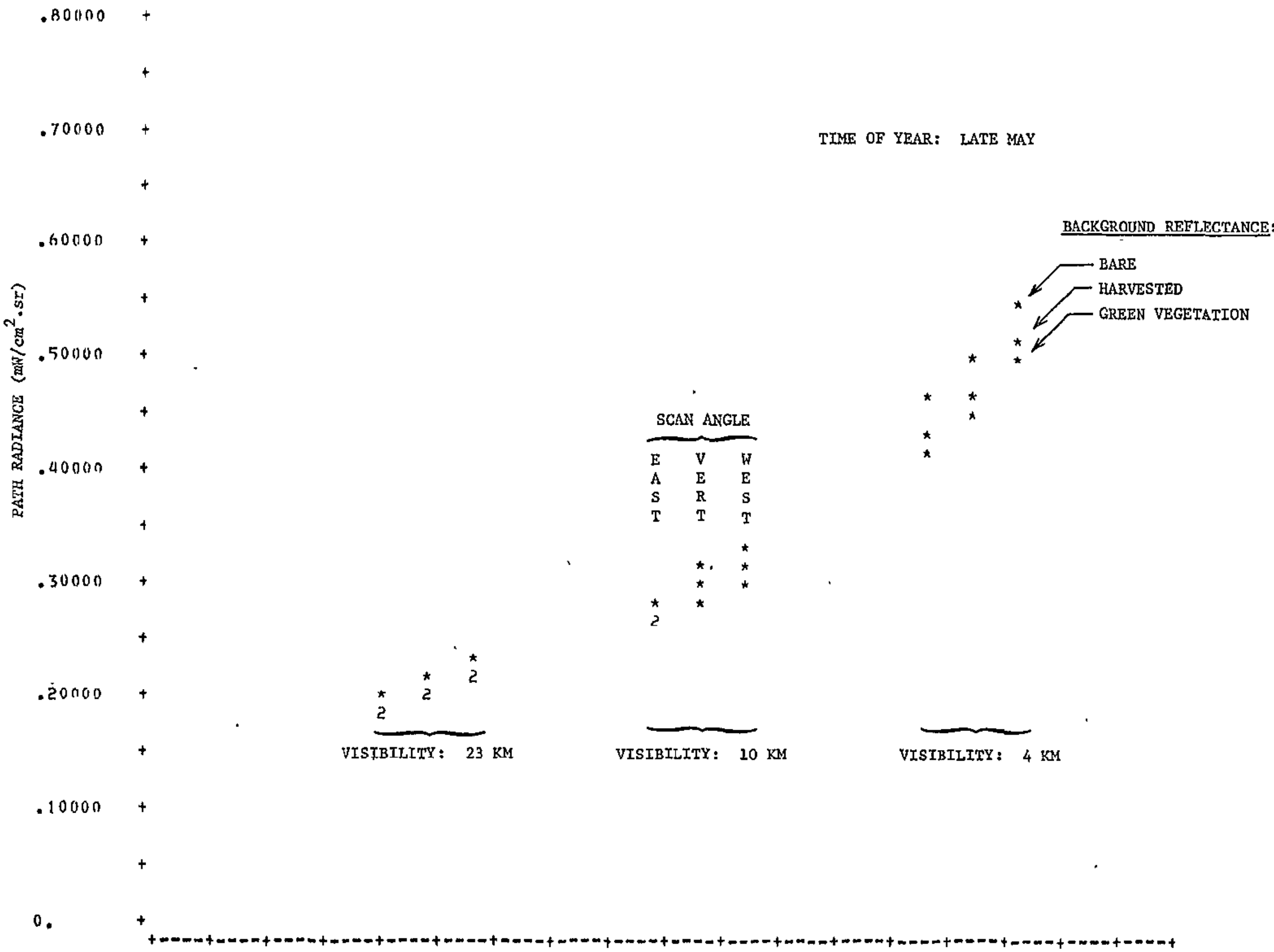

FIGURE 31. INFLUENCE OF SCAN ANGLE, ATMOSPHERIC VISIBILITY AND BACKGROUND REFLECTANCE ON INBAND PATH RADIANCE (LANDSAT BAND 6, 0.7–0.8 μm)

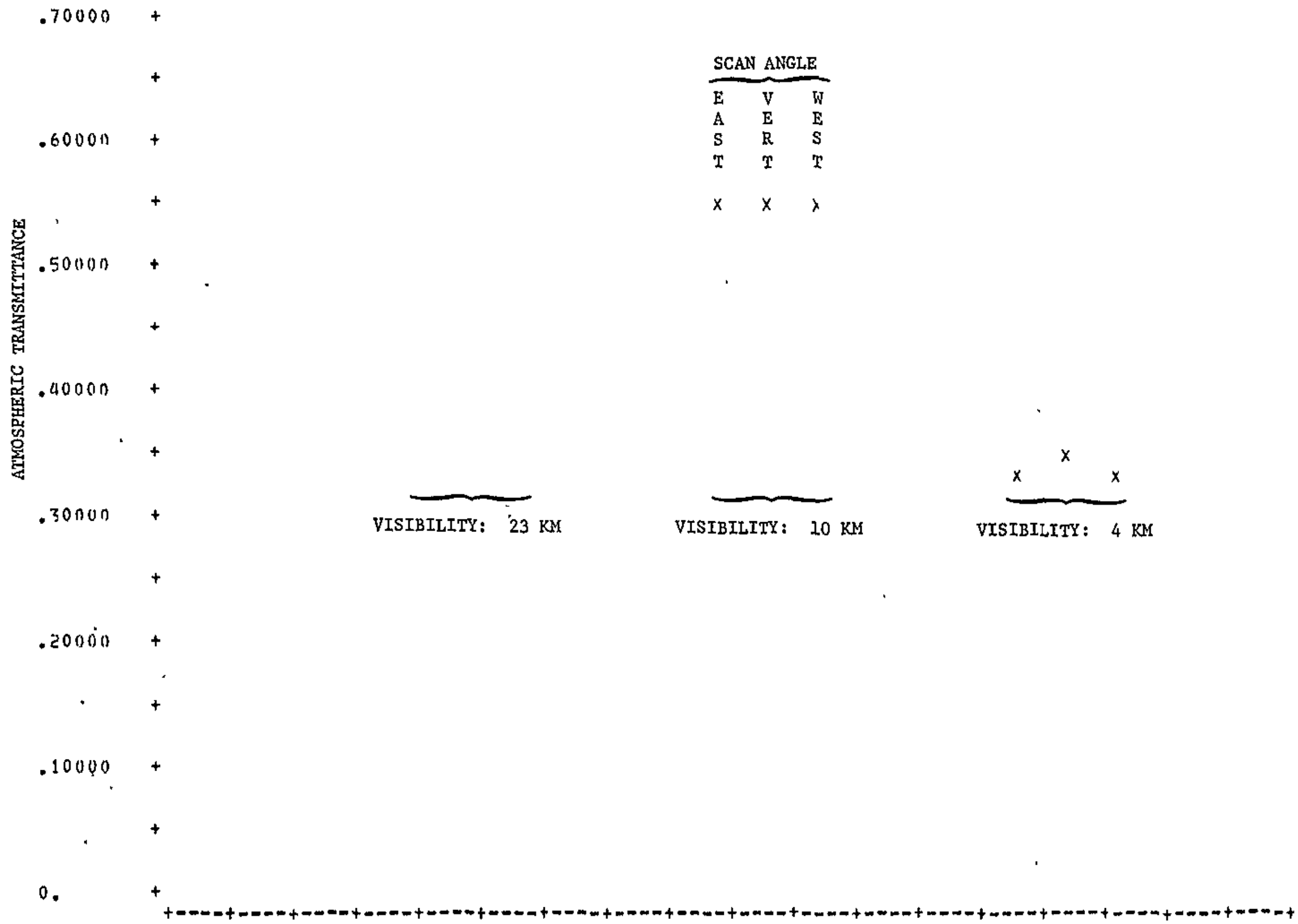

FIGURE 32. INFLUENCE OF SCAN ANGLE AND ATMOSPHERIC VISIBILITY ON INBAND ATMOSPHERIC TRANSMITTANCE (LANDSAT BAND 4, 0.5-0.6 μm)

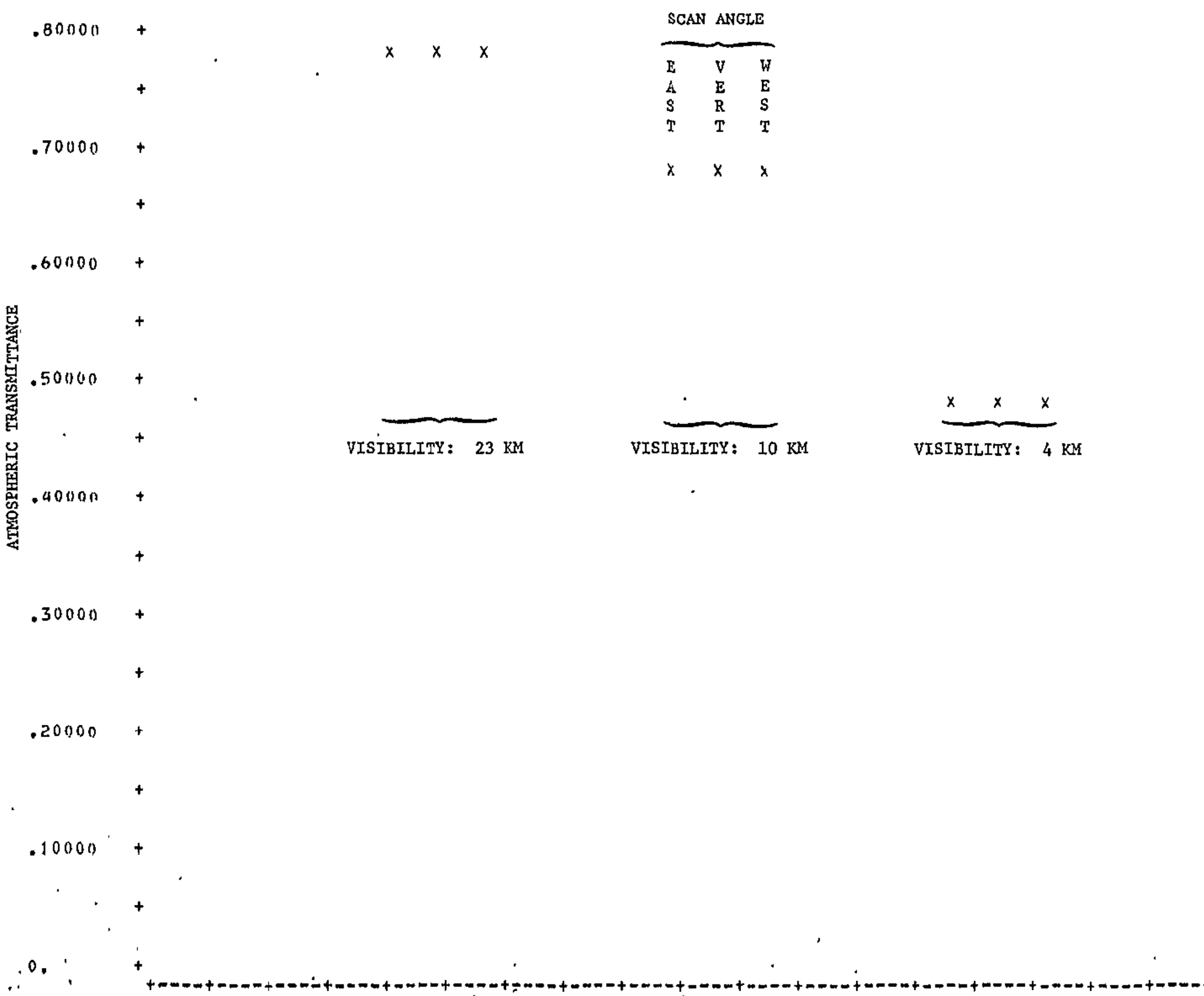

FIGURE 33. INFLUENCE OF SCAN ANGLE AND ATMOSPHERIC VISIBILITY ON INBAND ATMOSPHERIC TRANSMITTANCE (LANDSAT BAND 6, 0.7-0.8 μm)

an exhaustive analysis of this data set from being undertaken during the time frame of this effort. However, some analysis has been conducted in an attempt to determine, at least qualitatively, the effects on Landsat radiances of variations in the level of each of these factors of interest. Table 15 presents a series of average values of the simulated radiances in each Landsat band, each average being taken over all cases for a particular level of one factor. The levels and factors over which the averages are taken are indicated in the two leftmost columns of the table. This table is useful for indicating gross trends in the simulated radiances over the various levels of any particular factor.

Figs. 34-59 are scatter plots of simulated radiances in selected Landsat bands displaying both the domain of these radiances and their variability with respect to the various levels of particular subsets of factors. Figs. 34-36 are two-dimensional scatter plots of simulated radiances in selected pairs of bands; those bands being 4 vs 5, 6 vs 5, and 6 vs 7, respectively. It is of interest to compare these radiances scatter plots to the canopy reflectance scatter plots (Figs. 23 and 24). This comparison indicates a similar pattern in the variations of these two quantities, with the radiances containing somewhat more variation due to the various atmospheric factors and levels affecting these radiances. This increased variation is more noticeable in Bands 4 and 5, where atmospheric effects are most significant. Figs. 37-43 are identical to Fig. 35, except that each plot is for a particular growth stage. These plots illustrate the variability in the simulated radiances over all growth stages and within each particular growth stage. They also indicate the changing domain of the wheat canopy radiances as the canopy progresses through its various growth stages.

Figs. 44-57 contain displays of the factor effects on simulated radiances in Bands 5 and 6 for each of the seven wheat canopy growth stages. In each figure, 81 data points are plotted, one for each

TABLE 15. AVERAGE EFFECTS OF FACTOR LEVELS OVER THE ENSEMBLE OF SIMULATED RADIANCES

FACTOR	LEVEL	AVERAGE RADIANCE ($w/cm^2 \cdot sr$) VALUE IN LANDSAT BAND: BAND 4	BAND 5	BAND 6	BAND 7
Latitude	38^oN	.594	.514	.840	1.22
	46^oN	.553	.481	.792	1.16
Visual Range	4 km	.647	.541	.795	1.13
	10 km	.558	.487	.817	1.20
	23 km	.514	.465	.837	1.24
Background Reflectance	Bare Soil	.613	.542	.802	1.14
	Green Wheat	.512	.422	.833	1.25
	Harvested Wheat	.585	.529	.814	1.18
Soil Reflectance	Mean - Sigma	.540	.454	.751	1.09
	Mean	.573	.497	.815	1.19
	Mean + Sigma	.606	.542	.883	1.29
Canopy Density	Low	.623	.573	.808	1.11
	Base	.557	.473	.814	1.20
	High	.540	.448	.828	1.26

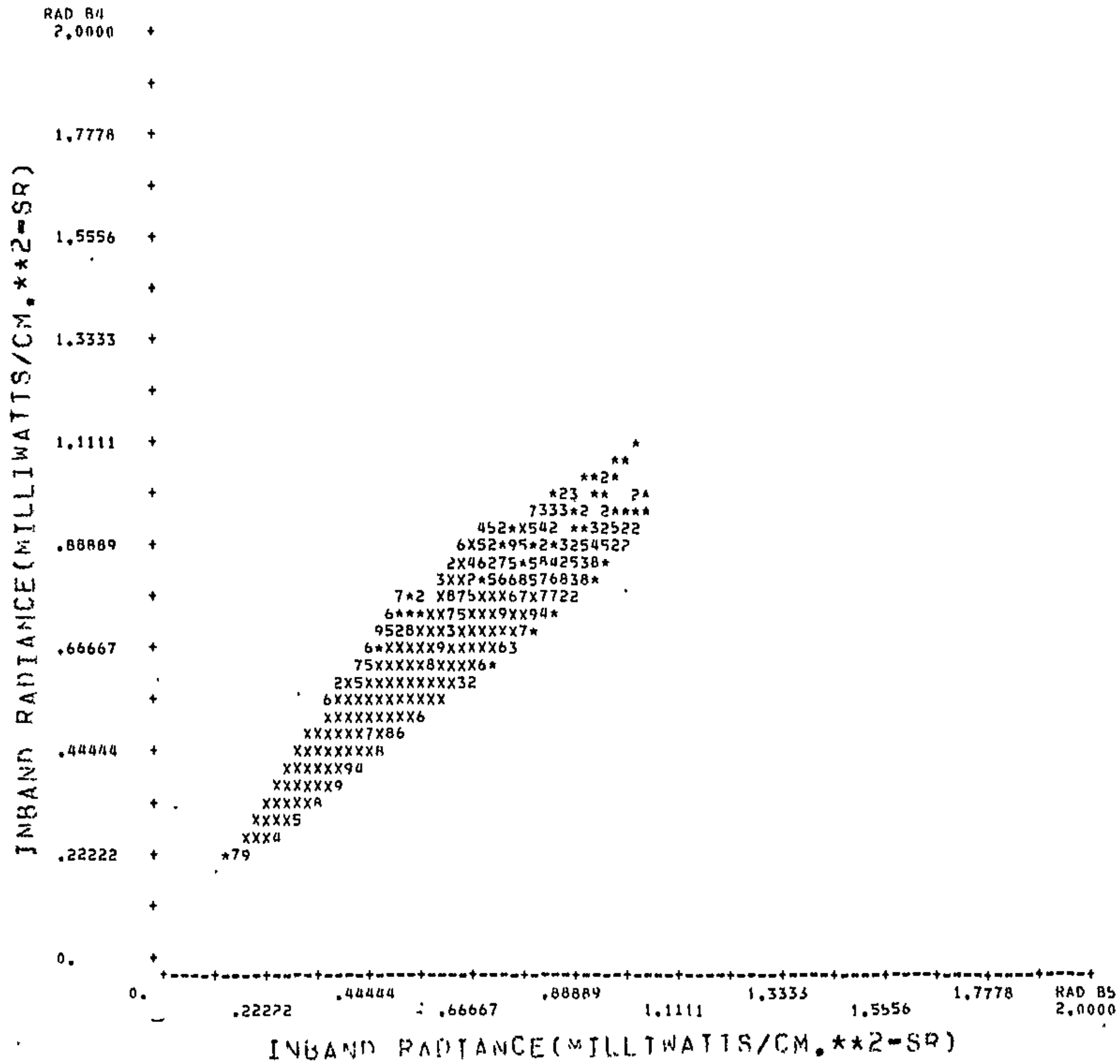

FIG.34 SPECTRAL DOMAIN OF SIMULATED LANDSAT WHEAT CANOPY RADIANCES FOR ALL GROWTH STAGES; BAND 4 VS. BAND 5

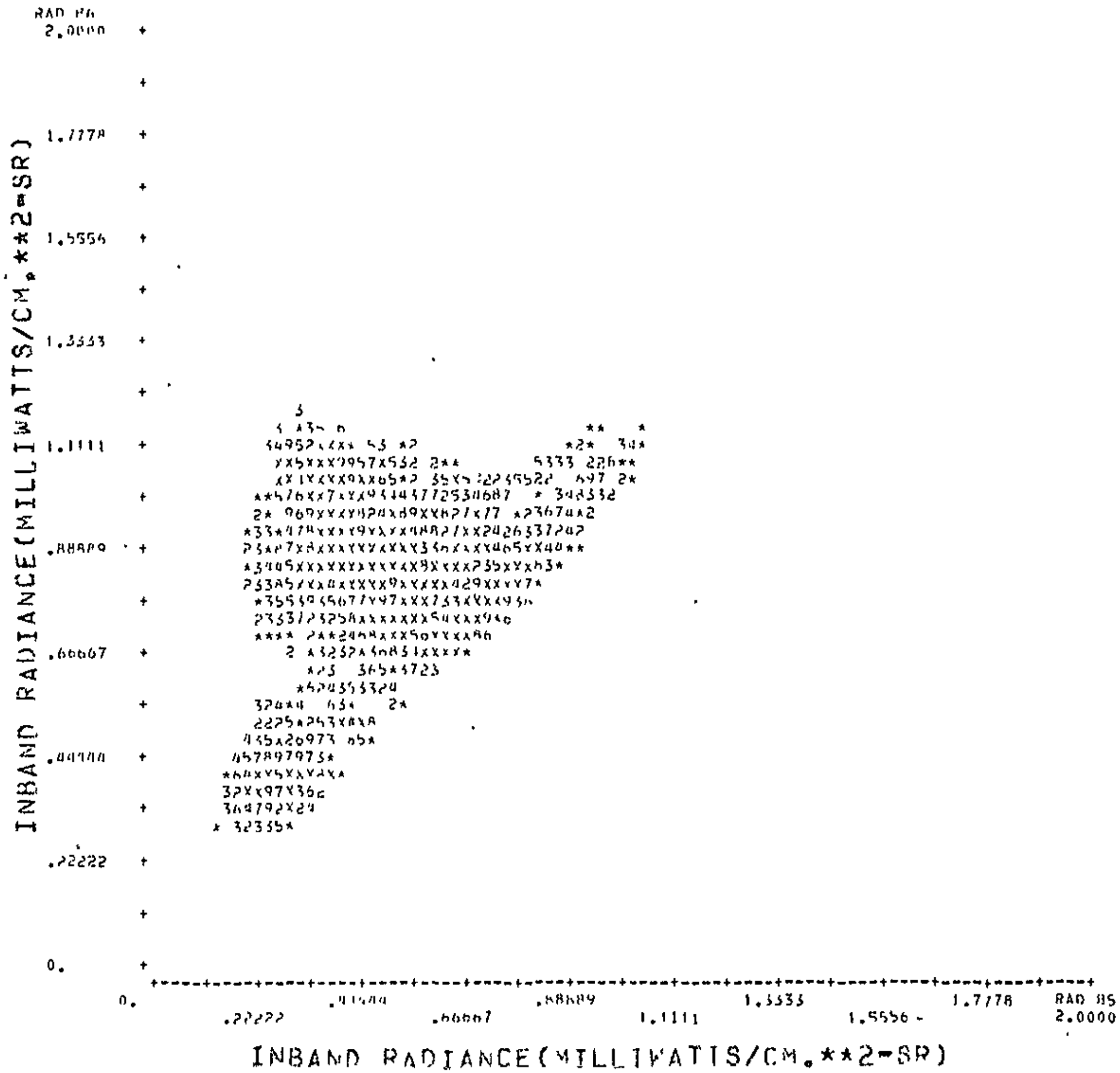

FIG.35 SPECTRAL DOMAIN OF SIMULATED LANDSAT WHEAT CANOPY RADIANCES FOR ALL GROWTH STAGES; BAND 6 VS. BAND 5

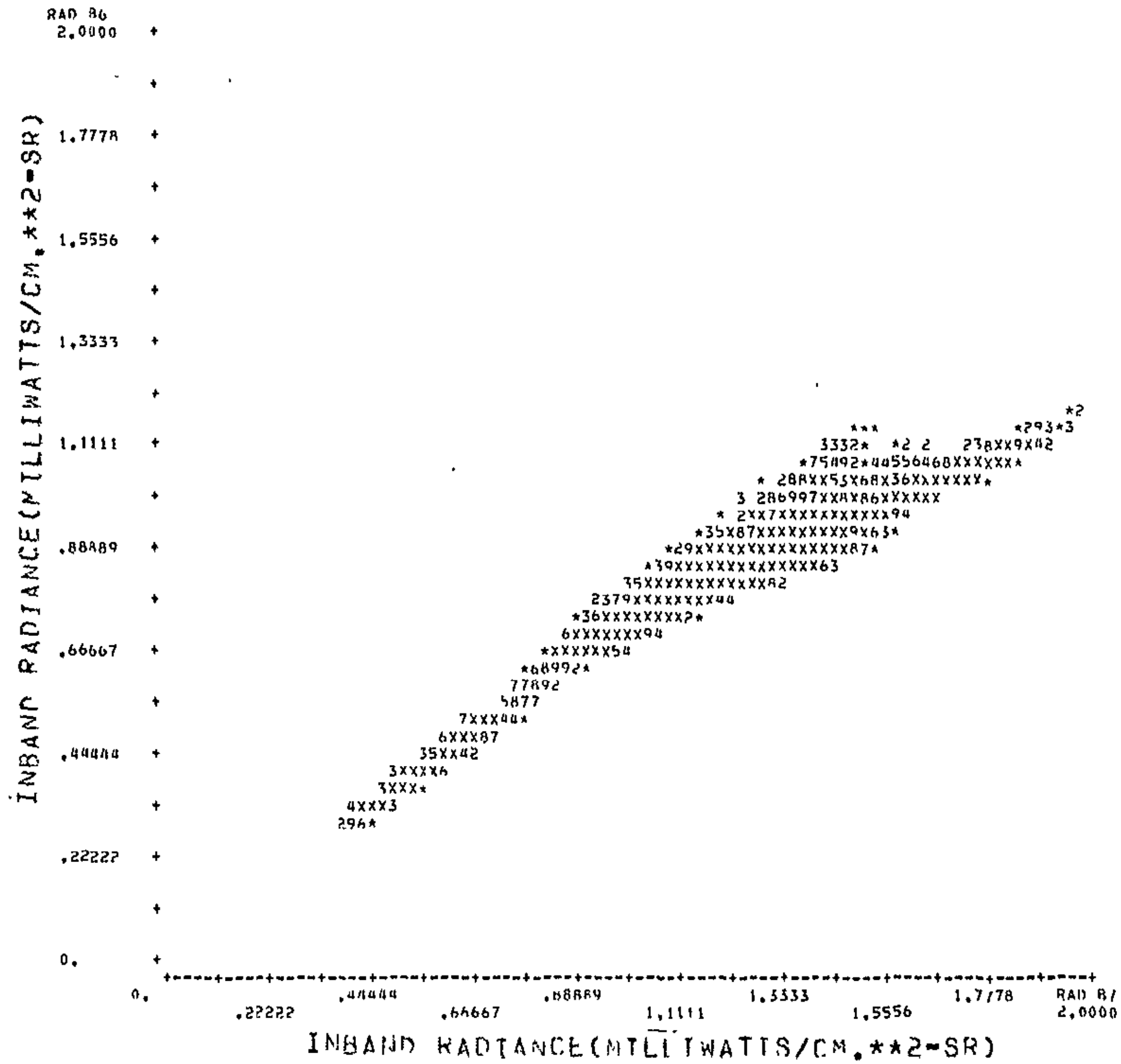

FIG.36 SPECTRAL DOMAIN OF SIMULATED LANDSAT WHEAT CANOPY RADIANCES FOR ALL GROWTH STAGES; BAND 6 VS. BAND 7

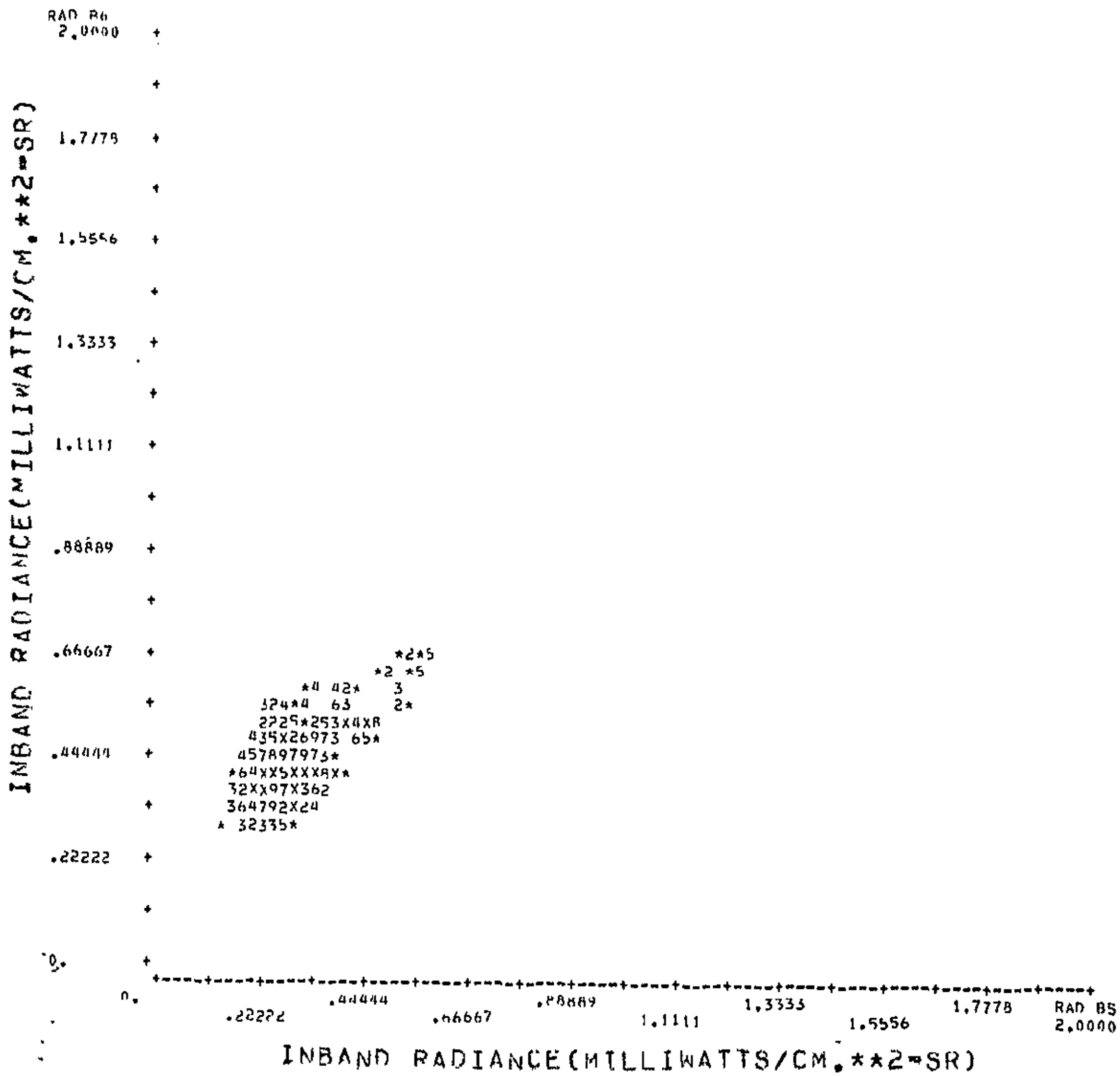

FIG.37 SPECTRAL DOMAIN OF SIMULATED LANDSAT WHEAT CANOPY RADIANCES FOR GROWTH STAGE 1; BAND 5 VS. BAND 6

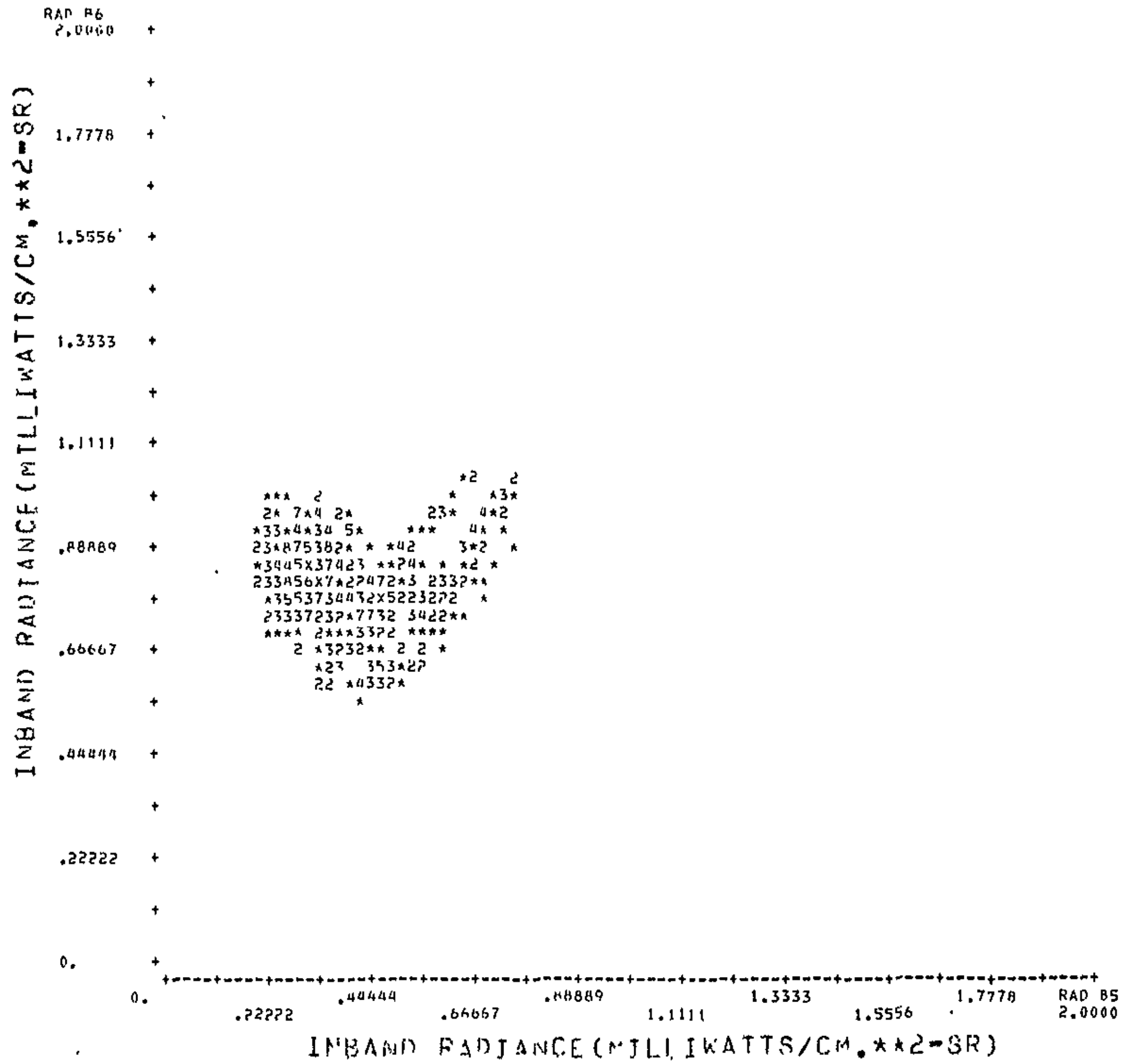

FIG.38 SPECTRAL DOMAIN OF SIMULATED LANDSAT WHEAT CANOPY RADIANCES
FOR GROWTH STAGE 2: BAND 5 VS. BAND 6

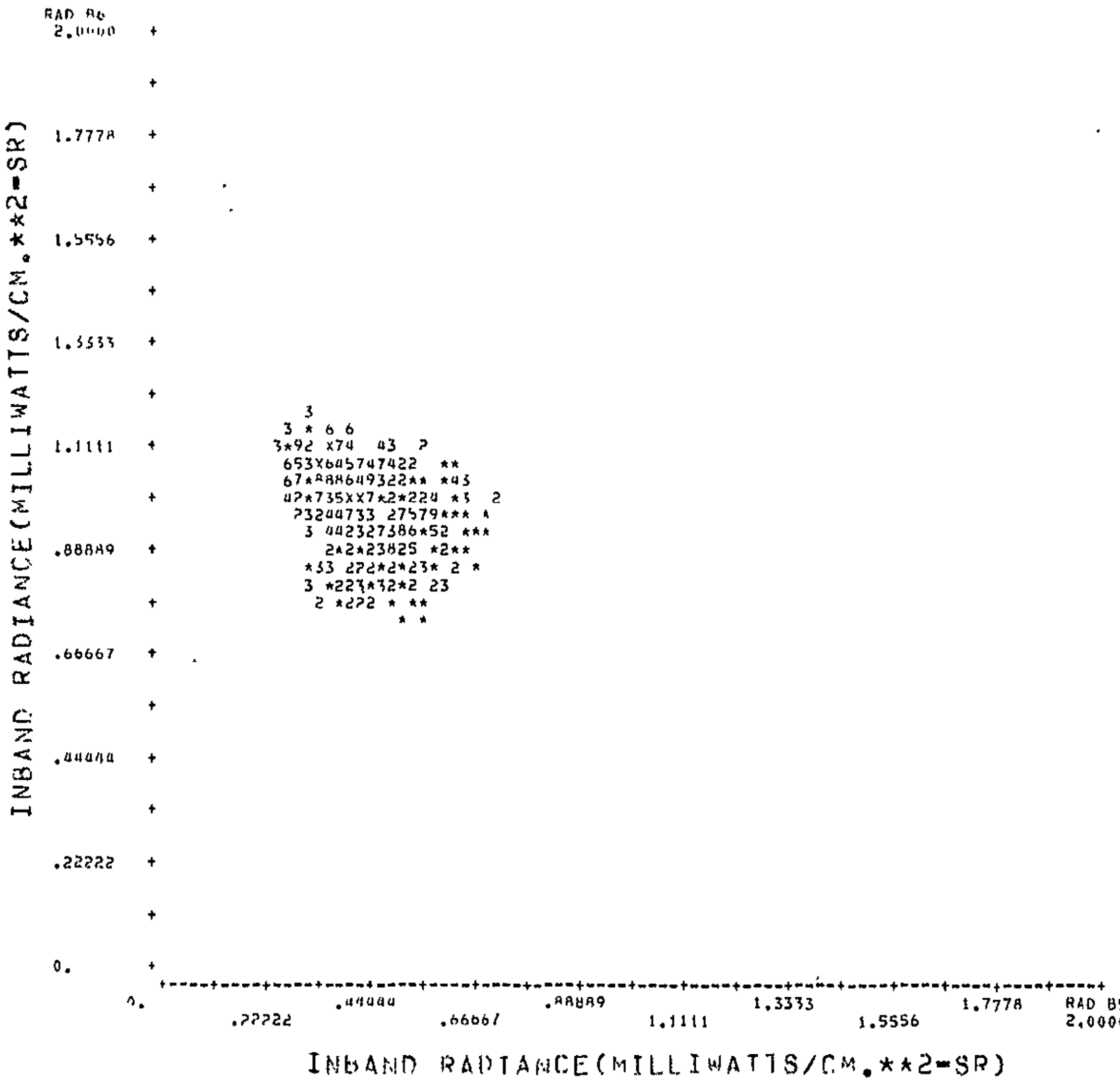

FIG.39 SPECTRAL DOMAIN OF SIMULATED LANDSAT WHEAT CANOPY RADIANCES
FOR GROWTH STAGE 3: BAND 5 VS. BAND 6

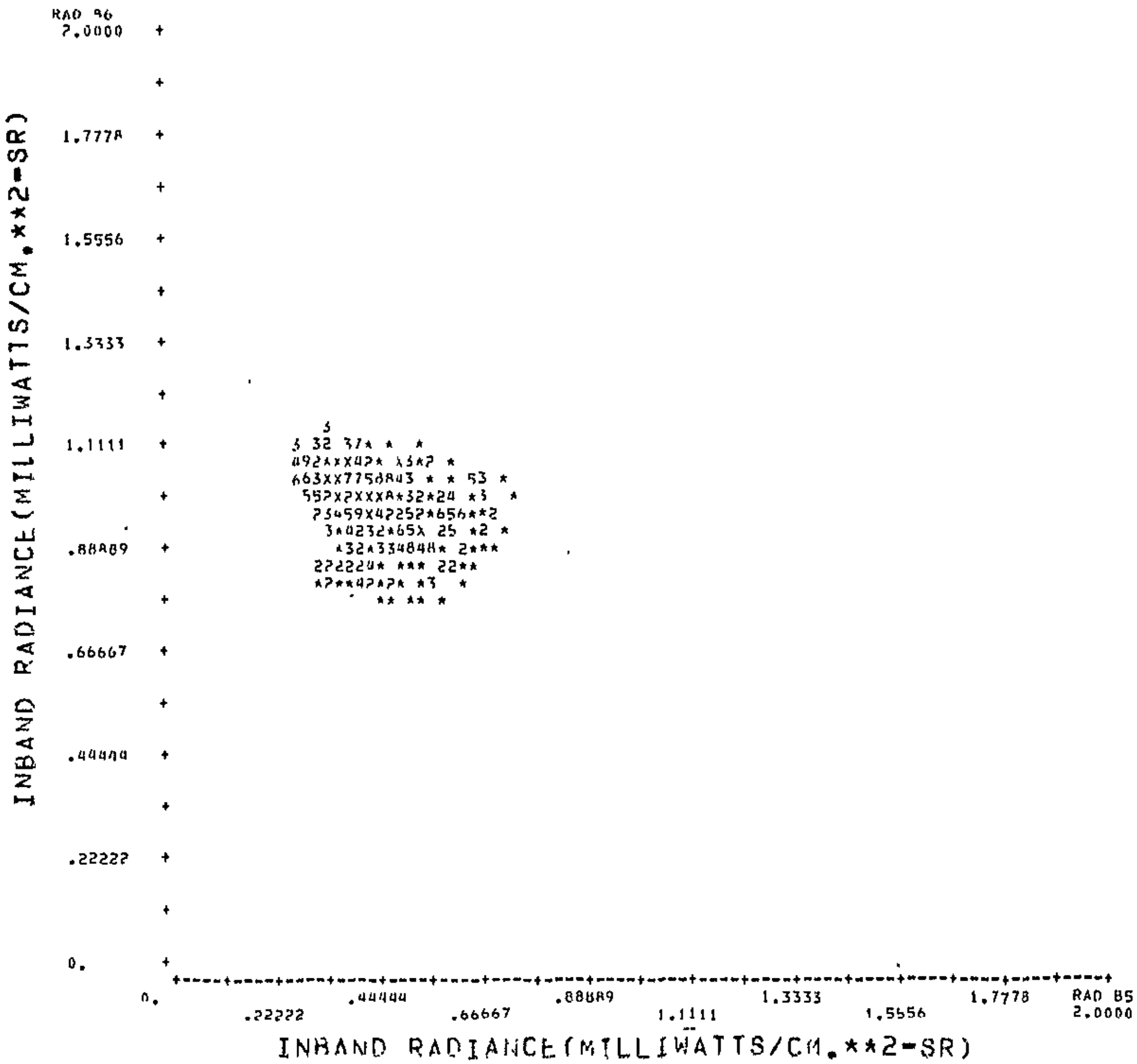

FIG.40 SPECTRAL DOMAIN OF SIMULATED LANDSAT WHEAT CANOPY RADIANCES FOR GROWTH STAGE 4; BAND 5 VS. BAND 6

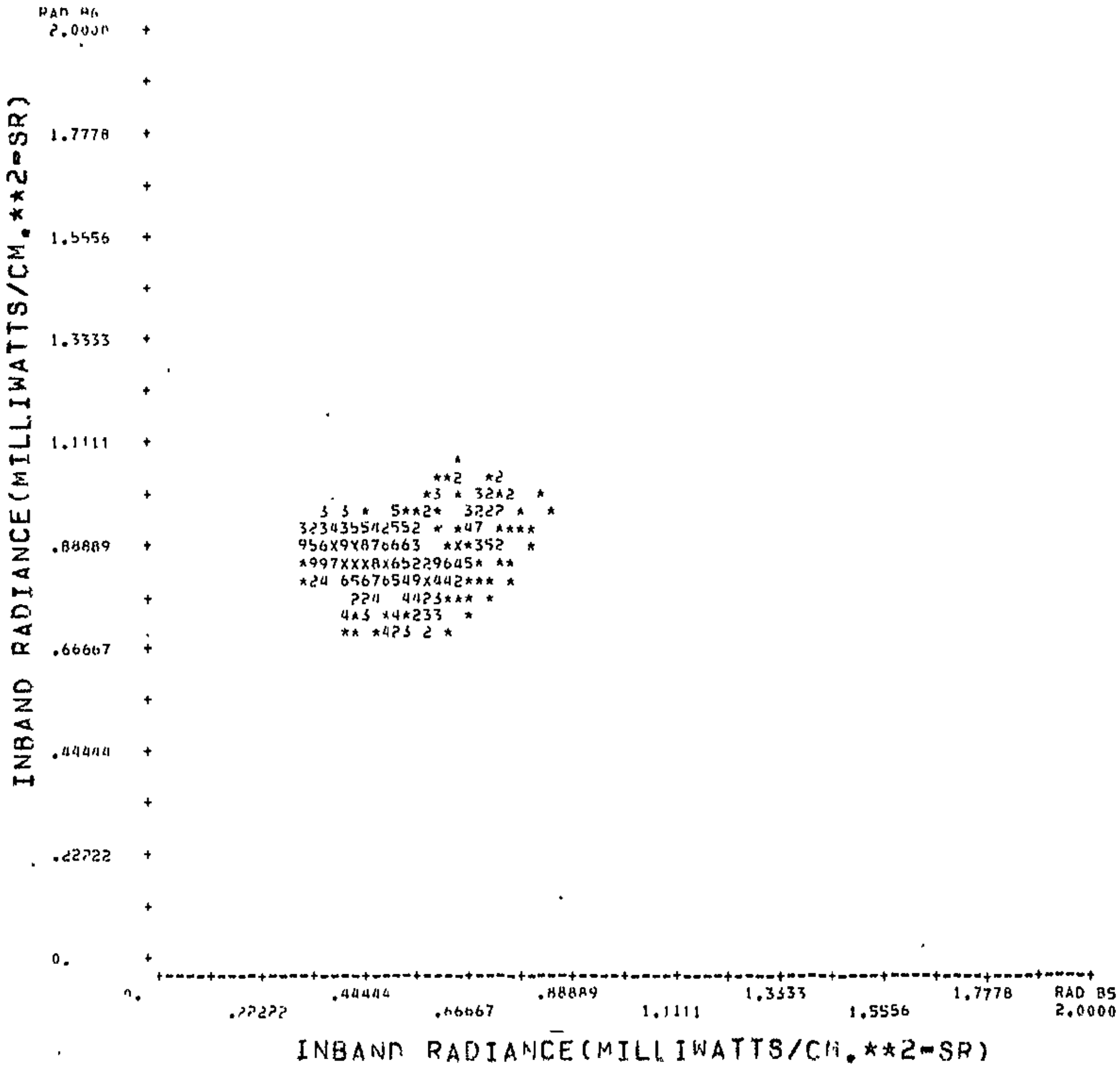

FIG.41 SPECTRAL DOMAIN OF SIMULATED LANDSAT WHEAT CANOPY RADIANCES
FOR GROWTH STAGE 5; BAND 5 VS. BAND 6

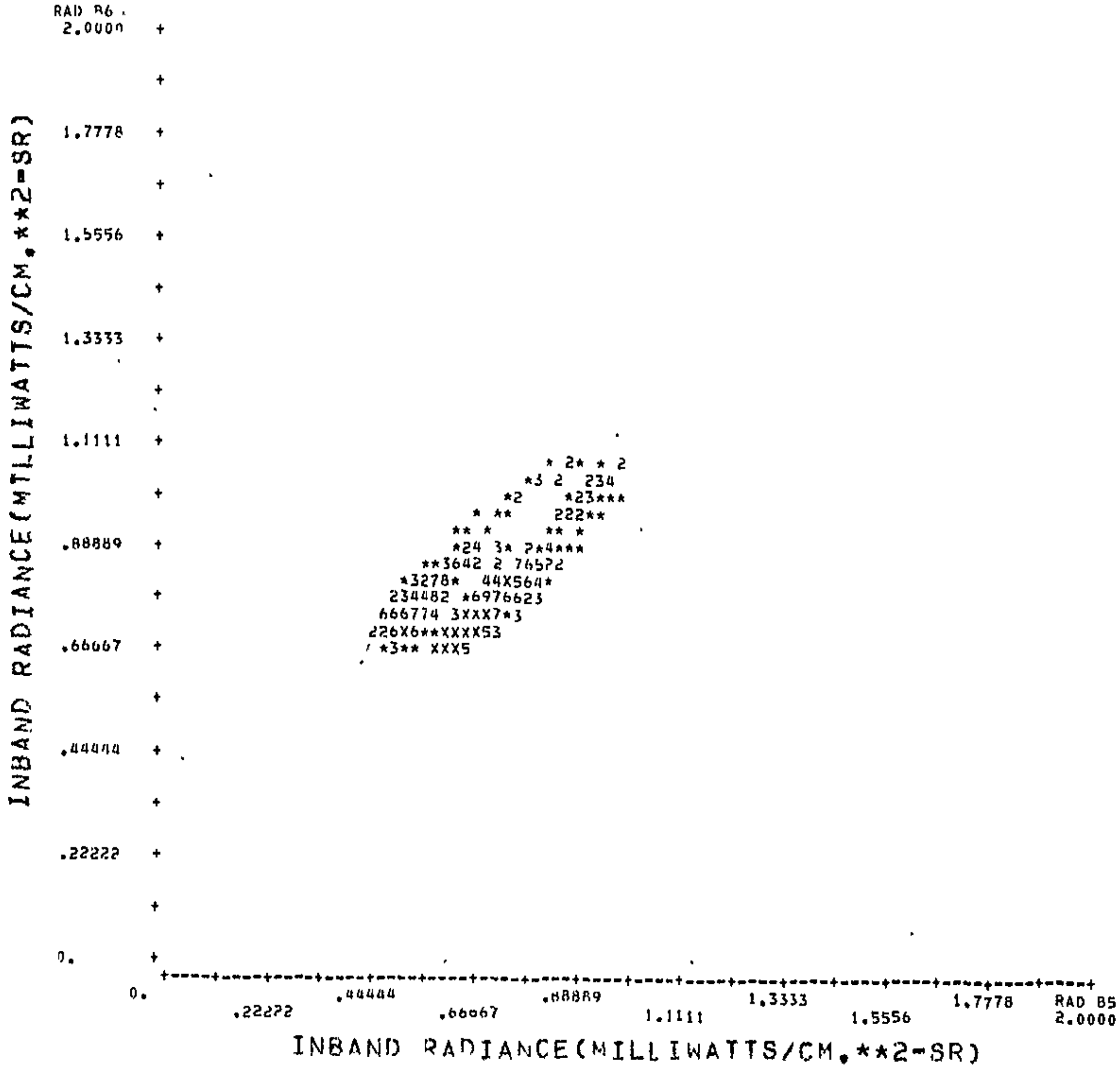

FIG.42 SPECTRAL DOMAIN OF SIMULATED LANDSAT WHEAT CANOPY RADIANCES FOR GROWTH STAGE 6: BAND 5 VS. BAND 6

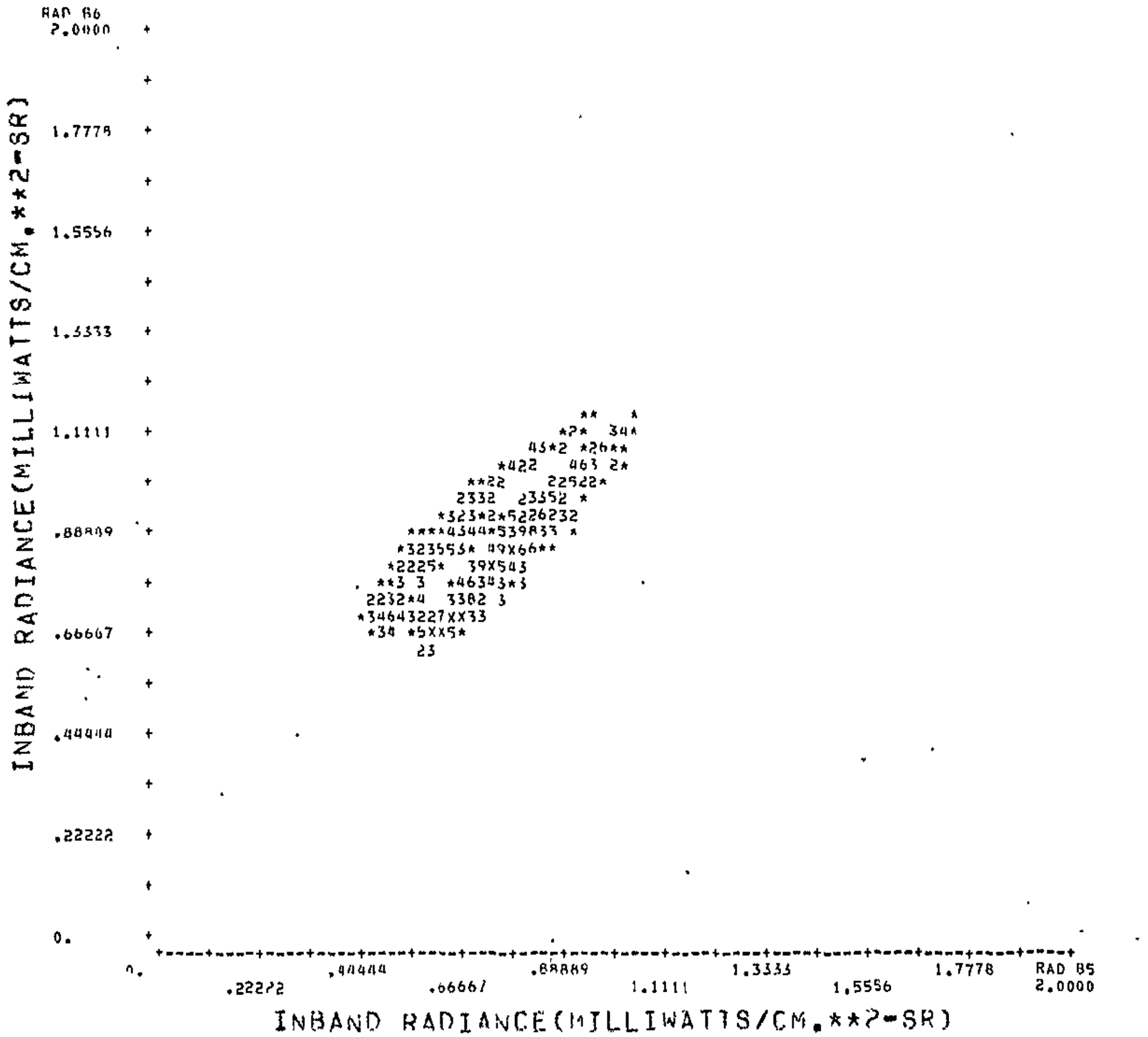

FIG.43 SPECTRAL DOMAIN OF SIMULATED LANDSAT WHEAT CANOPY RADIANCES FOR GROWTH STAGE 7; BAND 5 VS. BAND 6

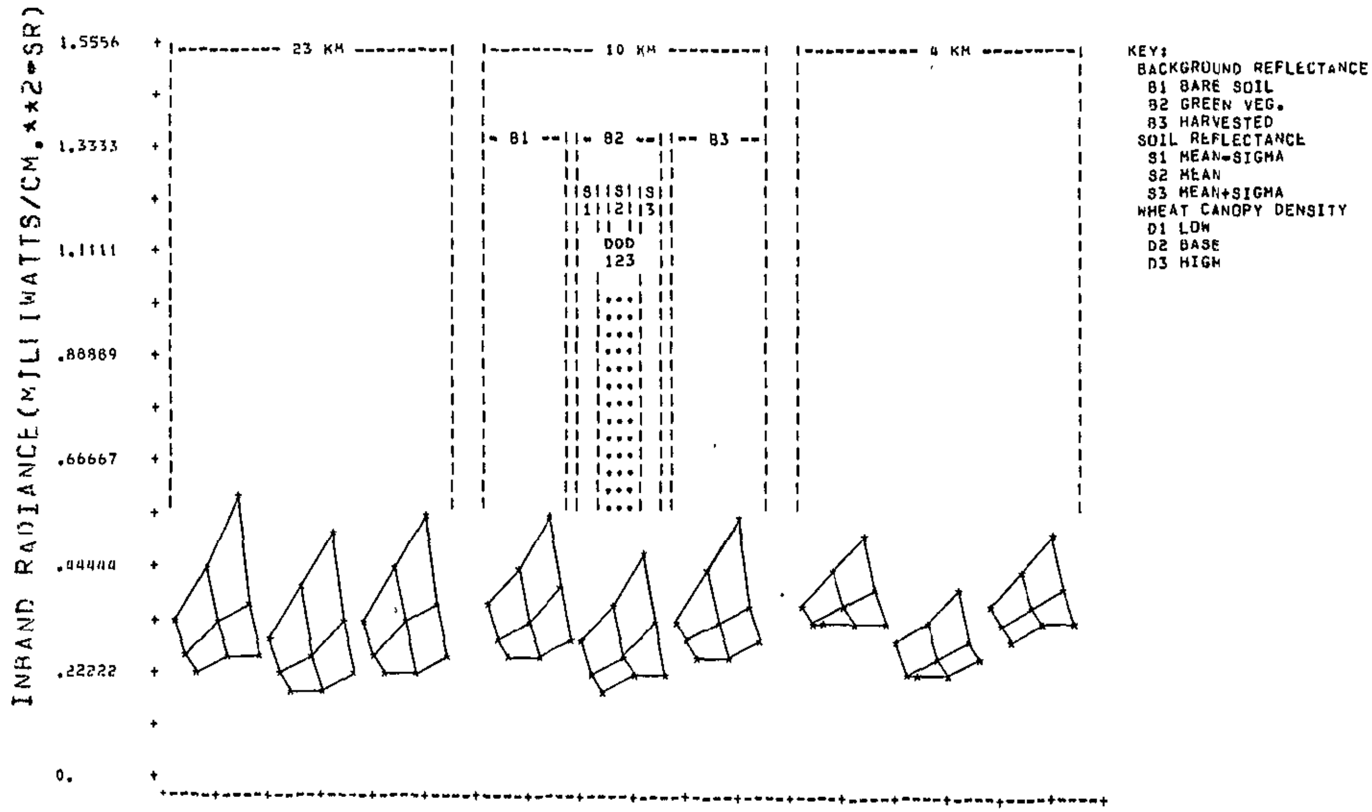

FIG.44 INFLUENCE OF CANOPY DENSITY, SOIL REFLECTANCE, BACKGROUND REFLECTANCE AND VISUAL RANGE ON SIMULATED LANDSAT WHEAT CANOPY RADIANCE (BAND 5) FOR GROWTH STAGE 1 (NADIR VIEW ANGLE, 38 DEG. N. LATITUDE)

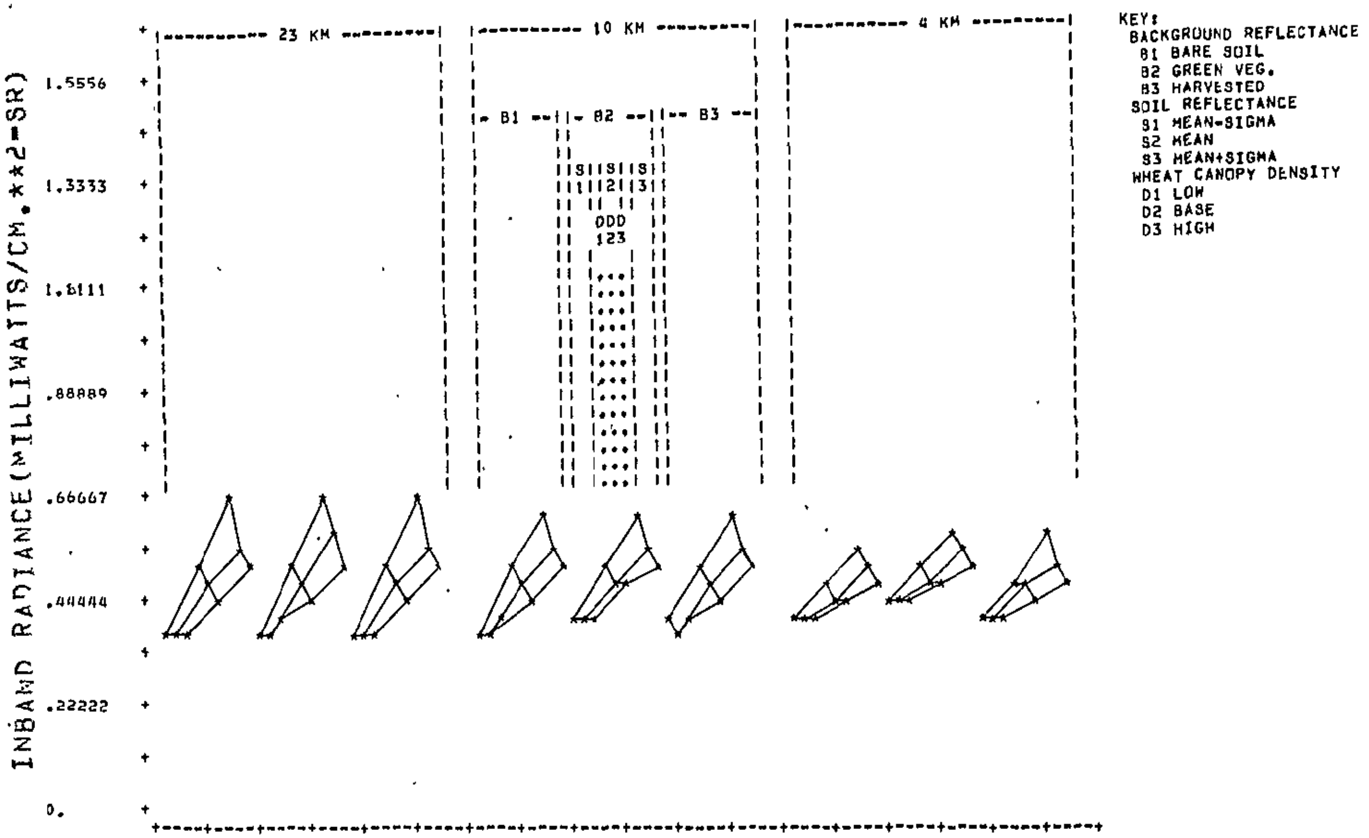

FIG. 45 INFLUENCE OF CANOPY DENSITY, SOIL REFLECTANCE, BACKGROUND REFLECTANCE AND VISUAL RANGE ON SIMULATED LANDSAT WHEAT CANOPY RADIANCE (BAND 6) FOR GROWTH STAGE 1 (NADIR VIEW ANGLE, 38 DEG. N. LATITUDE)

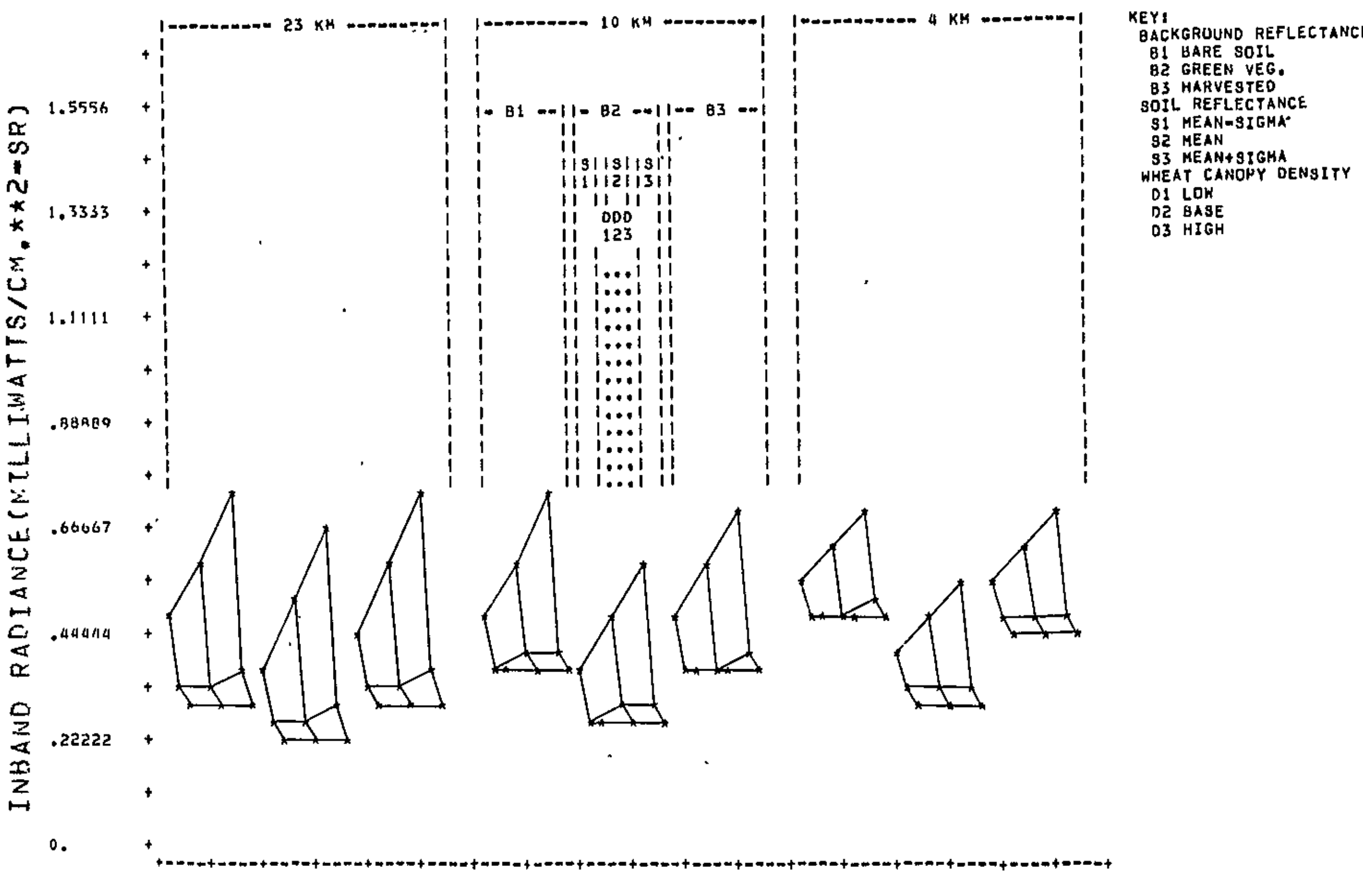

FIG.46 INFLUENCE OF CANOPY DENSITY, SOIL REFLECTANCE, BACKGROUND REFLECTANCE AND VISUAL RANGE ON SIMULATED LANDSAT WHEAT CANOPY RADIANCE (BAND 5) FOR GROWTH STAGE 2 (NADIR VIEW ANGLE, 38 DEG. N. LATITUDE)

ERIM
FORMERLY WILLOW RUN LABORATORIES, THE UNIVERSITY OF MICHIGAN

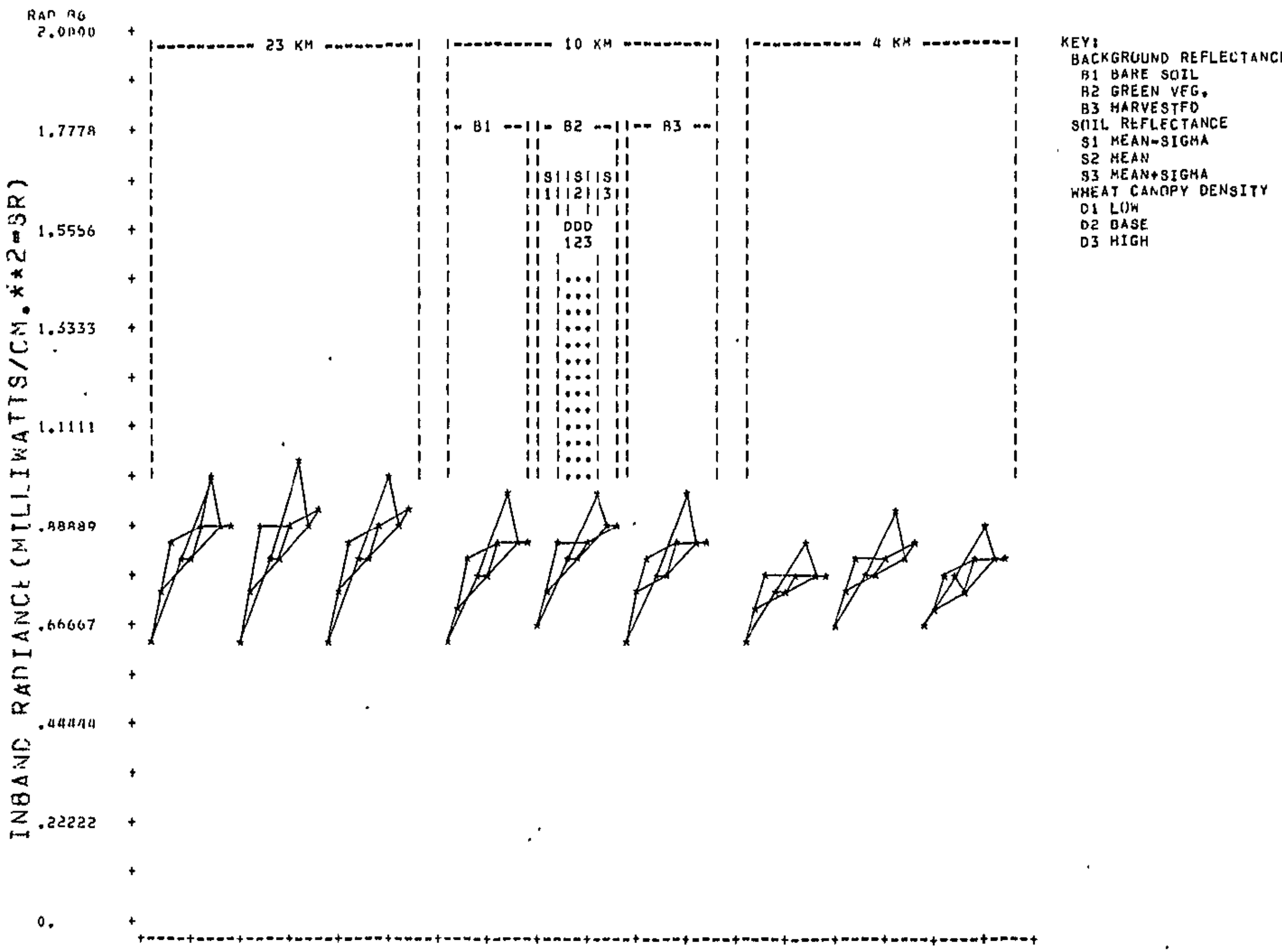

FIG.47 INFLUENCE OF CANOPY DENSITY, SOIL REFLECTANCE, BACKGROUND REFLECTANCE AND VISUAL RANGE ON SIMULATED LANDSAT WHEAT CANOPY RADIANCE (BAND 6) FOR GROWTH STAGE 2 (NADIR VIEW ANGLE, 38 DEG. N. LATITUDE)

ORIGINAL PAGE IS OF POOR QUALITY

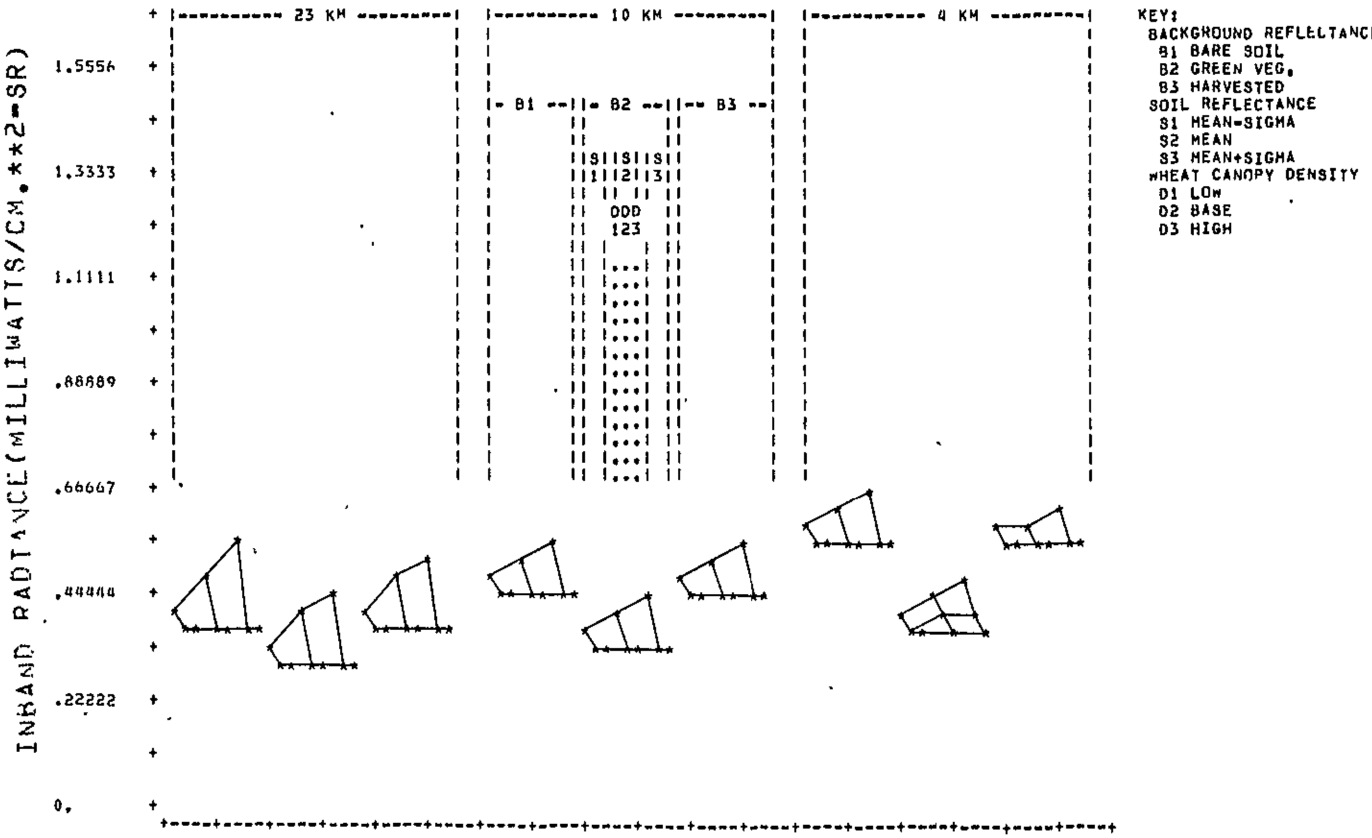

FIG.48 INFLUENCE OF CANOPY DENSITY, SOIL REFLECTANCE, BACKGROUND REFLECTANCE AND VISUAL RANGE ON SIMULATED LANDSAT WHEAT CANOPY RADIANCE (BAND 5) FOR GROWTH STAGE 3 (NADIR VIEW ANGLE, 38 DEG. N. LATTITUDE)

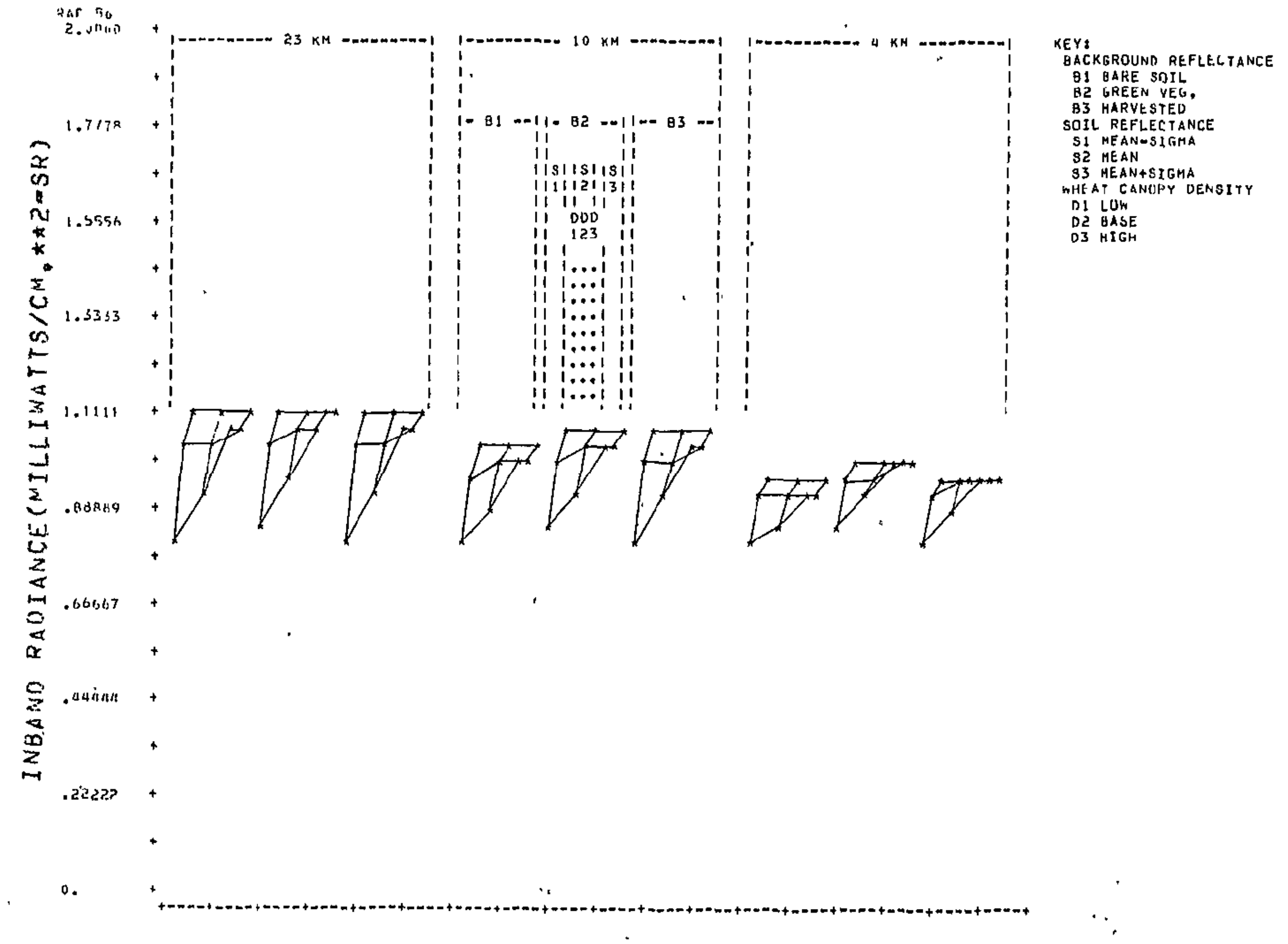

FIG.49 INFLUENCE OF CANOPY DENSITY, SOIL REFLECTANCE, BACKGROUND REFLECTANCE AND VISUAL RANGE ON SIMULATED LANDSAT WHEAT CANOPY RADIANCE (BAND 6) FOR GROWTH STAGE 3 (NADIR VIEW ANGLE, 38 DEG. N. LATITUDE)

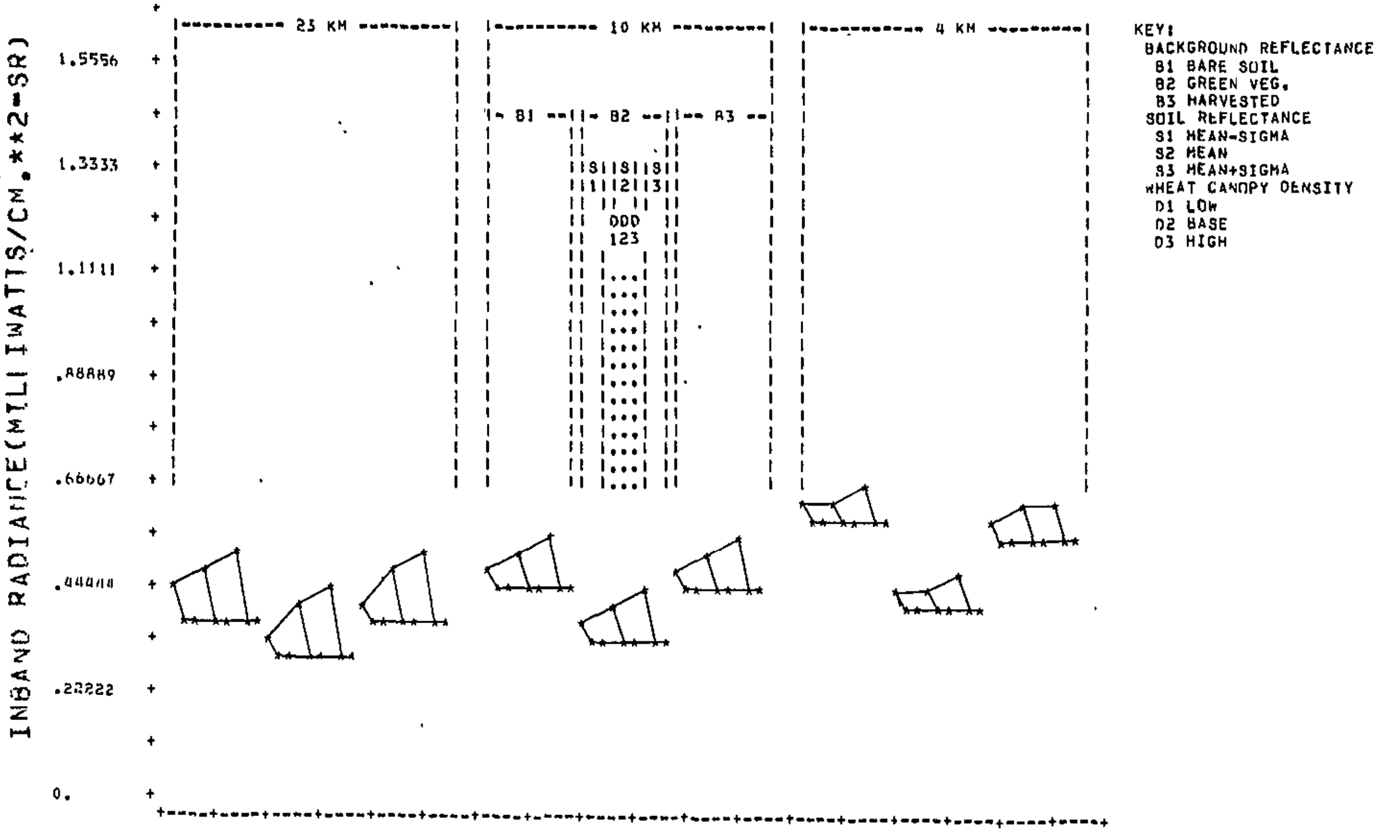

FIG.50 INFLUENCE OF CANOPY DENSITY, SOIL REFLECTANCE, BACKGROUND REFLECTANCE AND VISUAL RANGE ON SIMULATED LANDSAT WHEAT CANOPY RADIANCE (BAND 5) FOR GROWTH STAGE 4 (NADIR VIEW ANGLE, 38 DEG. N. LATITUDE)

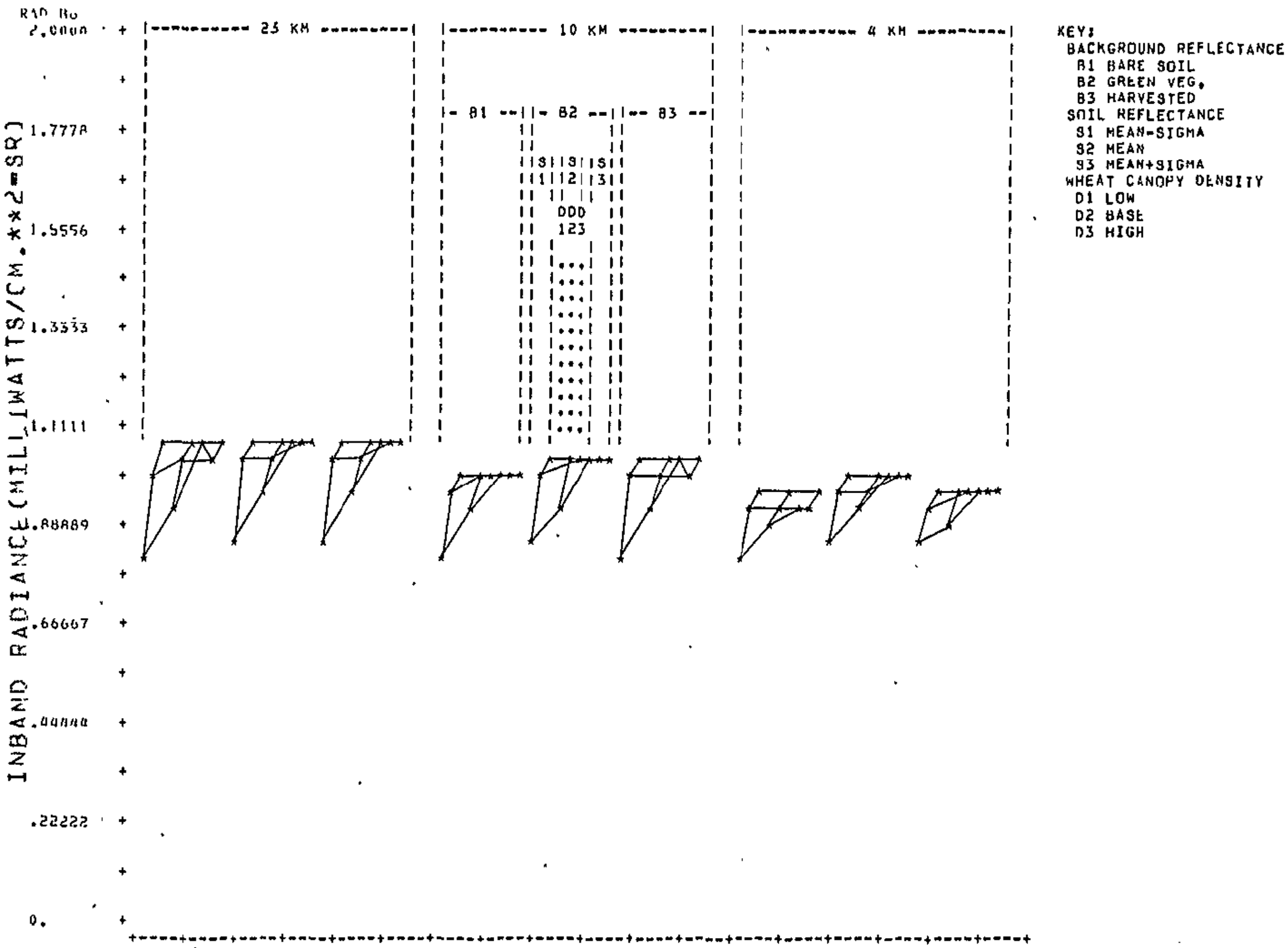

FIG.51 INFLUENCE OF CANOPY DENSITY, SOIL REFLECTANCE, BACKGROUND REFLECTANCE AND VISUAL RANGE ON SIMULATED LANDSAT WHEAT CANOPY RADIANCE (BAND 6) FOR GROWTH STAGE 4 (NADIR VIEW ANGLE, 38 DEG. N. LATITUDE)

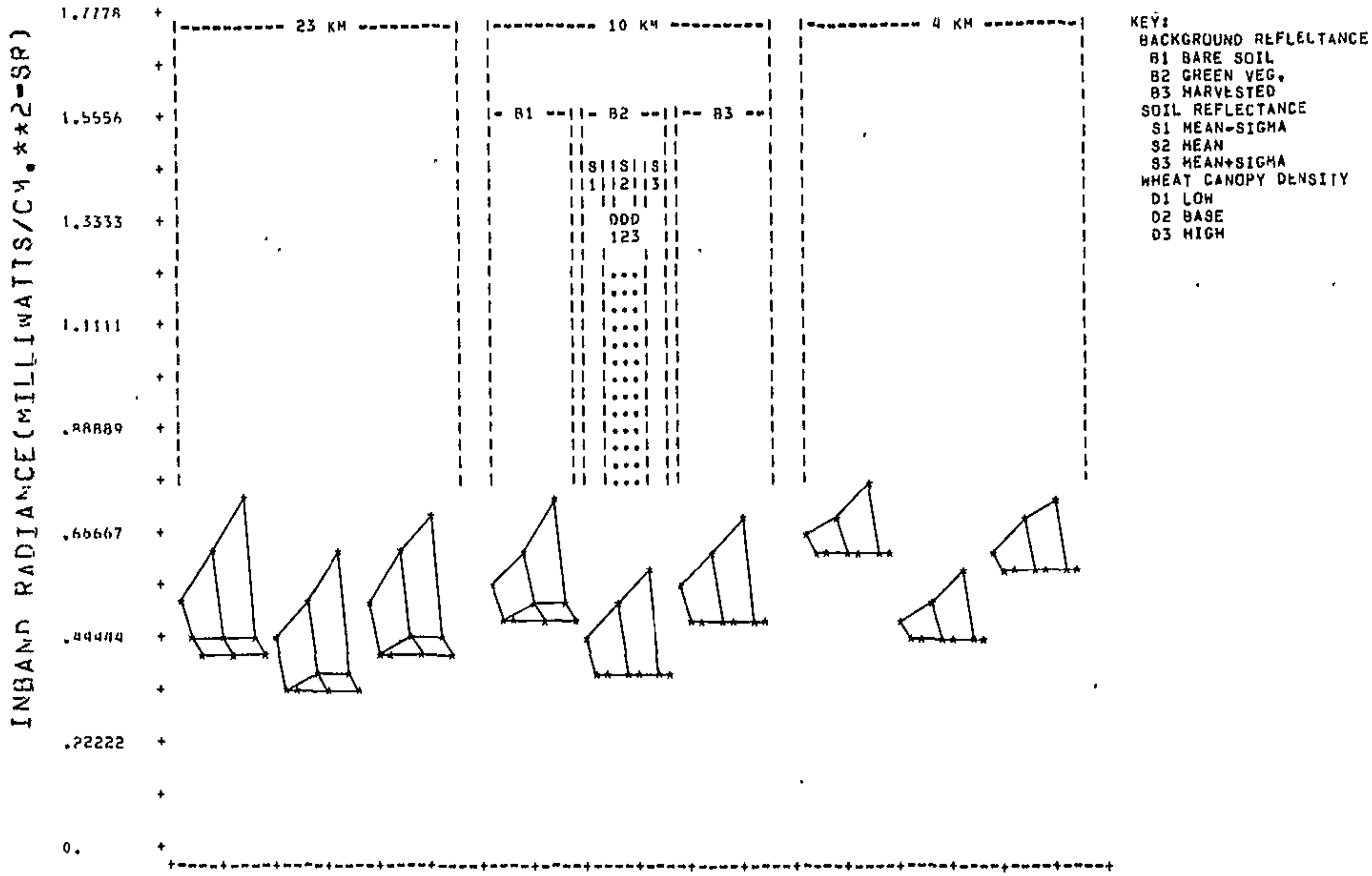

FIG.52 INFLUENCE OF CANOPY DENSITY, SOIL REFLECTANCE, BACKGROUND REFLECTANCE AND VISUAL RANGE ON SIMULATED LANDSAT WHEAT CANOPY RADIANCE (BAND 5) FOR GROWTH STAGE 5 (NADIR VIEW ANGLE, 38 DEG. N. LATITUDE)

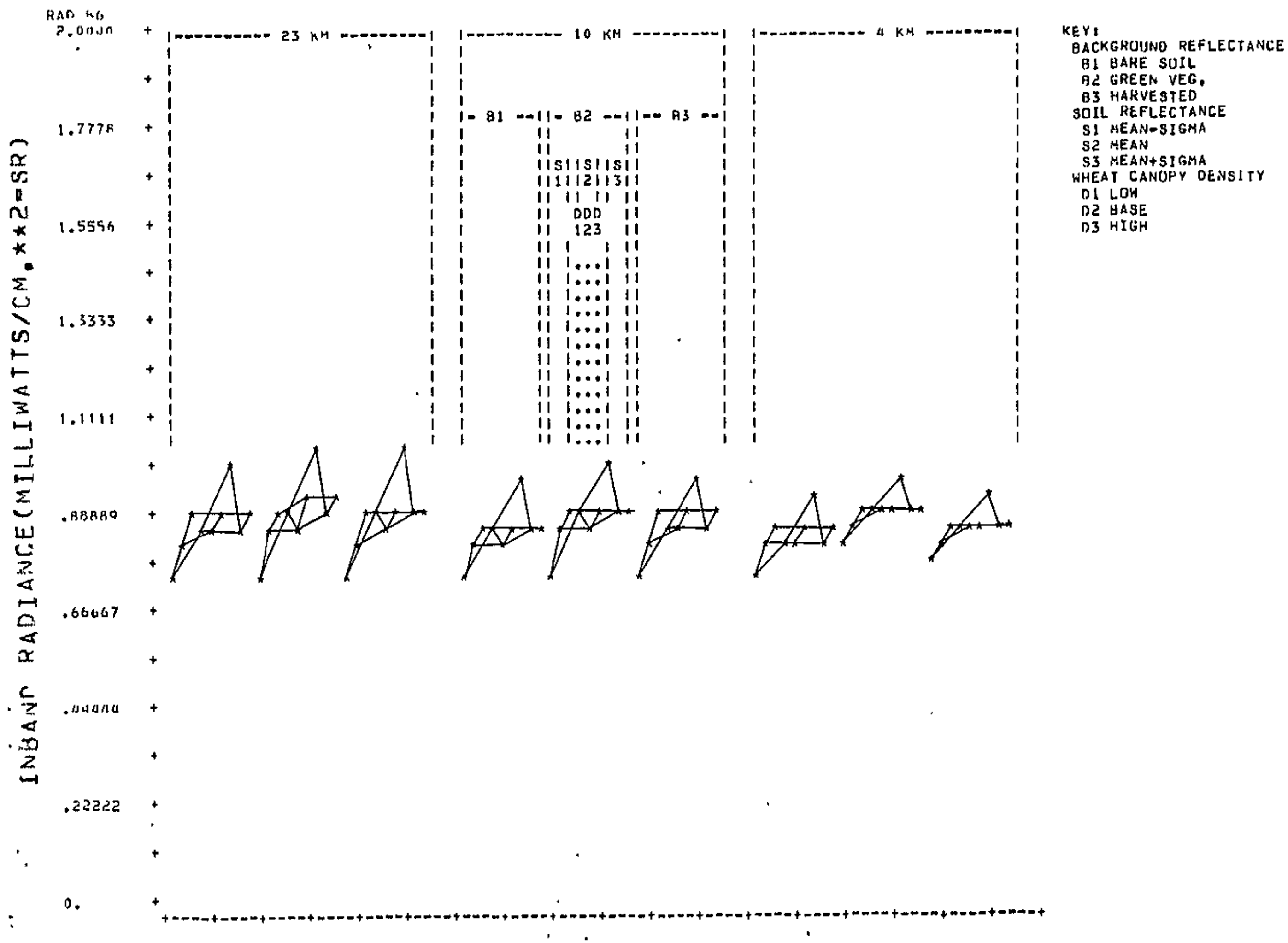

FIG.53 INFLUENCE OF CANOPY DENSITY, SOIL REFLECTANCE, BACKGROUND REFLECTANCE AND VISUAL RANGE ON SIMULATED LANDSAT WHEAT CANOPY RADIANCE (BAND 6) FOR GROWTH STAGE 5 (NADIR VIEW ANGLE, 38 DEG. N. LATITUDE)

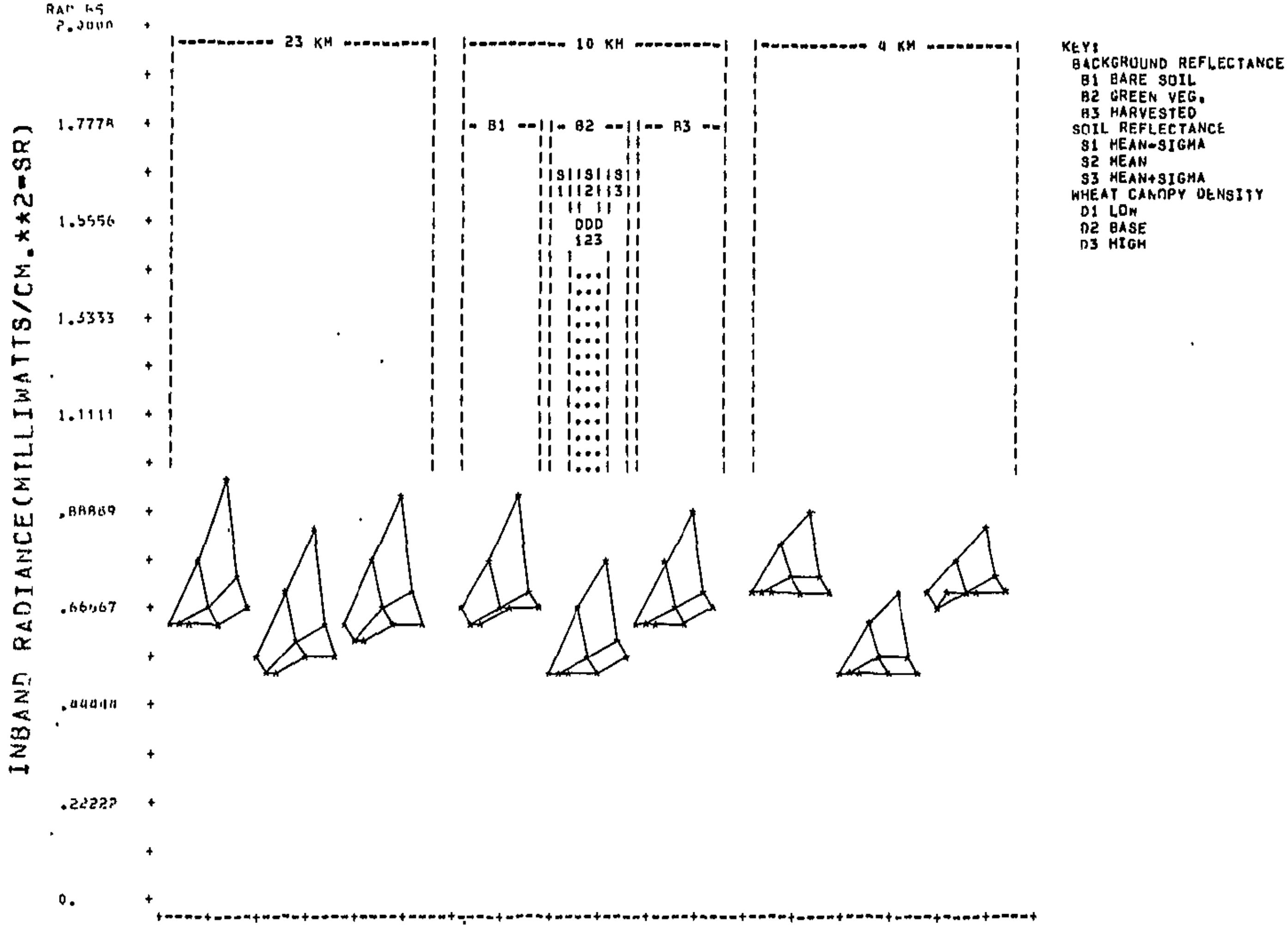

FIG.54 INFLUENCE OF CANOPY DENSITY, SOIL REFLECTANCE, BACKGROUND REFLECTANCE AND VISUAL RANGE ON SIMULATED LANDSAT WHEAT CANOPY RADIANCE (BAND 5) FOR GROWTH STAGE 6 (NADIR VIEW ANGLE, 38 DEG. N. LATITUDE)

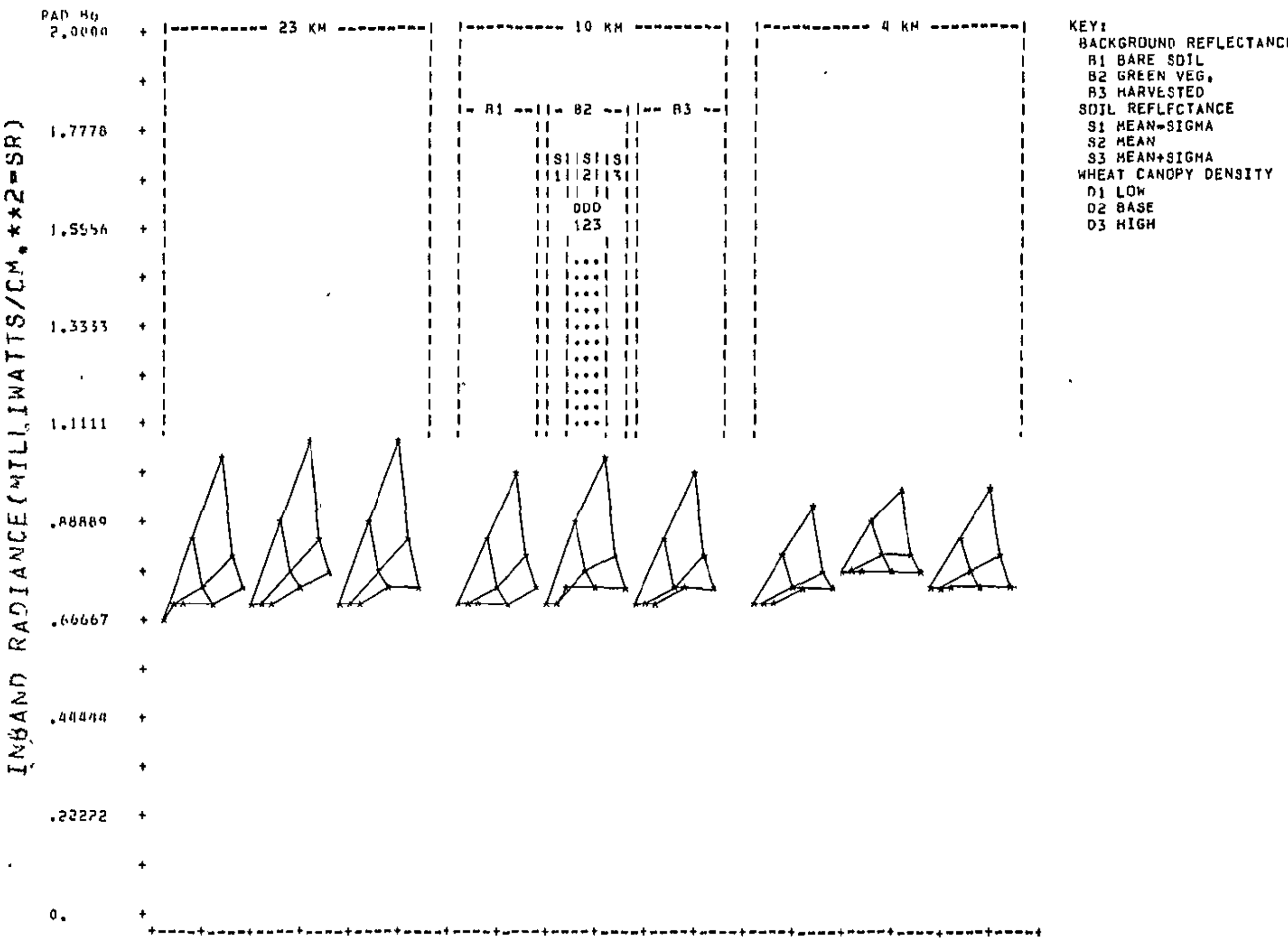

FIG.55 INFLUENCE OF CANOPY DENSITY, SOIL REFLECTANCE, BACKGROUND REFLECTANCE AND VISUAL RANGE ON SIMULATED LANDSAT WHEAT CANOPY RADIANCE (BAND 6) FOR GROWTH STAGE 6 (NADIR VIEW ANGLE, 38 DEG. N. LATITUDE)

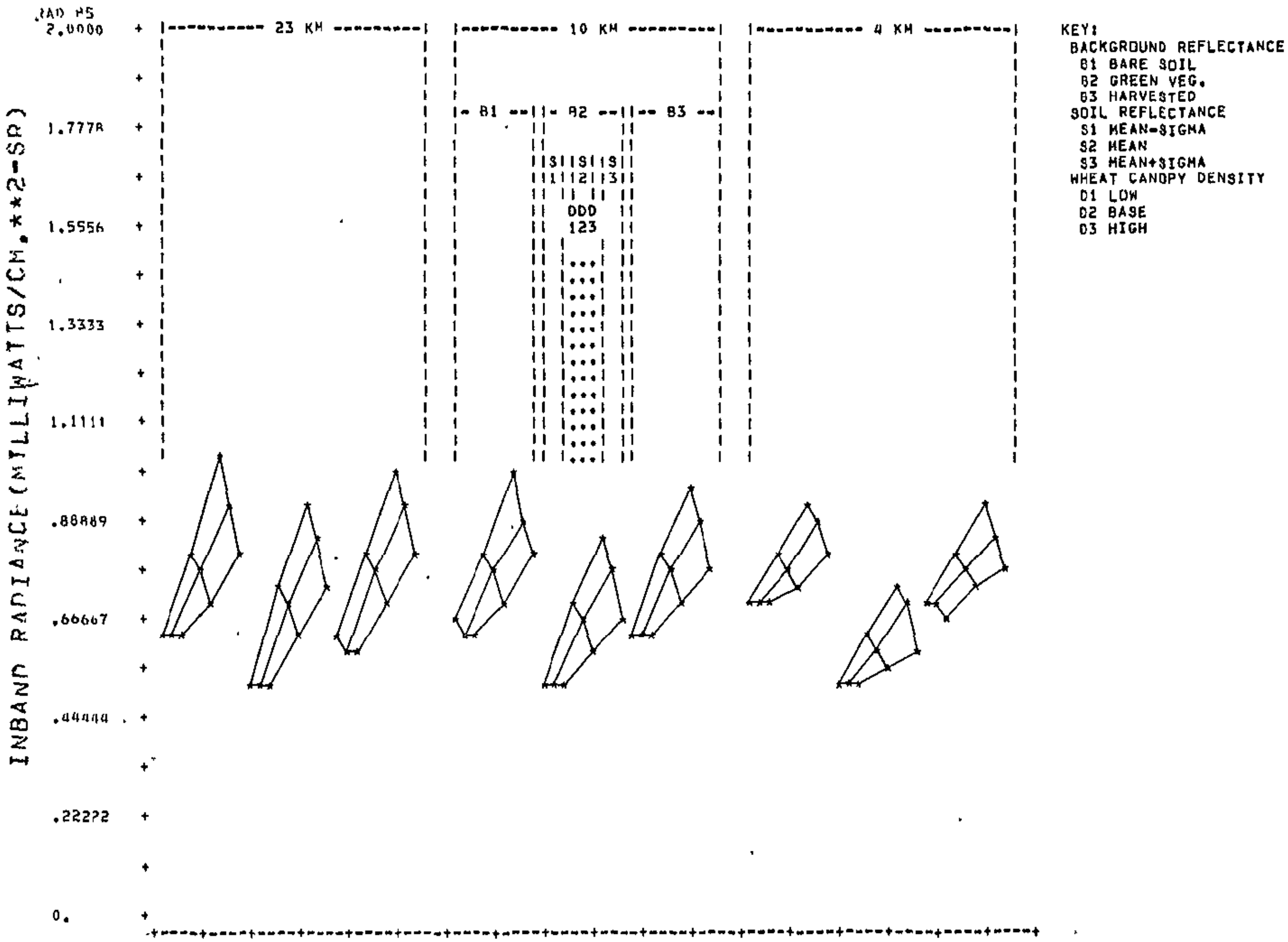

FIG.56 INFLUENCE OF CANOPY DENSITY, SOIL REFLECTANCE, BACKGROUND REFLECTANCE AND VISUAL RANGE ON SIMULATED LANDSAT WHEAT CANOPY RADIANCE (BAND 5) FOR GROWTH STAGE 7 (NADIR VIEW ANGLE, 38 DEG. N. LATITUDE)

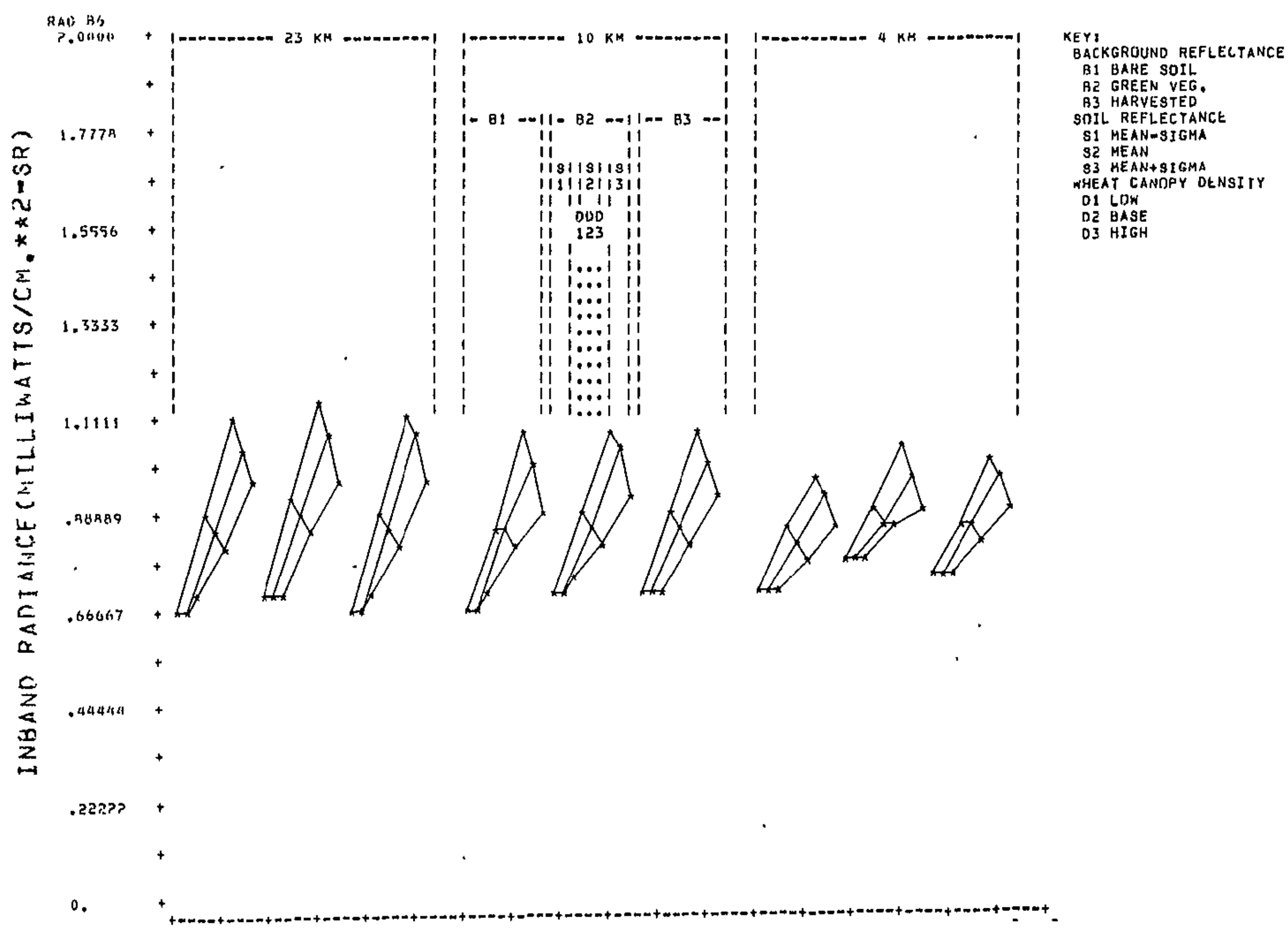

FIG.57 INFLUENCE OF CANOPY DENSITY, SOIL REFLECTANCE, BACKGROUND REFLECTANCE AND VISUAL RANGE ON SIMULATED LANDSAT WHEAT CANOPY RADIANCE (BAND 6) FOR GROWTH STAGE 7 (NADIR VIEW ANGLE, 38 DEG. N. LATITUDE)

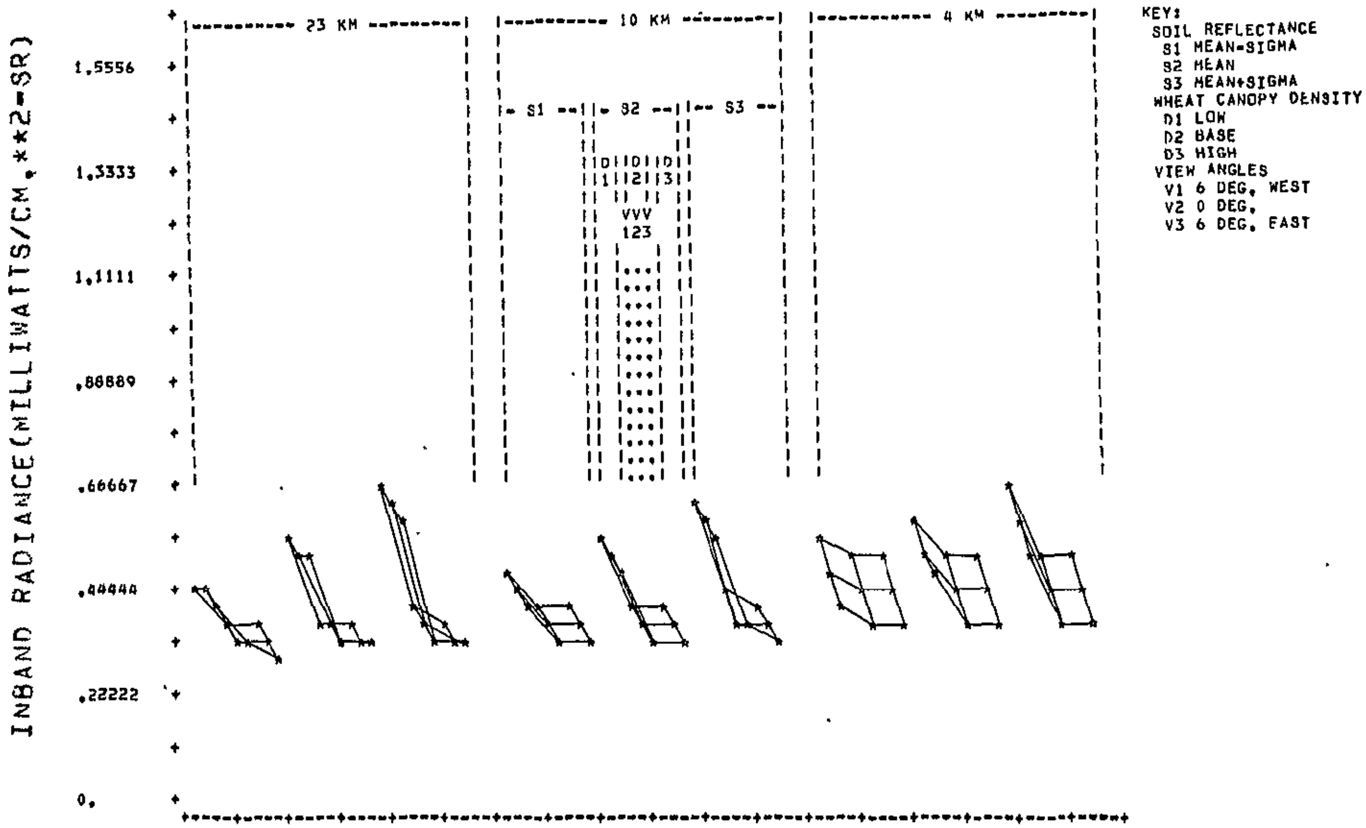

FIG.58 INFLUENCE OF VIEW ANGLE, CANOPY DENSITY, SOIL REFLECTANCE AND VISUAL RANGE ON SIMULATED LANDSAT WHEAT CANOPY RADIANCE (BAND 5) FOR GROWTH STAGE 5 (GREEN WHEAT BACKGROUND, 38 DEG. N. LATITUDE)

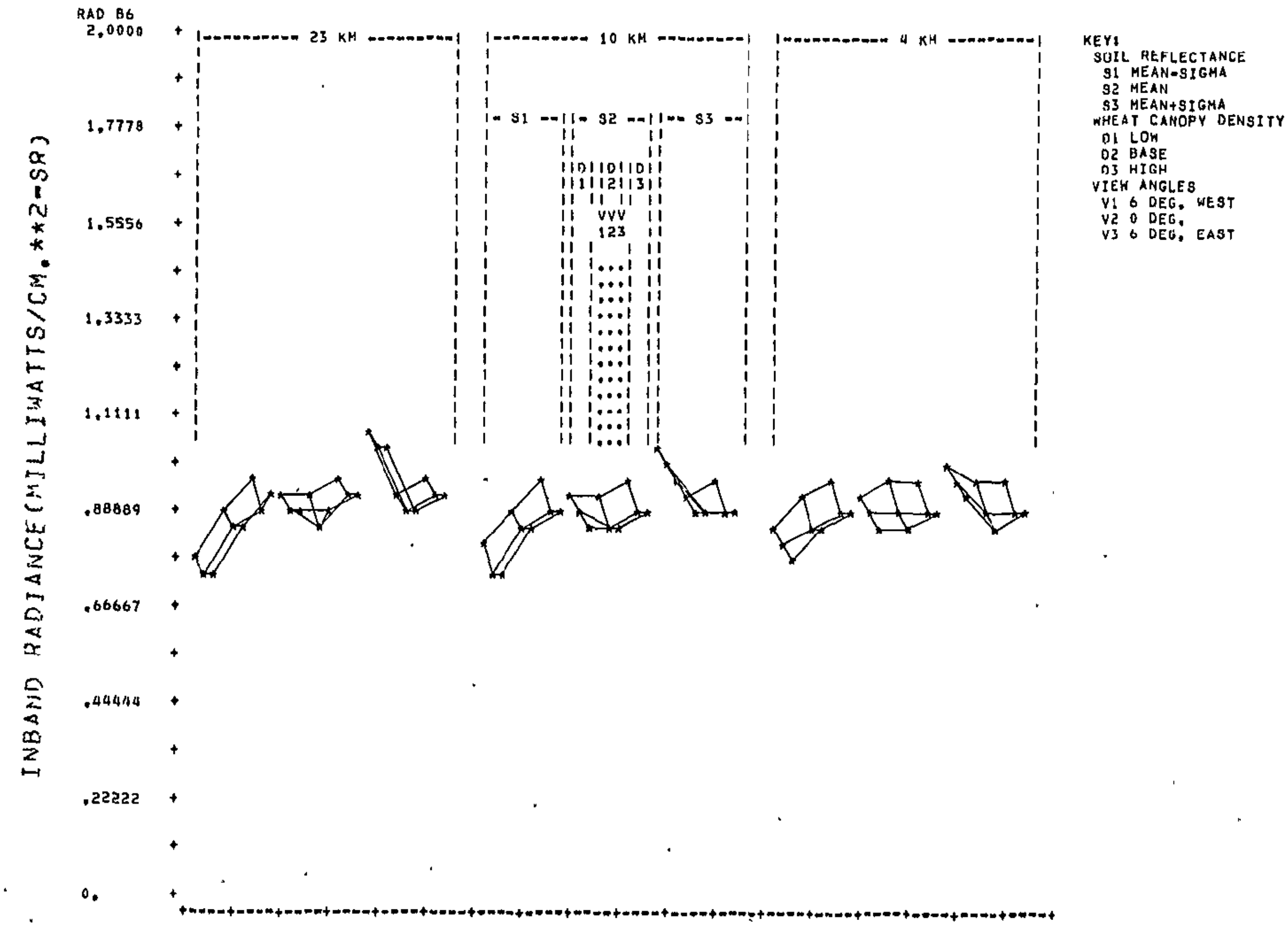

FIG.59 INFLUENCE OF VIEW ANGLE, CANOPY DENSITY, SOIL REFLECTANCE AND VISUAL RANGE ON SIMULATED LANDSAT WHEAT CANOPY RADIANCE (BAND 6) FOR GROWTH STAGE 5 (GREEN WHEAT BACKGROUND, 38 DEG. N. LATITUDE)

ORIGINAL PAGE IS OF POOR QUALITY

different combinations of three canopy density levels, three soil reflectance spectra, three background reflectance spectra, and three atmospheric visual ranges. All data points correspond to 38^{o}N latitude and a nadir view angle. As in Figs. 25-33, the abscissa variable has no physical significance; it has been defined solely for the purpose of displaying variations in the simulated radiances due to variations in the three levels of the four factors just mentioned. The factors, from most rapidly to most slowly varying, are: canopy density, soil reflectance, background reflectance and atmospheric visibility. The key in each figure indicates the order in which the levels of each factor vary. Each figure appears to be composed of nine distinct patterns drawn by connecting data points in a particular manner to aid in their interpretation. These patterns form three groups of three, each group corresponding to a particular atmospheric visual range, varying from 23 km (relatively clear) on the left to 4 km (very hazy) on the right. The three patterns within each group correspond to particular background reflectances, varying from left to right from bare soil to green wheat to harvested wheat. Each pattern is formed by the connection of nine data points, consisting of three groups of three data points. Successive groups of three points correspond to particular soil reflectance spectra ranging from the darkest soil (mean - sigma) on the left to the highest soil (mean + sigma) on the right. Successive data points within each group of three correspond to particular wheat canopy densities ranging from low density on the left to high density on the right. The nine patterns were formed by connecting the three data points corresponding to each soil for each canopy density and by connecting the three data points corresponding to each canopy density for each soil reflectance spectrum. These lines serve to geometrically organize each figure into a set of patterns, each pattern corresponding to a particular combination of atmospheric visual range and background reflectance spectrum. These lines also enable the variations in radiance due to changes in soil reflectance and canopy density to be easily followed in each of these figures.

Figs. 58-59 are additional display of simulated radiances in Bands 5 and 6, respectively, for Growth Stage 5 (senescing wheat), a green vegetation background reflectance spectrum, and 38°N latitude. The primary purpose of these two figures is to display the effects of view angle. The organization of these figures is similar to those just discussed, except that the factors, from most rapidly to most slowly varying, are: view angle, canopy density, soil reflectance and atmospheric visibility. Successive data points within each group of three correspond to particular view angles ranging from 6° in a westerly direction on the left to nadir to 6° in an easterly direction on the right. Each pattern corresponds to a particular combination of atmospheric visual range and soil reflectance spectrum. The nine patterns are formed by connecting the three data points corresponding to each density for each view angle and by connecting the three data points corresponding to each view angle for each density.

Examinations of these simulated radiances have yielded some interesting observations concerning the effects of variations in the levels of the factors listed in Table 12. These observations will next be discussed in terms of these individual factors.

6.6.1 LATITUDE EFFECTS

No significant differences were observed between simulated radiances corresponding to 38°N latitude and those corresponding to 46°N latitude. At the more Northerly latitude the sun zenith angle is lower, but between April and July the difference is less than 4°. This difference results in somewhat lower scene irradiances at 46° latitude which explains the lower average radiances in Table 15. This small difference, however, does not produce significant differences in the effects of the remaining factors on the simulated radiances.

6.6.2 ATMOSPHERIC VISIBILITY EFFECTS

Variations in the atmospheric visibility affect both atmospheric transmittance and path radiance. As atmospheric visibility decreases, atmospheric transmittance decreases and the amount of path radiance increases. The decreased atmospheric transmittance reduces the scene irradiance and the amount of reflected radiation reaching the scanner from the ground. Figs. 44-57 illustrate two general trends. The most apparent trend is the decreased variability in the radiances as visibility decreases. This trend can be attributed to the fact that the lower visibility radiances are composed more of path radiance, reducing their sensitivity to variations in the condition of the wheat canopy, i.e., its density and soil reflectance. A less obvious trend is that the radiances increase in the shorter wavelength bands (4 and 5) as visibility decreases and decrease in the longer wavelength bands (6 and 7). This trend is more apparent in Bands 4 and 7 than in Bands 5 and 6, as is borne out by the average radiance values in Table 15 for the different visual ranges. In the shorter wavelength bands, the increase in path radiance more than offsets the decrease in transmittance, resulting in an increase in radiance as visibility decreases. In the longer wavelength bands, path radiance is less significant and its increase does not offset the decrease in transmittance, resulting in a decrease in radiance as visibility decreases.

6.6.3 BACKGROUND REFLECTANCE EFFECTS

Fig. 21 illustrates the similarity between the bare soil and harvested wheat background reflectance spectra and also the distinctness of the green wheat background spectrum. Using nominal band limits for the four Landsat spectral bands, the bare soil background can be seen to be slightly brighter in Bands 4 and 5 but darker in Bands 6 and 7. Table 15 indicates that the radiances in Bands 4 and 5 are slightly higher for the bare soil background than for the harvested wheat background and that just the opposite is true in Bands 6 and 7. In any band, the radiance is higher for the brighter background due to the increased path radiance from this background. The green wheat background reflectance spectrum is darker than both the bare soil and harvested wheat spectra in Bands 4 and 5 and brighter in Band 7. The situation for Band 6 is unclear because of the abrupt transition in the green background spectrum within the band. Table 15 indicates again the increased average radiance for the brighter background. Figs. 44-57 clearly indicate the lower radiances in Band 5 for the green wheat background as opposed to the radiances for the two brighter backgrounds. In Band 6, the green background appears to be the brightest as indicated by the higher radiances corresponding to it.

6.6.4 SCANNER VIEW ANGLE EFFECTS

Figs. 58 and 59 illustrate typical scanner view angle effects on radiances for Growth Stage 5. The most obvious trend to note is the increased variation over the three view angles considered as atmospheric visibility decreases. This trend is due to the increase in path radiance as visibility decreases. The variation is greater in Band 5 than in Band 6 because of the greater significance of path radiance at the shorter wavelengths. In Band 5, radiances decrease (or at least don't increase) as the view angle moves from a westerly orientation through nadir to an easterly orientation from the Landsat ground track. With the morning sun in the East, the sun is most directly behind the path of observation of the scanner when it is looking into the West, resulting in the highest path radiance component for the westerly view angle. As the view angle swings into an easterly direction the scanner is looking more toward the direction of the sun, resulting in a decreasing path radiance component. (Ref. 19 contains a more detailed discussion of the relationship between path radiance and view angle.)

A different phenomenon related to view angle can be noted for Band 6 (Fig. 59). For the 23 km visual range, darkest soil, and high canopy density, the radiance decreases as the view angle shifts from a westerly direction to nadir and then increases as it shifts to an easterly direction. This trend contradicts the usual trend described in the previous paragraph. The explanation for the increase in radiance as the view angle shifts to the easterly direction is that, although the path radiance component does decrease as expected, the canopy reflectance increases, offsetting this decrease and resulting in a higher radiance. (The path radiance does not constitute as large a fraction of the signal in Bands 6 and 7 as it does in Bands 4 and 5.) The increased reflectance of the canopy at the 6° view angle is due to the bidirectional reflectance characteristic of the canopy. As the scanner shifts from the westerly view angle to nadir, the path radiance decreases and the canopy reflectance also decreases. The decrease in canopy reflectance is attributable to the fact that the soil is darker than the crop and more soil is visible at the nadir view angle. As the scanners view angle shifts to the easterly direction, the less soil is visible again and the canopy reflectance increases, offsetting the path radiance decrease.

6.6.5 SOIL REFLECTANCE EFFECTS

Figs. 44-57 illustrate the increase in radiance which occurs for a constant canopy density as soil brightness (reflectance) increases. The average radiances in Table 15 for the various soil levels support this observed increase in radiance as soil brightness increases. The brighter soils reflect more of the radiation which penetrates through the canopy layers to the soil. The variation in radiance is greatest when the canopy density is low and less as the canopy density increases. In fact, in some cases for base and high density canopies, soil brightness has no noticeable effect on radiance. For such high density canopies, essentially no radiation emerges from the canopy after being reflected by the soil. This invariance to soil brightness is most prominent for Growth Stages 3 and 4 for which the percent cover is greatest. The figures also indicate that radiances in Band 6 are more sensitive to soil brightness variations than radiances in Band 5. The canopy is more transparent at the longer wavelengths, allowing more radiation to penetrate through the canopy layers and increasing the sensitivity to soil brightness variations. Thus one would expect Band 7 to exhibit effects similar to those of Band 6 and those of Band 4 to be similar to Band 5 effects.

6.6.6 WHEAT CANOPY DENSITY EFFECTS

The variations in radiance due to differences in wheat canopy density can be seen in Figs. 44-57 to be greater, generally, for changes from low to base density than from base to high density. Table 13 indicates that the greater change in percent ground cover occurs between the low and base densities, explaining this trend. The amount of variation in the radiances is determined by the relative reflectance characteristics of the soil and canopy layers in each spectral band. The average radiance values in Table 15 show a decrease in Bands 4 and 5 as density increases and an increase in Bands 6 and 7. When the soil and crop canopy layers are spectrally similar in a particular band, density variations have little effect on radiance. For instance, in Band 6 for Growth Stage 6 (Fig. 55), the darkest soil and the crop layers are indeed spectrally similar.

An interesting phenomenon occurs in several cases and is related to canopy density effects. For example, in Band 6 for Growth Stage 5 (Fig. 53), radiance decreases as canopy density varies from low to base density and then increases as density varies from base to high density for a 23 km visual range and the brightest soil. This somewhat surprising result can be attributing to "shadowing" within the canopy, according to the following postulated explanation. The crop is darker than the soil, so that an increase in density from low to base level results in a decrease in radiance. But the increased density also causes shadows to be cast in the canopy (particularly due to stalks) which are even darker than the crop. When the density is further increased to the high level, the canopy is filled in to a higher degree, replacing shadowed regions with highly reflecting crop material, thereby increasing the observed radiance.

6.6.7 MULTITEMPORAL PATTERNS OF WHEAT RADIANCES

One objective of LACIE is to exploit the multitemporal characteristics of wheat signatures, where possible, to improve recognition performance. Consequently, the temporal patterns of wheat signatures and the effects of the various factors on these patterns are of interest. The simulation modeling results provide insight on this subject.

Temporal trajectories, in spectral space, of the simulated radiances from nine different wheat canopies are presented in Fig. 60. The temporal dependence of radiances in Bands 5 and 6 is presented for each possible combinations of the three soil brightnesses and three canopy densities. Each of the seven points in each plot represents one growth stage. These radiance values are for a nadir scanner view angle, 10 km visual range, 38°N latitude, and a green wheat background. Substantial differences exist in the specific shapes of the patterns, although there is a common overall trend.

The previously discussed effects of soil reflectance (Sec. 6.6.5) and wheat canopy density (Sec. 6.6.6), and their interactions, are evident here in Fig. 60. The high-density canopies portrayed in the right-hand column of plots, show little influence of soil brightness for Growth Stages 2-6, which have relatively high percentages of vegetative cover. The differences observed there between Growth Stages 6 (Ripe) and 7 (Harvested) clearly depend on soil brightness. The effects of soil brightness also are apparent in the low-density canopies of the left-hand column of plots.

6.7 DISCUSSION

Landsat radiances have been simulated for each of several wheat canopy growth stages for a variety of levels of factors determining the exact nature of the canopy and the atmosphere. These factors and

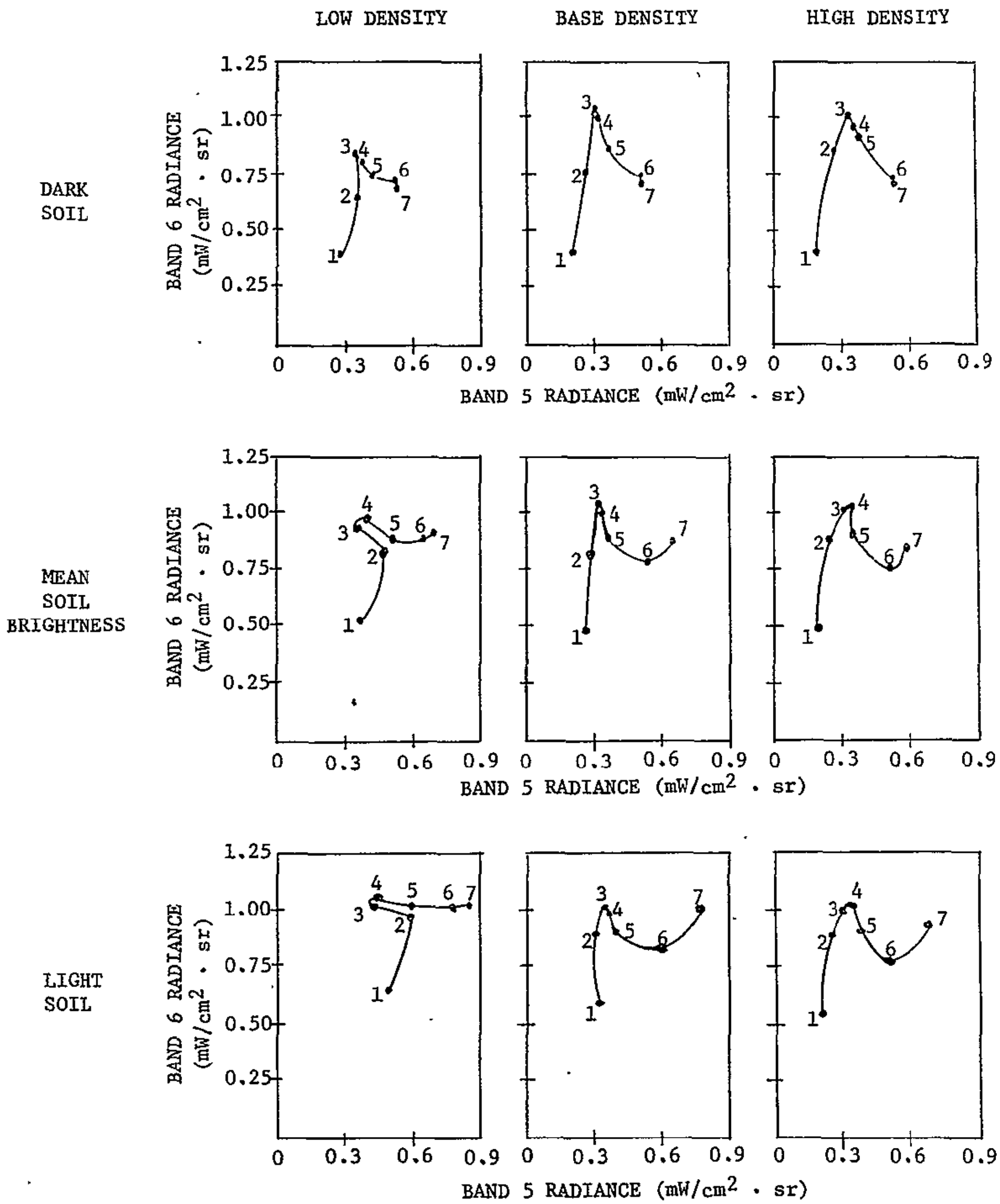

FIGURE 60. INFLUENCE OF SOIL BRIGHTNESS AND WHEAT CANOPY DENSITY ON MULTITEMPORAL PATTERNS OF SIMULATED WHEAT RADIANCES. Nadir Scanner View Angle, 10 km Visual Range, 38°N Latitude, and Green Wheat Background. Numbers Indicate Wheat Canopy Growth Stage.

their particular levels were listed earlier in Table 12. A qualitative analysis of the effects of variations in the levels of these factors has been conducted.

A slight decrease in radiance was noted at 46°N latitude as compared to 38°N latitude, but no significant difference was observed in the radiance variations at these two latitudes for the various levels of the other factors investigated.

The effects of differences in atmospheric visibility conditions were characterized in terms of their effect on atmospheric transmittance and path radiance. As visual range decreases, transmittance also decreases and path radiance increases. Path radiance effects are most significant in the shorter wavelength bands and the overall variation in the radiance in each band as visual range varies is determined by the relative changes in transmittance and path radiance. Also, in these shorter wavelength bands, because of the significance of path radiance, less sensitivity was observed to variations in factors affecting the canopy.

The background reflectance spectrum affects the magnitude of the path radiance component of the total simulated radiance, as well as diffuse irradiance. The brighter the background in any particular band, the greater the path radiance is also. The differences in three backgrounds investigated was most apparent in the shorter wavelength bands where path radiance is most significant. The bare soil and harvested wheat backgrounds resulted in almost identical radiance values; the green wheat background resulted in lower values in the shorter wavelength bands and higher values in the longer wavelength bands.

The effect of the different scanner view angles were found to depend on changes in both the path radiance component and the bidirectional canopy reflectance. Some significant changes in total radiance were observed for the different view angles, the amount of this change being determined by the relative position of the sun and the direction of view of the scanner. The bidirectional reflectance of the canopy is determined by the amount of soil, crop, and shadow which are observed for a particular view angle. In the shorter wavelength bands, changes in radiance for the different view angles are primarily dependent on changes in the path radiance component; in the longer wavelength bands they depend primarily on changes in the canopy reflectance.

Variations in soil brightness resulted in increased radiance as brightness increased. The amount of this increase depended on the canopy density which determines how much radiation penetrates through the canopy to the soil. These variations were generally more significant in the longer wavelength bands because of the higher canopy transmittance in these bands. The effect of canopy density depends to a large part on the relative brightness of the soil and the crop. A greater change in radiance was observed between low and base density canopies than between base and high density canopies.

The temporal variation of the wheat canopy was observed in two bands over the seven stages of growth for each combination of soil brightness and canopy density. Substantial differences in the patterns were observed which could have a strong effect on multitemporal techniques for the recognition of wheat.

The accuracy of the simulated radiances is predicated on the accuracy of the Suits canopy reflectance model and the Turner radiative transfer model. The accuracy of both models has been examined in the past and has been found to be acceptable. The data which have been generated as part of this effort, however, would permit further verification of these models. The simulated radiances could be compared against actual Landsat data values and field measurement data. This comparison would not only allow the two models to be further verified but also allow the appropriateness of the canopy and atmospheric data used in the simulation to be evaluated. At the same time calibration factors could be determined to convert the radiance values into Landsat data values. Limited comparisons between some of the simulated values and radiometric field measurements data acquired by the LACIE field measurements team are made in Sec. 7.

The analysis of the simulated radiances has thus far been only qualitative, but should be made more quantitative. The calibration factors mentioned in the previous paragraph should be utilized to analyze these data in terms of their equivalent Landsat data values to tie them closer to LACIE processing operations. More levels of the various factors might be included to more precisely determine the effects of these factors. One factor in particular for which more levels should be investigated is visual range (See Sec. 7). Similar simulations should also be undertaken for spring wheat and other crops which compete with wheat in recognition processing.

Improvements should be made to the overall simulation model to make it more general and readily useable. A capability for simulating the covariance matrix for a particular set of canopy conditions and atmospheric conditions should also be added to the model. The model could be made more general by allowing the background reflectance spectrum to be the canopy reflectance spectrum itself. In the present arrangement, this would be impractical when many different canopy characteristics are considered. The model might also be used with a more developed sensor system model to simulate an entire data set based on the arrangement of crops within the scene and the particular conditions of each field and the atmosphere.

7
ANALYSES OF FIELD MEASUREMENT DATA

One part of the overall LACIE effort is a Field Measurements Project [20]. The data acquired in this field measurement activity are directly applicable to studies of the type carried out and described in the preceding sections. The major focus of these field measurements has been on detailed spectral reflectance measurements of wheat fields and selected other targets, made from both truck-mounted and helicopter-borne spectroradiometers. Reduced versions of these data were not available for analysis during the performance period of this investigation.

Useful ancillary measurements were also made in support of both the primary spectral measurements and Landsat overpasses and to provide additional inputs for modeling efforts. Analyses are presented below of the atmosphere optical thickness measurements, broad-band irradiance measurements, and broad-band crop reflectance measurements made by members of the field measurements team.

7.1 ATMOSPHERE OPTICAL THICKNESS MEASUREMENTS

During the 1974-75 crop year and also for the fall of 1975 optical thickness measurements were made at three LACIE "supersites" in support of the helicopter data collection flights and associated Landsat overpasses. The data, collected by a Volz type solar radiometer, were taken at approximately ten minute intervals throughout the day for 47 days of the year. The optical thicknesses were then tabulated for the bands centered at the wavelengths 380 nm, 500 nm, 610 nm, 748.7 nm, 873.0 nm, and 1040 nm. We received useable versions of these data in mid-March of 1976; although it was then stated that this was to be an interim data set, we have nevertheless carried out a preliminary analysis of the data.

The optical thickness, $\tau_o(\lambda)$ of the atmosphere is defined as

$$\tau_o(\lambda) = \int_0^\infty \kappa_\lambda(x)\ dz \qquad (10)$$

where $\kappa_\lambda(x)$ is the volume extinction coefficient of the atmosphere as a function of wavelength λ and altitude z [21]. Optical depth is a dimensionless parameter which is used to specify the optical state of the atmosphere. It can be determined experimentally by measuring the direct solar irradiance at sea level for a specific angle of the sun, i.e.,

$$E(\lambda) = E_o(\lambda)\ \exp[-\tau_o(\lambda)\ \sec\ \theta_o] \qquad (11)$$

where $E(\lambda)$ is the measured irradiance, $E_o(\lambda)$ is the extraterrestrial irradiance at the top of the atmosphere, and θ_o is the solar zenith angle. It is assumed here that the detector has a flat collecting area the normal of which is parallel to the direction of the incoming solar radiation. In actual calculations the annual variation of $E_o(\lambda)$ should be taken into account by using the ratio $(\overline{r}/r)^2$ where $\overline{r}$ is the mean Earth-Sun distance and r is the variable Earth-Sun distance.

Our understanding of the calibration procedures used for the optical thickness measurements is based on Ref. 22. Because of the difficulty in obtaining absolute radiometric calibrations, it was decided by the measurement team that calibrations would be made using the thin atmosphere at Pike's Peak, Colorado. This was done for one sensor (#1003) for the period November 1974 through May 1975. June through August calibrations were based on lab measurements ratioed back to the Pike's Peak values. Data for other sensors were based upon calibration constants more recently obtained at Garden City, Kansas, and at JSC.

For a given location and time of year the optical thickness can be determined from the following equation:

$$J(\lambda) = J_o(\lambda)\ \exp[-\tau_o(\lambda)\ \sec\ \theta_o] \qquad (12)$$

where $J_o(\lambda)$ is the response of the particular sensor at the top of Earth's atmosphere. Because of different gain settings for each spectral channel the values of $J_o(\lambda)$ do not correspond to the values of the extraterrestrial irradiance at the top of the atmosphere. This is clearly indicated in Fig. 61 for the three sensors #1025, #1023, #1030.

By monitoring the sensor output $J(\lambda)$ as a function of sun angle θ_o, values for the constant $J_o(\lambda)$ were determined for each radiometer band, but these values are subject to considerable uncertainty because of changes in atmospheric conditions throughout the measurement days. In a telephone conversation with Dr. White at JSC, we learned that a more detailed and careful calibration of the sensors will be performed in Arizona where hopefully the atmospheric conditions are more stable than they were at the previous calibration sites. In any case, we have analyzed some of the data for the interim data set for the LACIE intensive test sites.

An example of the temporal fluctuations in the optical thickness during one day at a site in northwest North Dakota is illustrated in Fig. 62. For this case there were two sensors at the same location and yet they give us entirely different values of optical thickness, values of which usually lie outside the estimated uncertainty limits; one sensor (#1030) was used only this one day, while the other was used frequently. It should be noted also that the changes from time to time in each case are about the same, which indicates that the calibration constants were different by a constant scale factor. The optical thickness should be independent of such factors and this example clearly points out that one must be quite careful in the determination of the calibration constants. In any case, the graph indicates the magnitude of the temporal fluctuation in optical thickness measurements.

Another question of importance in the investigation of the relationship between optical thickness and Landsat multispectral data is

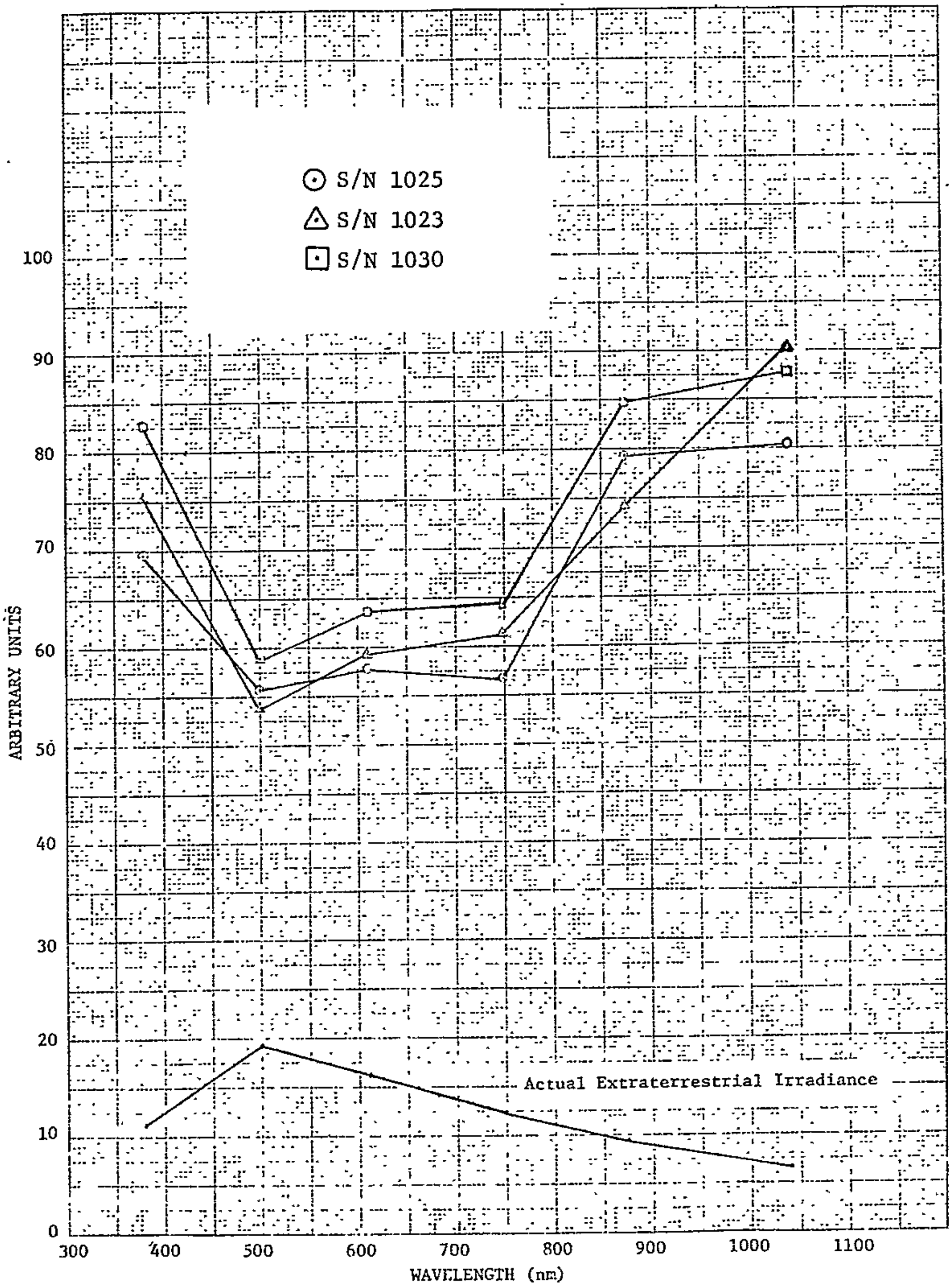

FIGURE 61. J_o VALUES AS A FUNCTION OF WAVELENGTH

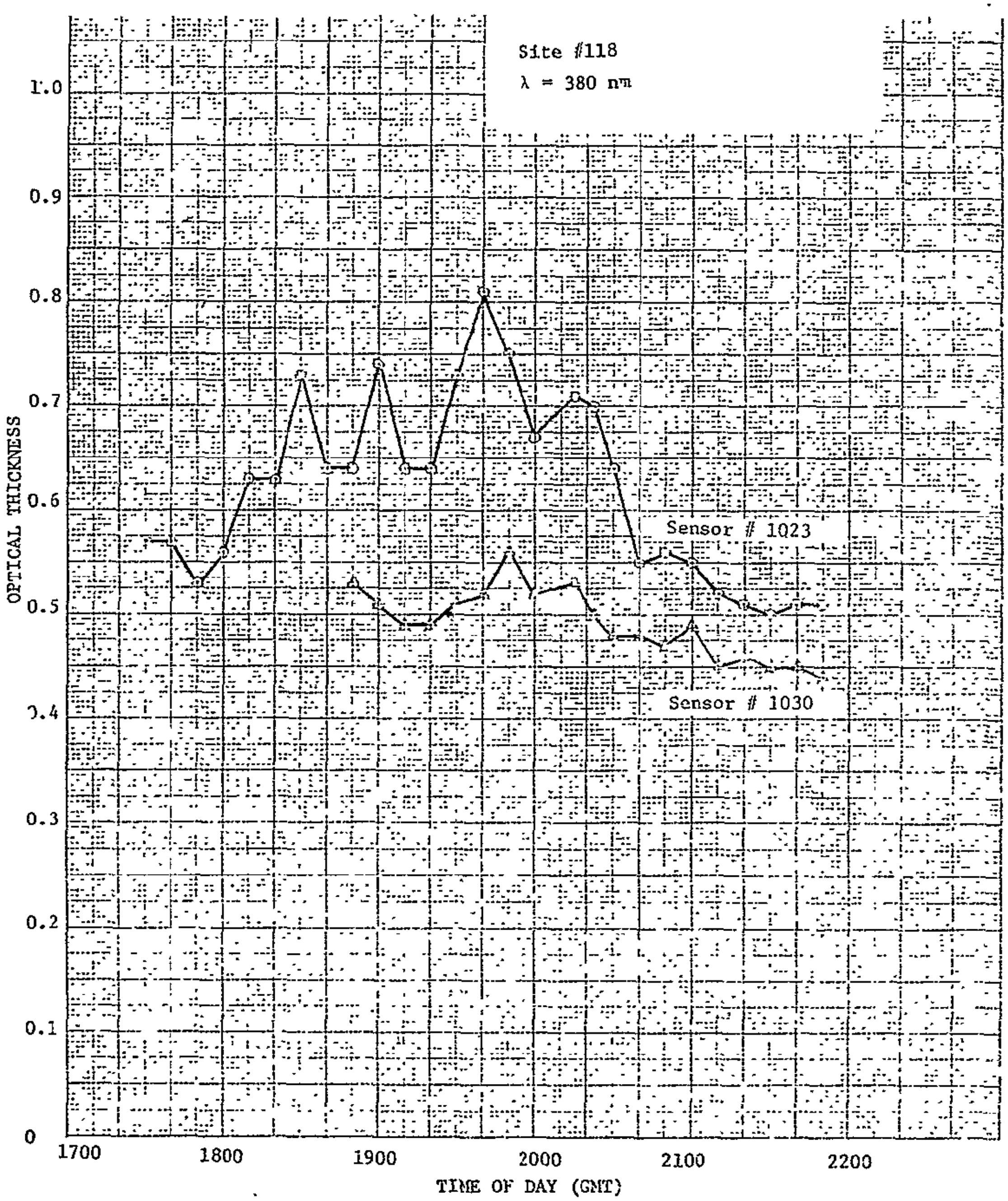

FIGURE 62. OPTICAL THICKNESS VS. TIME OF DAY; 7/18/75

the spectral variation in optical thickness. In Fig. 63 the optical thickness for an aerosol-free (Rayleigh) atmosphere and for an atmosphere with a sea level visual range of ∿23 km are illustrated. The latter values were taken from an Elterman model based upon measurements, and were used for the 'clear' atmosphere in the model calculations discussed in Sec. 6. The data points between the two curves represent five values of optical thickness measured in mid-morning over western Kansas between June 1975 and December 1975. The arrangement of points varies somewhat from channel to channel but the graph indicates that the visual range for that period was very high, i.e., greater than about 30 km.

Finally, the fluctuation in optical thickness between spectral bands over an extended period of time should be examined. An example is depicted in Fig. 64 for a month in the summer of 1975; values for the first two channels (380 nm and 500 nm) and their ratio are plotted. The significance of the observed fluctuations is not known because of the large uncertainties associated with the instrument calibrations. The ratio of bands seems to have about the same changes as the optical thickness values themselves.

In conclusion, we can say that this <u>interim</u> data set is interesting in that it does provide some information on magnitudes and the temporal and spectral variability in optical thickness. Hopefully, the next data set will have improved calibration constants and more reliable values of optical thickness. In any case, considering the difficulties involved in the collection of these data we now have a better idea of the variability in the optical properties of Earth's atmosphere. Also, the recommendation can be made that atmospheres with visual ranges greater than 23 km should be simulated, in addition to those already done, to represent the full range of conditions under which wheat will be observed.

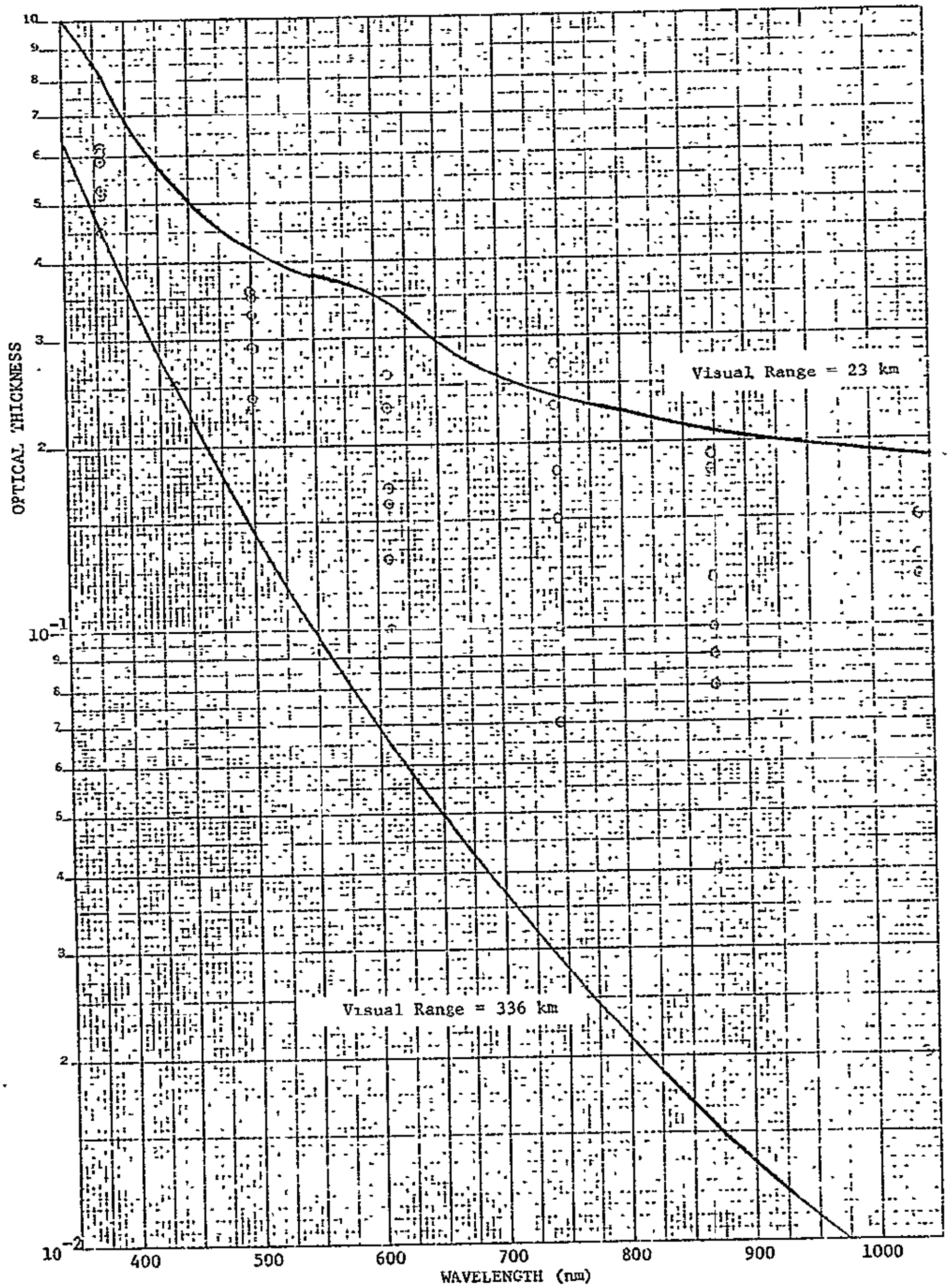

FIGURE 63. SPECTRAL OPTICAL THICKNESS AT THE SAME TIME (1610 HRS. GMT) ON VARIOUS DAYS FROM JUNE 1975 TO DECEMBER 1975 AT SITE NO. 76

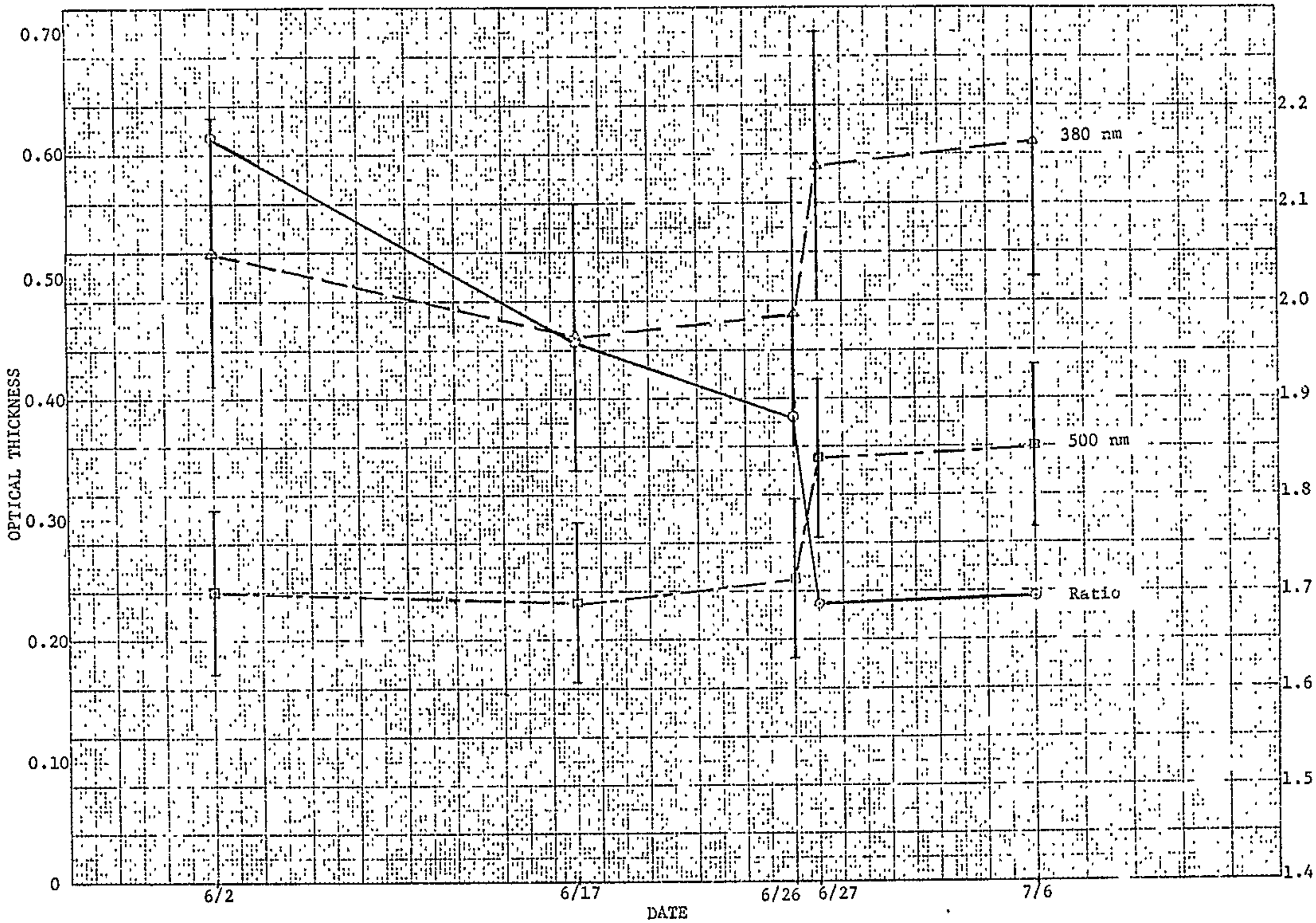

FIGURE 64. VARIATION IN OPTICAL THICKNESS DURING THE SUMMER OF 1975 AT 1610 HRS. GMT AT SITE NO. 76 FOR 380 nm, 500 nm, AND THEIR RATIO

7.2 BROAD-BAND IRRADIANCE MEASUREMENTS

Radiometers with broad-band spectral characteristics similar to those of the Landsat multispectral scanner were used by Texas A&M University in the Finney Kansas ITS and by Purdue/LARS in the Williams North Dakota ITS to make selected ancillary measurements. One of these measurements was that of the ratio of diffuse (non-direct) to total irradiance, from which the ratio of diffuse to direct irradiance can be calculated. The average diffuse-to-direct ratios for over sixty measurements at the sites are presented in Table 16. The corresponding values used in the theoretical simulations of wheat radiances were substantially greater. This provides another indication that clearer atmospheres should be simulated in addition to those already employed, agreeing with the observation based on the optical thickness measurements.

7.3 BROAD-BAND CROP REFLECTANCE MEASUREMENTS

These same broad-band radiometers were also used to measure crop reflectances, e.g., both wheat and bare soil reflectances at the two sites. Fig. 65(a) presents a scatter diagram of Band 6 vs. Band 5 reflectances measured for winter wheat at the Finney ITS throughout the growing season. This plot agrees well with a similar display in Fig. 23 of the theoretical reflectance calculations discussed earlier (See Sec. 6.4). The major differences are that the lowest reflectance values in Band 5 are lower for the measurements than for the calculations and bright-bare-soil effects are not evident in the measured data. The measurements were acquired primarily at five different stages of growth from an irrigated field with a relatively dense canopy at each growth stage. A similar diagram for spring wheat, measured on three dates in North Dakota, is presented in Fig. 65(b).

The multitemporal patterns of these reflectance values are presented in Fig. 66. The winter wheat pattern of Fig. 66(a) should not be compared directly to the multitemporal patterns of Fig. 60 since the latter figure displays radiance values which include atmospheric and

TABLE 16. AVERAGES OF BROAD-BAND GROUND SPECTRAL MEASUREMENTS MADE BY THE LACIE FIELD MEASUREMENTS TEAM

QUANTITY	UNITS	VALUE IN LANDSAT BAND: 4	5	6	7
1. Diffuse/Direct Irradiance	Dimensionless	0.137	0.104	0.107	0.119
2. Soil Reflectance	Dimensionless				
a. Mean		0.130	0.157	0.214	0.263
b. Standard Deviation		0.060	0.049	0.057	0.068

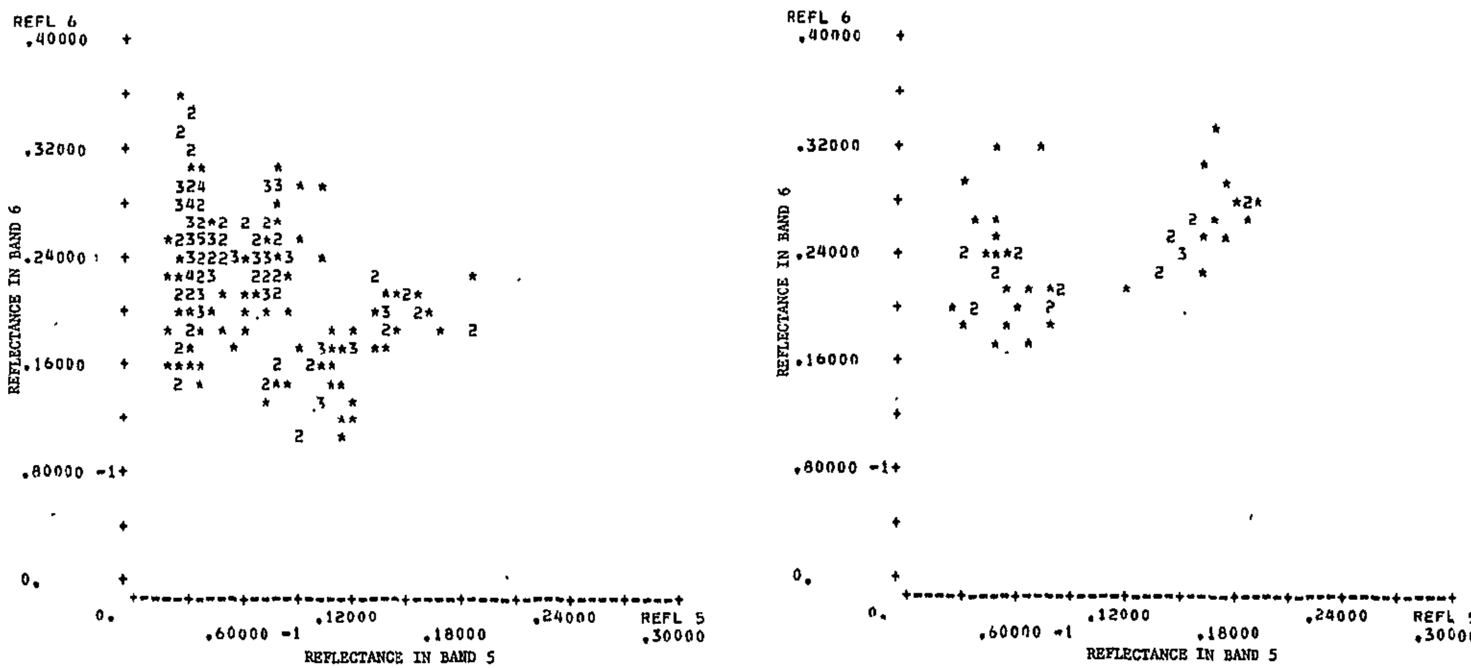

(a) Winter Wheat, Finney Kansas ITS

(b) Spring Wheat, Williams N. Dakota ITS

FIGURE 65. SCATTER DIAGRAMS OF 1975 FIELD RADIOMETER MEASUREMENTS OF WHEAT REFLECTANCE, LANDSAT BAND 6 VS BAND 5

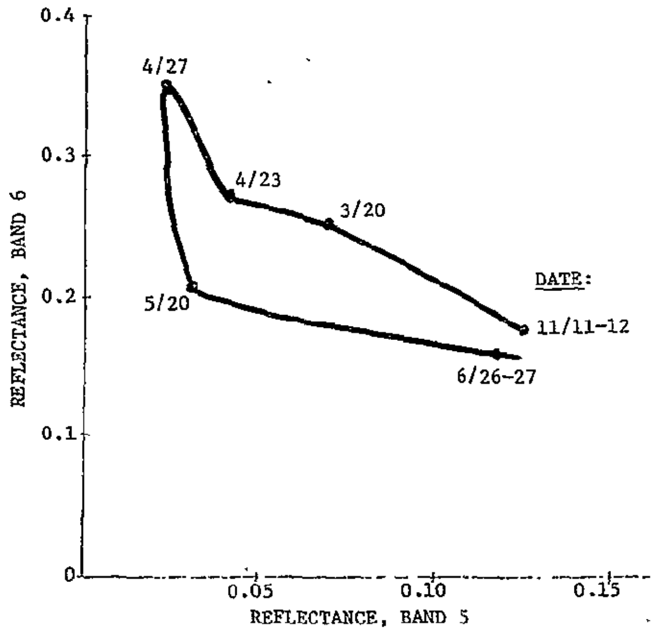

(a) Winter Wheat, Finney Kansas ITS

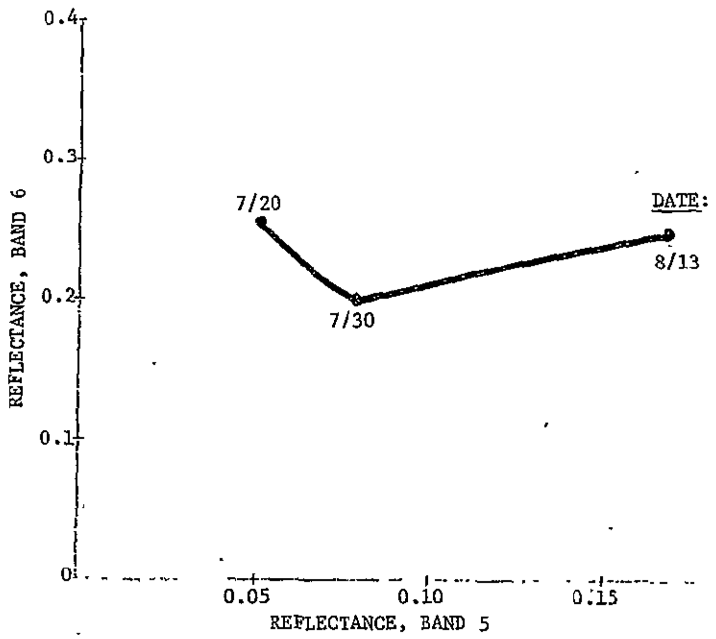

(b) Spring Wheat, Williams N. Dakota ITS

FIGURE 66. AVERAGED 1975 FIELD MEASUREMENTS OF MULTITEMPORAL WHEAT FIELD REFLECTANCES IN LANDSAT BANDS, MADE USING BROAD-BAND RADIOMETERS

irradiance effects as well as reflectance effects.

Soil reflectance values also were measured with the broad-band ratiometers. Mean values and standard deviations in the four bands also are presented in Table 16. These average soil reflectances agree quite well with the mean bare soil spectrum used in the wheat canopy simulations (See the 'bare' spectrum of Fig. 21) in Bands 6 and 7 but are somewhat lower in Bands 4 and 5, which would contribute to the lowest measured reflectances being lower than the lowest calculated ones.

REFERENCES

1. Malila, W. A., R. C. Cicone and J. M. Gleason, Wheat Signature Modeling and Analysis for Improved Training Statistics: Supplement, Simulated LANDSAT Wheat Radiances and Radiance Components, NASA CR-____, ERIM 109600-66-F_S, Environmental Research Institute of Michigan, Ann Arbor, Michigan, May 1976.

2. Malila, W. A., J. M. Gleason and R. C. Cicone, Investigation of Spatial Misregistration Effects in Multispectral Scanner Data, NASA CR-____, ERIM 109600-68-F, Environmental Research Institute of Michigan, Ann Arbor, Michigan, May 1976.

3. "Farm Facts, 1973-1974, Kansas Crop and Livestock Information for 1973 and Preliminary Estimates for 1974", Kansas State Board of Agriculture, Topeka, Kansas.

4. "Preliminary LACIE II CAMS Detailed Analysis Procedures", JSC-09681, prepared by LEC, Johnson Space Center, Houston, Texas, May 1975.

5. Malila, W. A., R. H. Hieber and A. P. McCleer, "Correlation of ERTS MSS Data and Earth Coordinate Systems", Proceedings of Conference on Machine Processing of Remotely Sensed Data, Purdue University, West Lafayette, Indiana, October 16-18, 1973, pp. 2b-1 thru 2b-13; (Also ERIM No. 193300-18-SA/J, August 1973).

6. Malila, W. A., D. P. Rice and R. C. Cicone, Final Report on the CITARS Effort by the Environmental Research Institute of Michigan, NASA CR-____, ERIM 109600-12-F, Environmental Research Institute of Michigan, Ann Arbor, Michigan, April 1975.

7. Richardson, W. and A. P. Pentland, Evaluation of Algorithms for Estimating Wheat Acreage from Multispectral Scanner Data, NASA CR-____, ERIM 109600-69-F, Environmental Research Institute of Michigan, Ann Arbor, Michigan, May 1976.

8. Horwitz, H. M., J. T. Lewis and A. P. Pentland, Estimating Proportions of Objects from Multispectral Scanner Data, NASA CR-____, ERIM 109600-13-F, Environmental Research Institute of Michigan, Ann Arbor, Michigan, May 1975.

9. Malila, W. A., "Radiation Balance Mapping With Multispectral Scanner Data", Remote Sensing of Earth Resources, Vol. 1, edited by F. Shahrokhi, University of Tennessee Space Institute, Tullahoma, Tennessee, 1972.

REFERENCES (Continued)

10. Lambeck, P. F. and D. P. Rice, Signature Extension Using Transformed Cluster Statistics and Related Techniques, NASA CR-____, ERIM 109600-70-F, Environmental Research Institute of Michigan, Ann Arbor, Michigan, May 1976.

11. Crane, R. B. and W. Richardson, "Rapid Processing of Multispectral Scanner Data Using Linear Techniques", Remote Sensing of Earth Resources, Vol. 1, edited by F. Shahrokhi, University of Tennessee Space Institute, Tullahoma, Tennessee, 1972.

12. Kauth, R. J. and G. S. Thomas, System for Analysis of Landsat Agricultural Data: Automatic Computer Assisted Proportion Estimation of Local Areas, NASA CR-____, ERIM 109600-67-F, Environmental Research Institute of Michigan, Ann Arbor, Michigan, May 1976, Section 4.2.1.

13. Engvall, J. and J. Tubbs, "A Non-Parametric Approach to Classifying Remote Sensed Data", to be published in Proceedings of the Symposium on Machine Processing of Remotely Sensed Data, West Lafayette, Indiana, June 1976.

14. Turner, R. E., Radiative Transfer in Real Atmospheres, NASA CR-____, ERIM 190100-24-T, Environmental Research Institute of Michigan, Ann Arbor, Michigan, July 1974.

15. Suits, G. H., "The Calculation of the Directional Reflectance of a Vegetative Canopy", Remote Sensing of Environment, Vol. 2: 117-125, 1972.

16. Multispectral Scanner System for ERTS, NASA CR-132758, Space and Communications Group, Hughes Aircraft Company, El Segundo, California, August 1972.

17. Earth Resources Technology Satellite Data Users Handbook, NASA Goddard Space Flight Center, Greenbelt, Maryland, 15 February 1972 (and subsequent revisions).

18. Condit, H. R., "The Spectral Reflectance of American Soils", Photogrammetric Engineering, Vol. XXXVI, No. 9:955-966, September 1970.

19. Malila, W. A., J. M. Gleason, and R. C. Cicone, Final Report on Atmospheric Modeling Related to Thematic Mapper Scan Geometry, NASA CR-____, ERIM 119300-5-F, Environmental Research Institute of Michigan, Ann Arbor, Michigan, April 1976.

REFERENCES (Continued)

20. Field Measurements Research for Remote Sensing of Wheat, Data Acquisition Plan, NASA/Johnson Space Center, (EOD), Houston, Texas, August 1975.

21. Turner, R. E., W. A. Malila and R. F. Nalepka, "Importance of Atmospheric Scattering in Remote Sensing", Proceedings of the Seventh International Symposium on Remote Sensing of Environment, Willow Run Laboratories of the Institute of Science and Technology, The University of Michigan, Ann Arbor, Michigan, 1971, pp. 1651-1697.

22. Memorandum to Dr. M. C. McEwen, NASA/JSC-TF3, from W. P. White, Request for Approval of a Solar Radiometer Data Delivery Plan, LEC Reference No. 643-757, Lockheed Electronics Company, Houston, Texas, 20 January 1976.

Technical and Final Report Distribution List

NASA Contract NAS9-14123

NAME	NUMBER OF COPIES
NASA/Johnson Space Center Earth Observations Division Houston, Texas 77058	
ATTN: Mr. Robert MacDonald/TF	(1)
ATTN: Mr. B. Erb/TF2	(1)
ATTN: Dr. F. Hall/TF2	(1)
ATTN: Mr. J. Murphy/TF2	(1)
ATTN: Mr. A. Grandfield/TF3	(10) + 1 Reproducible
ATTN: Mr. J. Dragg/TF4	(1)
ATTN: Earth Resources Data Facility/TF12	(8)
NASA/Johnson Space Center Earth Resources Program Office Office of the Program Manager Houston, Texas 77058	
ATTN: Mr. Clifford E. Charlesworth/HA	(1)
ATTN: Mr. William E. Rice/HA	(1)
NASA/Johnson Space Center Earth Resources Program Office Program Analysis & Planning Office Houston, Texas 77058	
ATTN: Dr. O. Glenn Smith/HD	(1)
NASA/Johnson Space Center Earth Resources Program Office Systems Analysis and Integration Office Houston, Texas 77058	
ATTN: Mr. Richard A. Moke/HC	(1)
ATTN: Mr. M. Jay Harnage, Jr./HC	(1)
NASA/Johnson Space Center Technical Library Branch Houston, Texas 77058	
ATTN: Ms. Retha Shirkey/JM6	(4)

NAME	NUMBER OF COPIES
NASA/Johnson Space Center Management Services Division Houston, Texas 77058 ATTN: Mr. John T. Wheeler/AT3	(1)
NASA/Johnson Space Center Technical Support Procurement Houston, Texas 77058 ATTN: Mrs. Ruth Elder/BB63	(1)
Earth Resources Laboratory, GS Mississippi Test Facility Bay St. Louis, Mississippi 39520 ATTN: Mr. D. W. Mooneyhan	(1)
EROS Data Center U.S. Department of Interior Sioux Falls, South Dakota 57198 ATTN: Mr. G. Thorley	(1)
Department of Mathematics Texas A&M University College Station, Texas 77843 ATTN: Dr. Larry Guseman	(1)
NASA/Johnson Space Center Mission Planning & Analysis Division Houston, Texas 77058 ATTN: Mr. Eugene Davis/FA	(1)
U.S. Department of Agriculture Agricultural Research Service Washington, D.C. 20242 ATTN: Dr. Robert Miller	(1)

NAME	NUMBER OF COPIES
U.S. Department of Agriculture Soil & Water Conservation Research Division P.O. Box 267 Weslaco, Texas 78596 ATTN: Dr. Craig Wiegand	(1)
U.S. Department of Interior USGA National Center Mail Stop 115 Geography Program Reston, Virginia 22092 ATTN: Dr. James R. Anderson	(1)
Director, Remote Sensing Institute South Dakota State University Agriculture Engineering Building Brookings, South Dakota 57006 ATTN: Mr. Victor I. Myers	(1)
U.S. Department of Interior Fish & Wildlife Service Bureau of Sport Fisheries & Wildlife Northern Prairie Wildlife Research Center Jamestown, North Dakota 58401 ATTN: Mr. Harvey K. Nelson	(1)
U.S. Department of Agriculture Forest Service 240 W. Prospect Street Fort Collins, Colorado 80521 ATTN: Dr. Richard Driscoll	(1)
U.S. Department of Interior Geological Survey Water Resources Division 500 Zack Street Tampa, Florida 33602 ATTN: Mr. A.E. Coker	(1)

NAME	NUMBER OF COPIES
U.S. Department of Interior Geological Survey 801 19th Street, N.W. Washington, DC 20242 ATTN: Mr. M. Deutsch	(1)
U.S. Geological Survey 801 19th Street, N.W., Room 1030 Washington, DC 20242 ATTN: Dr. Jules D. Friedman	(1)
U.S. Department of Interior Geological Survey Federal Center Denver, Colorado 80225 ATTN: Dr. Harry W. Smedes	(1)
U.S. Department of Interior Geological Survey Water Resources Division 901 S. Miami Ave. Miami, Florida 33130 ATTN: Mr. Aaron L. Higer	(1)
University of California School of Forestry Berkeley, California 94720 ATTN: Dr. Robert Colwell	(1)
Environmental Remote Sensing Applications Laboratory Oregon State University Corvallis, Oregon 97331 ATTN: Dr. Barry J. Schrumpf	(1)

NAME	NUMBER OF COPIES
U.S. Department of Interior Director, EROS Program Washington, DC 20244 ATTN: Mr. J. M. Denoyer	(1)
U.S. Department of Interior Geological Survey GSA Building, Room 5213 Washington, DC 20242 ATTN: Mr. W.A. Fischer	(1)
NASA Wallops Wallops Station, Virginia 23337 ATTN: Mr. James Bettle	(1)
Purdue University Purdue Industrial Research Park 1220 Potter Drive West Lafayette, Indiana 47906	
ATTN: Dr. David Landgrebe	(1)
ATTN: Mr. Terry Phillips	(1)
ATTN: Dr. Marvin Bauer	(1)
ATTN: Dr. Philip Swain	(1)
U.S. Department of Interior EROS Office Washington, DC 20242 ATTN: Dr. Raymond W. Fary	(1)
U.S. Department of Interior Geological Survey 801 19th Street, N.W. Washington, DC 20242 ATTN: Mr. Charles Withington	(1)

NAME	NUMBER OF COPIES
U.S. Department of Interior EROS Office Washington, DC 20242 ATTN: Mr. William Hemphill	(1)
Chief of Technical Support Western Environmental Research Laboratories Environmental Protection Agency P.O. Box 15027 Las Vegas, Nevada 89114 ATTN: Mr. Leslie Dunn	(1)
NASA/Langley Research Mail Stop 470 Hampton, Virginia 23365 ATTN: Mr. William Howle	(1)
U.S. Geological Survey Branch of Regional Geophysics Denver Federal Center, Building 25 Denver, Colorado 80225 ATTN: Mr. Kenneth Watson	(1)
NAVOCEANO, Code 7001 Naval Research Laboratory Washington, DC 20390 ATTN: Mr. J. W. Sherman, III	(1)
U.S. Department of Agriculture Administrator Agricultural Stabilization and Conservation Service Washington, DC ATTN: Mr. Kenneth Frick	(1)
Pacific Southwest Forest & Range Experiment Station U.S. Forest Service P. O. Box 245 Berkeley, CA 94701 ATTN: Mr. R. C. Heller	(1)

NAME	NUMBER OF COPIES
United States Department of Agriculture/Forestry Service Division of Forest Economics and Marketing Resources 1200 Independence Avenue Washington, D.C. 20250 ATTN: Dr. P. Weber	(1)
University of Texas at Dallas Box 688 Richardson, Texas 75080 ATTN: Dr. Patrick L. Odell	(1)
Department of Mathematics University of Houston Houston, Texas 77004 ATTN: Dr. Henry Decell	(1)
Institute for Computer Services and Applications Rice University Houston, Texas 77001 ATTN: Dr. M. Stuart Lynn	(1)
U.S. National Park Service Western Regional Office 450 Golden Gate Avenue San Francisco, California 94102 ATTN: Mr. M. Kolipinski	(1)
U.S. Department of Agriculture Statistical Reporting Service Room 4833, South Bldg. Washington, D.C. 20250 ATTN: G. F. Hart/W. H. Wigton	(2)
U.S. Department of Agriculture Statistical Reporting Service Washington, DC 20250 ATTN: Mr. H. L. Trelogan, Administrator	(1)

NAME	NUMBER OF COPIES
Ames Research Center National Aeronautics and Space Administration Moffett Field, California 94035	
ATTN: Dr. D. M. Deerwester	(1)
Goddard Space Flight Center National Aeronautics and Space Administration Greenbelt, Maryland 20771	
ATTN: Mr. W. Nordberg, 620	(1)
ATTN: Mr. W. Alford, 563	(1)
Lewis Research Center National Aeronautics and Space Administration 21000 Brookpark Road Cleveland, Ohio 44135	
ATTN: Dr. Herman Mark	(1)
John F. Kennedy Space Center National Aeronautics and Space Administration Kennedy Space Center, Florida 32899	
ATTN: Mr. J. P. Claybourne/AA-STA	(1)
NASA/Langley Mail Stop 214 Hampton, Virginia 23665	
ATTN: Mr. James L. Raper	(1)
Texas A&M University Institute of Statistics College Station, TX 77843	
ATTN: Dr. H. O. Hartley	(1)
Texas Tech University Department of Mathematics P. O. Box 4319 Lubbock, TX 79404	
ATTN: Dr. T. Boullion	(1)

NAME	NUMBER OF COPIES
Department of Watershed Sciences Colorado State University Fort Collins, Colorado 80521 ATTEN: Dr. James A. Smith	(1)
Lockheed Electronics Co. 16811 El Camino Real Houston, Texas 77058 ATTN: Mr. R. Tokerud	(1)
University of Tulsa Math-Sciences Department 600 South College Tulsa, Oklahoma 74104 ATTN: Dr. William A. Coberly	(1)
IBM Corporation 1322 Space Park Drive Houston, Texas 77058 ATTN: Dr. D. Ingram	(1)
S&D - DIR Marshall Space Flight Center Huntsville, Alabama 35812 ATTN: Mr. Cecil Messer	(1)
Code 168-427 Jet Propulsion Laboratory 4800 Oak Grove Drive Pasadena, California 91103 ATTN: Mr. Fred Billingsley	(1)
NASA Headquarters Washington, DC 20546	
ATTN: Mr. W. Stoney/ER	(1)
ATTN: Mr. Leonard Jaffe/ER	(1)
ATTN: Mr. M. Molloy/ERR	(1)
ATTN: Mr. James R. Morrison	(1)

NAME	NUMBER OF COPIES
Mr. James D. Nichols Space Sciences Laboratory, Rm. 260 University of California Berkeley, CA 94720	(1)
EXXON Production Research Co. P. O. Box 2189 Houston, TX 77001 ATTN: Mr. J. O. Bennett	(1)
Texas A&M University Remote Sensing Center College Station, Texas 77843 ATTN: Mr. J. C. Harlan	(1)
U.S. Department of Agriculture 12th & Independence, SW Room 3745-S Washington, D.C. 20250 ATTN: Mr. Clark Ison LACIE Project Office (FAS)	(1)
University of Arkansas Mathematics Department Fayetteville, Arkansas 72704 ATTN: Dr. Jack D. Tubbs	(1)